TRISO Fuel Performance: Modeling, Integration into Mainstream Design Studies, and Application to a Thorium-fueled Fusion-Fission Hybrid Blanket

by

Jeffrey James Powers

A dissertation submitted in partial satisfaction of the
requirements for the degree of
Doctor of Philosophy

in

Engineering - Nuclear Engineering

in the

Graduate Division

of the

University of California, Berkeley

Committee in charge:

Professor Ehud Greenspan, Chair
Professor Brian Wirth
Professor Per Peterson
Professor Richard Norgaard

Fall 2011

TRISO Fuel Performance: Modeling, Integration into Mainstream Design Studies, and Application to a Thorium-fueled Fusion-Fission Hybrid Blanket

Copyright 2011
by
Jeffrey James Powers

Abstract

TRISO Fuel Performance: Modeling, Integration into Mainstream Design Studies, and Application to a Thorium-fueled Fusion-Fission Hybrid Blanket

by

Jeffrey James Powers

Doctor of Philosophy in Engineering - Nuclear Engineering

University of California, Berkeley

Professor Ehud Greenspan, Chair

This study focused on creating a new tristructural isotropic (TRISO) coated particle fuel performance model and demonstrating the integration of this model into an existing system of neutronics and heat transfer codes, creating a user-friendly option for including fuel performance analysis within system design optimization and system-level trade-off studies. The end product enables both a deeper understanding and better overall system performance of nuclear energy systems limited or greatly impacted by TRISO fuel performance. A thorium-fueled hybrid fusion-fission Laser Inertial Fusion Energy (LIFE) blanket design was used for illustrating the application of this new capability and demonstrated both the importance of integrating fuel performance calculations into mainstream design studies and the impact that this new integrated analysis had on system-level design decisions.

A new TRISO fuel performance model named TRIUNE was developed and verified and validated during this work with a novel methodology established for simulating the actual lifetime of a TRISO particle during repeated passes through a pebble bed. In addition, integrated self-consistent calculations were performed for neutronics depletion analysis, heat transfer calculations, and then fuel performance modeling for a full parametric study that encompassed over 80 different design options that went through all three phases of analysis. Lastly, side studies were performed that included a comparison of thorium and depleted uranium (DU) LIFE blankets as well as some uncertainty quantification work to help guide future experimental work by assessing what material properties in TRISO fuel performance modeling are most in need of improvement.

A recommended thorium-fueled hybrid LIFE engine design was identified with an initial fuel load of 20MT of thorium, 15% TRISO packing within the graphite fuel pebbles, and a 20cm neutron multiplier layer with beryllium pebbles in flibe molten salt coolant. It operated at a system power level of 2000 MW_{th}, took about 3.5 years to reach full plateau power, and was capable of an End of Plateau burnup of 38.7 %FIMA if considering just the neutronic constraints in the system design; however, fuel performance constraints led to a maximum credible burnup of 12.1 %FIMA due to a combination of internal gas pressure and irradiation

effects on the TRISO materials (especially PyC) leading to SiC pressure vessel failures. The optimal neutron spectrum for the thorium-fueled blanket options evaluated seemed to favor a hard spectrum (low but non-zero neutron multiplier thicknesses and high TRISO packing fractions) in terms of neutronic performance but the fuel performance constraints demonstrated that a significantly softer spectrum would be needed to decrease the rate of accumulation of fast neutron fluence in order to improve the maximum credible burnup the system could achieve.

To my Lord and friend, Jesus Christ. All I have and am is Yours.

To my wife, Sarah. Your support, encouragement, and love are incredible.

To my friends and family, old and new. I appreciate all of your kind words and prayers.

Acknowledgments

As with any multi-year work effort of substantial scale, a large number of people deserve thanks and recognition for their role in helping me complete this research and dissertation. I'm quite sure that I'll forget to recognize some of them here and I apologize ahead of time for any such omissions - I assure anyone that I forget to mention by name here that it's not for a lack of genuine thankfulness and gratitude in my heart towards you, it's simply my mind failing me at the moment.

I would first like to acknowledge my thesis committee members for their efforts. As my thesis chair, Ehud Greenspan oversaw the whole of my research, provided excellent feedback regarding neutronic analysis and overall design study efforts, and asked numerous insightful questions that opened me to new lines of thought that I had not previously considered. Brian Wirth served as a committee member but in reality was effectively a co-chair for my thesis; Brian's tireless support and help were essential in addressing some of the materials challenges in this work, developing my fuel performance model, and giving guidance in setting direction for my research. Per Peterson and Richard Norgaard, my other committee members, also provided helpful insights during my work and furthermore offered stimulating discussions related to my work but outside of the scope of my actual dissertation, delving into policy and economics and other issues.

I would be remiss if I did not acknowledge the formative impact that Timothy Trumbull, John Ward, and Jonathan Witter have had on my career. They have been great friends and mentors and their excellence in their respective areas of Nuclear Engineering was a major motivating factor in my decision to pursue graduate studies. Furthermore, Tim Trumbull and John Ward both assisted me in choosing this area of study for my doctoral thesis and I sincerely appreciate their thoughts and time in helping me make that decision. I'm truly blessed to count you guys as my friends and to have been able to learn from you.

Next, I would like to acknowledge the LIFE team at LLNL for providing me a home for my research and teaching me a great deal about a broad range of topics. Jeff Latkowski has been an excellent supervisor and mentor, asking important questions while also steadfastly supporting me in all sorts of ways, and he got me started at LLNL by taking a chance bringing me on for a summer research opportunity over three years ago that has blossomed into this work. Kevin Kramer, Max Fratoni, and Jeff Seifried all influenced my work and helped me complete my studies. Kevin and Max in particular taught me how to use various computer codes I needed for my research and helped guide my neutronic analysis. Ryan Abbott deserves far more credit than I can possibly give him here; he always took time out of his schedule to help answer heat transfer or mechanical design questions that I had, provided me with and taught me to use his MathCAD heat transfer model for my design study, and above all else is a good friend with whom I thoroughly enjoy having many interesting conversations over lunch or coffee. Lesa Christman has provided administrative support for me the entire time I've been on the LIFE project and has essential in getting things done at LLNL and pointing me to the right resources for questions I have.

Several friends and colleagues at UC Berkeley also made valuable contributions to this work and have been a source of support during my studies. In particular, Tommy Cisneros has been a great help in neutronic modeling and analysis as well as issues related to thorium fuels. Mike Laufer has been a rock solid friend that has provided continual support during coursework and research and has always been there when I have thermal hydraulics or heat transfer questions; our conversations over a cup of coffee have become a fixture in my graduate student experience and I'll sincerely miss them. Raluca (Scarlat) Meric de Bellefon and Vladimir Mozin have both also been with me since the beginning of my time at UC Berkeley; they've shared with me in the toil of coursework, helped me prepare for examinations, offered feedback on my research, and are good friends. Lisa Zemelman, the Graduate Student Affairs Officer for the Nuclear Engineering department at UC Berkeley, has been a tremendous help in navigating the bureaucracy of the UC system and helping me stay on track to complete my studies.

Numerous people helped me during my development of the TRIUNE fuel performance model. In particular, Dave Petti and John Maki of Idaho National Laboratory were extremely helpful in answering my questions and providing feedback on my assumptions and methods. Jaime Marian and Paul DeMange of LLNL supplied continual feedback along the way and gave freely of their own time to meet with me and discuss my progress and issues. Lance Snead, John Hunn, and others at ORNL gave important feedback regarding ongoing experimental work as well as some information regarding the capabilities and limitations of current TRISO manufacturing processes and technologies.

I am deeply thankful for my wife, Sarah, who not only has supported me emotionally and spiritually throughout my graduate studies but also made significant contributions to my research through her knowledge and skills. She's shown incredible patience and encouragement over the past 4.5 years and I'm looking forward to having more time to live out life with her after I've completed this work. I would also like to thank my family, both old and new, for their unending encouragement and prayers. My parents have always supported me, been there to give advice, and no matter what believed in me. Several friends have likewise been a solid support base for me during this time, in particular Jonny Lobel and Mike Mayer as well as some friends at Regeneration Church in Oakland. All of these people have lifted me and my work up in prayer, listened to my frustrations, offered encouragement, and reminded me that there's more to life than grad school. God has truly blessed me by surrounding me with such friends and family.

Lastly, I would like to acknowledge the Lawrence Scholar Program and the Institutional Computing Grand Challenge program at LLNL. The Lawrence Scholar Program has funded my time during my research over the past two and a half years and the allocations from the Institutional Computing Grand Challenge program have provided the computing time for all of my depletion analyses over the past three years. Both of these programs were instrumental in enabling me to complete my graduate studies.

Contents

List of Figures

List of Tables

Nomenclature

Abbreviations

BOL	Beginning of Life
CEA	Commissariat à l'Énergie Atomique
CEGA	Combustion Engineering-General Atomics
CVD	Carbon Vapor Deposition (or carbon vapor deposited)
DOE	Department of Energy (U.S.)
DU	Depleted Uranium
EFPD	Effective Full Power Days
EOL	End of Life
FIMA	Fissions per Initial Metal Atom (≤ 1.0)
FPM	Fuel Performance Model
GA	General Atomics
IIDC	Irradiation-Induced Dimensional Change (shrinkage and swelling)
INEEL	Idaho National Engineering and Environmental Laboratory
INL	Idaho National Laboratory (formerly INEEL)
IPyC	Inner Pyrolytic Carbon
LANL	Los Alamos National Laboratory
LIFE	Laser Inertial Fusion-based Energy
LLNL	Lawrence Livermore National Laboratory
MA	Minor Actinide
MHR	Modular Helium Reactor
MIT	Massachusetts Institute of Technology
NGNP	Next Generation Nuclear Plant
OPyC	Outer Pyrolytic Carbon
ORNL	Oak Ridge National Laboratory
PyC	Pyrolytic Carbon
SiC	Silicon Carbide
SNL	Sandia National Laboratory
TD	Theoretical density
TRISO	Tristructural isotropic
TRU	Transuranic
UCB	University of California, Berkeley

Symbols

ε	strain [μm/μm]
Φ	fast neutron fluence [10^{25} n-m^{-2} , (E_n >0.18 MeV)]
t	fast neutron fluence [10^{25} n-m^{-2} , (E_n >0.18 MeV)] or time [seconds or days]
k	thermal conductivity [W/m-K]
E	modulus of elasticity (Young's modulus) of a coating layer [MPa]
c	irradiation creep coefficient for a PyC layer [MPa n-m^{-2}, (E_n >0.18 MeV)]
σ	stress [MPa]
μ	Poissons ratio of a coating layer
ν	Poissons ratio in creep for a PyC layer
$\dot{S}$	dimensional change rate [(n-m^{-2})$^{-1}$]
$\overline{\dot{S}}$	average dimensional change rate over a time increment [(n-m^{-2})$^{-1}$]
u	radial displacement [μm]
r	radial coordinate [μm]
p	radial stress/pressure acting on the inner surface of a coating layer [MPa]
q	radial stress/pressure acting on the outer surface of a coating layer [MPa]
α	thermal expansion coefficient of a coating layer [K^{-1}]
$\overline{\alpha}$	average thermal expansion coefficient of a coating layer over a time increment [K^{-1}]
$\dot{T}$	rate of temperature change [K (10^{25} n-m^{-2})$^{-1}$]
$\overline{\dot{T}}$	average rate of temperature change over a time increment [K (10^{25} n-m^{-2})$^{-1}$]

Subscripts

a,b	Inner or outer (radius)
buff	Buffer layer
center	Center of the fuel kernel and TRISO particle
I	IPyC layer
kern	Kernel
O	OPyC layer
r	Radial direction
S	SiC layer
SiC	SiC layer
t	Tangential direction
TD	Theoretical density

Chapter 1

Introduction

Modern society demands increasingly large supplies of energy to meet the needs and desires of the current population and continue human development. Economic impacts can be clearly felt when energy prices change, as demonstrated by the effect that sharp increases in US gasoline prices in recent years had on the bank accounts and transportation plans for large numbers of people; even more fundamental, however, is the demonstrated impact that achieving at least some minimal level of energy supply and use has on basic quality of life factors such as life expectancy and literacy [1, 2]. Developing an understanding of our current energy use represents a key first step toward being able to intelligently approach energy supply and production challenges; to that end, Figure 1.1 summarizes estimated energy use in the US for 2010 while Figure 1.2 summarizes estimated energy use across the entire world for 2007.

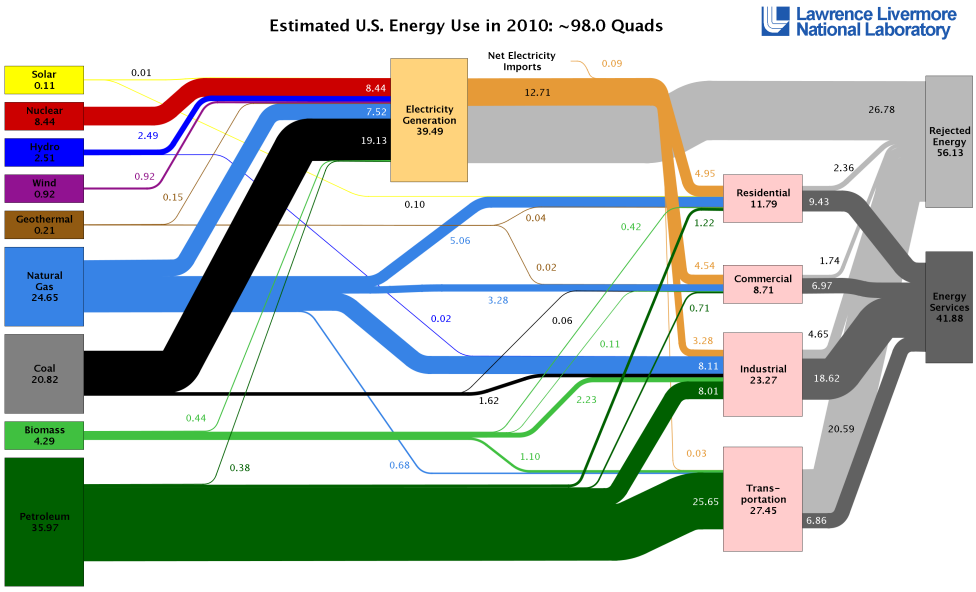

Figure 1.1: Estimated energy use in the US for 2010 [3].

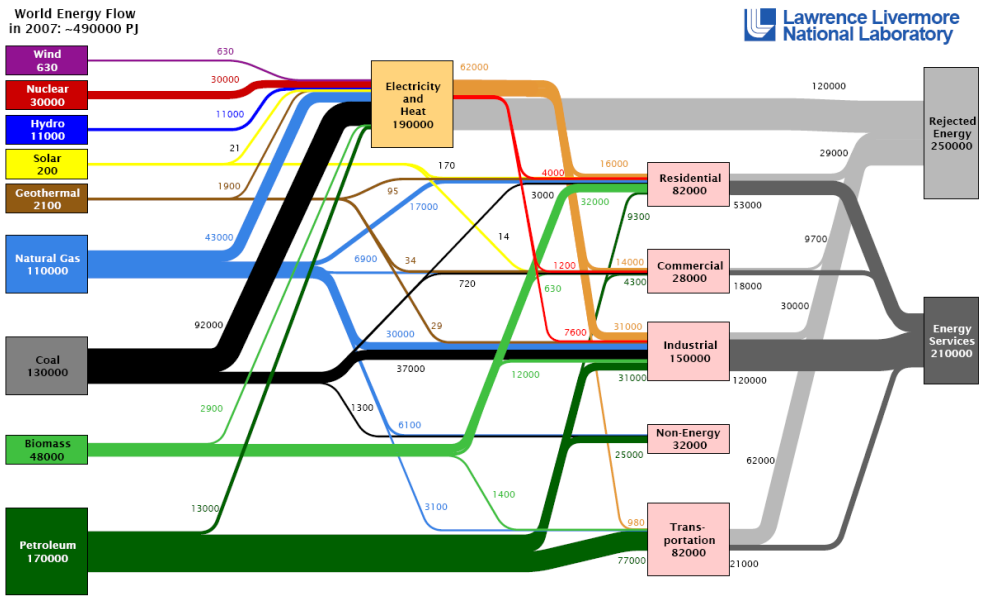

Figure 1.2: Estimated world energy use for 2007 [4].

These energy flow charts highlight the key role that electricity production plays in the energy system of the US and the world as a whole. Though projections of future energy supply and demand vary considerably, it seems clear that the overall demand for energy worldwide will continue to grow as the global population increases and emerging countries such as China and India continue to modernize. In light of the growing concern about possible global climate change due to greenhouse gas (GHG) emissions, there is an ongoing debate about which technologies to invest in for electricity generation [1, 5, 6, 7]. Nuclear fission energy systems that utilize fuels such as uranium and thorium will continue to be an important source of clean, low carbon electricity production and the total electricity generation from nuclear fission plants may in fact need to expand as part of the effort to simultaneously meet energy demand while reducing overall carbon emissions [1, 8, 9]. Designing next generation nuclear energy systems and developing models to understand and predict the performance of current and future nuclear fuels thus not ensures the safe, secure, and reliable operation of nuclear energy — it potentially benefits the Earth's atmosphere in crucial ways.

This chapter introduces topics related to tristructural isotropic (TRISO) coated fuel particles and hybrid fusion-fission Laser Inertial Fusion-based Energy (LIFE) systems. Section 1.1.1 provides background information on TRISO coated fuel particles, while Section 1.1.2 summarizes existing TRISO particle fuel performance models (FPMs) and identifies some of their key challenges and limitations. Previous works have reviewed the design and fuel performance modelling of TRISO fuel particles; more extensive information than the summary provided below can be found in those sources [10, 11]. Section 1.1.3 gives a broad description of the motivation for, and design of, hybrid LIFE engines. Section 1.2 then defines the objective of this dissertation and outlines the structure of this document.

1.1 Background review

1.1.1 TRISO Coated Fuel Particles

Tristructural isotropic (TRISO) fuel particles represent the chosen fuel technology for various nuclear reactor design projects that involve goals of high coolant temperatures or high burnup performance of nuclear fuel. TRISO fuel was originally developed and used in Germany for the AVR reactor, a 46 MW_{th} (15 MW_e) prototype pebble bed reactor, and the Thorium High Temperature Reactor (THTR-300), a 750 MW_{th} (300 MW_e) reactor; both of these reactors were high-temperature gas-cooled reactors (HTGRs) [12, 13, 14]. China currently uses TRISO fuel in its 10 MW_{th} prototype pebble bed High Temperature Reactor (HTR-10), and Japan uses TRISO fuel in its 30 MW_{th} prismatic core High Temperature Test Reactor (HTTR) [15, 16, 17]. TRISO fuel programs currently exist in the United States (US), France, the United Kingdom, Russia, and South Africa. The Next Generation Nuclear Plant (NGNP) program in the US, along with other projects in the US and around the world, plans to use TRISO fuel [18]. Figure 1.3 shows a micrograph of a TRISO fuel particle that has been colored to highlight the different regions.

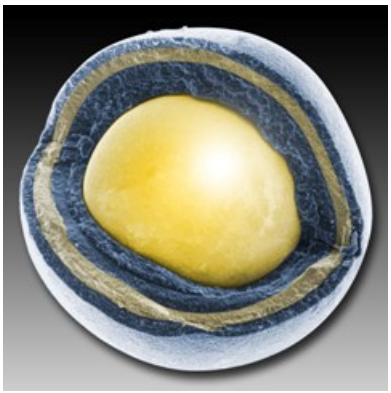

Figure 1.3: An artistically colored microscopic image of a TRISO fuel particle cracked open to show the fuel kernel and coating layers.

As seen above, TRISO particles typically consist of five distinct regions. At the center of the particle is the fuel kernel, which contains the nuclear fuel (uranium, plutonium, thorium, or transuranic elements) usually in an oxide or oxycarbide form. A porous carbon buffer surrounding the kernel attenuates recoiling fission fragments and accommodates internal gas buildup and particle dimensional changes. The outer layers consist of an inner pyrolytic carbon (IPyC) layer, a silicon carbide (SiC) layer, and an outer pyrolytic carbon (OPyC) layer. The PyC layers are dense pyrolytic carbon, typically at about 90% of their theoretical density of 2.2 g/cm^3 [19]. The SiC layer acts as the main pressure vessel for the particle and provides a diffusion barrier to prevent the release of gaseous and metallic fission products (FPs). The PyC layers protect the SiC layer from chemical attack during TRISO particle

operation, act as additional diffusion barriers to FPs, and the IPyC protects the fuel kernel from corrosive gases used to deposit the SiC layer. The possibility of replacing the SiC layer with ZrC has been suggested and is currently being evaluated [20, 21, 22, 23].

Table 1.1 provides typical dimensions and densities for a UO_2 TRISO particle, based upon a German 500μm kernel [19]. The actual dimensions and densities vary according to design purposes and manufacturing processes. Recent studies have shown that variations in manufacturing methods and processes can yield drastic differences in the quality and capabilities of the TRISO particles produced [24]. Theoretical densities listed in this table come from the most relevant references found in the literature [25, 26].

Table 1.1: Nominal parameters for a German UO_2 TRISO Particle [19]

Layer	**Density[g/cm^3]**		**Outer Radius**	**Thickness**
	Actual	**Theoretical**	**[μm]**	**[μm]**
Kernel	10.96	-	250	500 (diameter)
Buffer	1.1	2.26	345	95
IPyC	1.7	2.26	385	40
SiC	3.2	3.21	420	35
OPyC	1.7	2.26	460	40

While the TD of the kernel is not listed, exercising careful controls of kernel manufacturing processes generally yields nearly full density fuel. Figure 1.4 provides a simple illustration of a TRISO particle, as reproduced from Reference [27]. Figure 1.5 shows a micrograph of an actual TRISO particle, taken from Reference [28], in which the porous nature of the buffer and some cracking in the coating layers are visible.

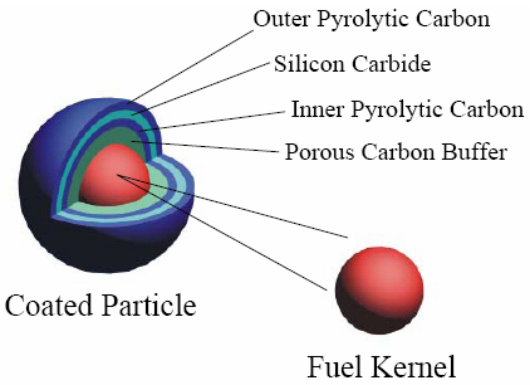

Figure 1.4: Illustrative cutaway drawing of a TRISO particle, as reproduced from Ref. [27].

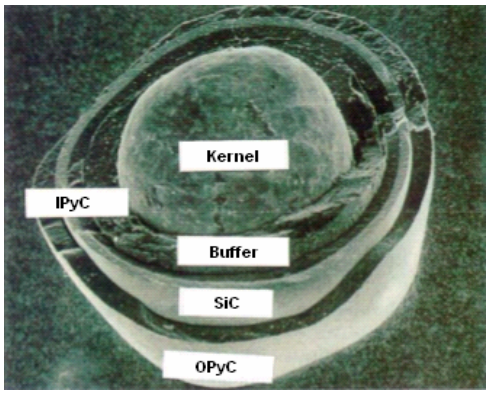

Figure 1.5: Micrograph of an actual TRISO fuel particle, as reproduced from Ref. [28].

Almost all nuclear energy systems that use TRISO fuel particles load large numbers of small particles into larger fuel assembly forms; spherical pebbles and prismatic blocks, shown in Figure 1.6 and Figure 1.7 respectively, are the two predominant final fuel forms. Reference [11] provides a fairly extensive review of the historical database of irradiation experiments that have been performed using TRISO fuel particles of various designs. Understanding the full implications, limitations, and status of these experiments presents a significant challenge. Figure 1.8 and Figure 1.9 attempt to summarize and synthesize some of this information by displaying it visually rather than in tabular form.

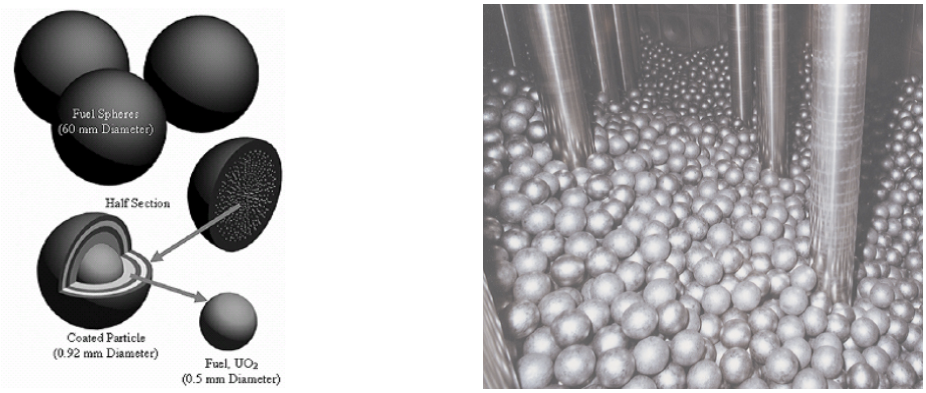

(a) (b)

Figure 1.6: Pictures of (a) TRISO particles packing into a graphite pebble, and (b) graphite fuel pebbles packed into a reactor bed with control devices going through the bed.

(a) (b) (c)

Figure 1.7: Pictures of (a) TRISO particles, (b) a fuel compact with TRISO particles packed into a graphite matrix, and (c) the final prismatic block loaded with fuel compacts.

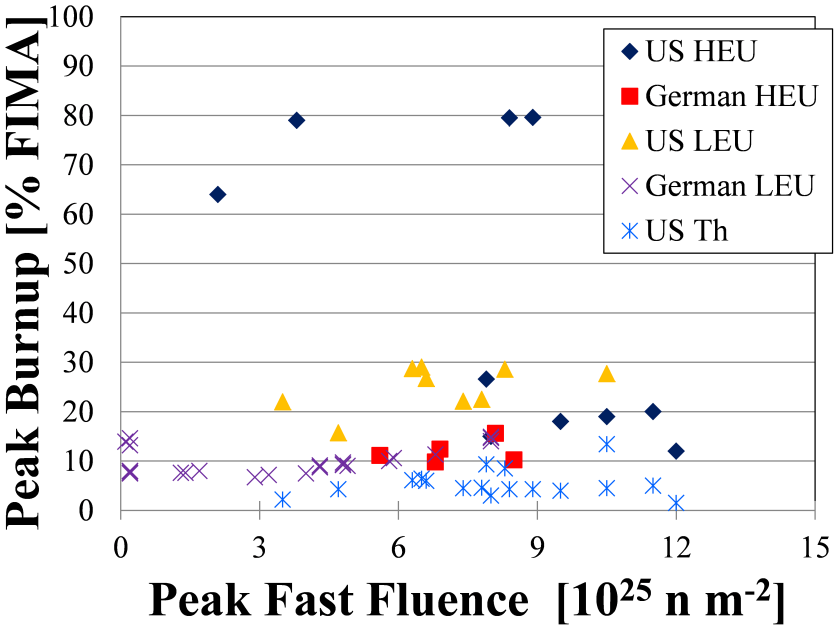

Figure 1.8: A scatter plot of the peak burnup and neutron fast fluence observed in various TRISO irradiation experiments, using source data from Reference [11].

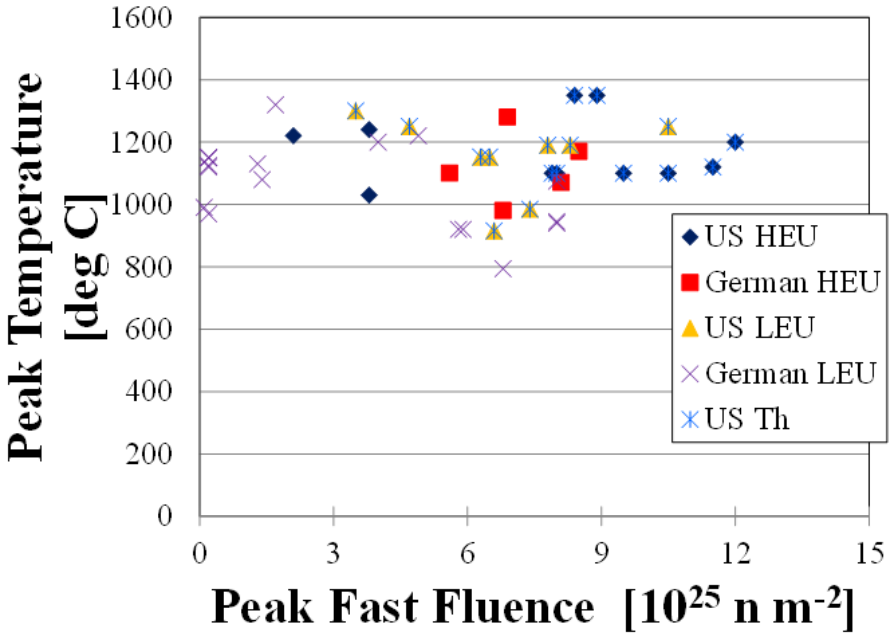

Figure 1.9: A scatter plot of the peak temperature and neutron fast fluence observed in various TRISO irradiation experiments, using source data from Reference [11].

It should be noted that the majority of the HEU data points in the figures above were from experiments where fissile fuel was being used to drive fertile fuel (e.g., thorium). Similarly, it appears that all of the thorium data in the figures above came from experiments that used fissile fuel to drive the fertile fuel; none of the experiments used just thorium by itself. It is also worth noting that while design applications may examine high burnup and high fluence use of TRISO fuel, the existing experimental data lacks any data for fertile fuels with burnup levels above about 15% FIMA or fast fluence levels above roughly 10^{26} n-m^{-2}; in addition, the experimental data available in the literature has other factors buried in it, such as different manufacturing techniques that have been used over time, that complicate matters when interpreting and applying the data [29].

1.1.2 TRISO Fuel Performance Modeling

Numerous TRISO fuel performance models (FPMs) have been developed over the years. Different organizations and projects generally each created their own model due to the unavailability of other models, and/or the developers desire to either customize the code to their specific needs or to address improvements in knowledge. Most TRISO FPMs involved projects using uranium dioxide fuel kernels. Furthermore, most of these fuel kernels were stoichiometric (e.g., UO_2) rather than hypostoichiometric (e.g., $UO_{1.7}$).

The existing FPMs can be categorized in various ways. One method divides them into models that use closed-form analytical solutions for the stress-strain-displacement

relationships and those that use numerical approaches, such as finite element analysis or methods (FEA or FEM). The various techniques used for heat transfer solutions, internal gas generation, and pressure calculations can greatly affect the predicted results; however, such differences generally do not represent as fundamental a difference in solution technique and code capabilities as selecting between closed-form or numerical methods for solving the stress-strain-displacement equations.

The dominant approach to calculating the stresses, strains, and displacements necessary in a TRISO FPM to predict fuel performance has been a closed-form analytical solution developed at INL [19, 30, 31]. This approach reduces the problem to a 1D symmetric sphere and then solves the system of equations from the center of the fuel kernel radially outward to the OPyC/matrix interface boundary. This is a simplification in that it ignores asphericity, temperature gradients across a TRISO particle, and other factors; however, it enables the model to calculate failure fractions for large sets of simulated TRISO particles within reasonable time frames. Greg Miller at INL laid the groundwork for such a closed-form solution [30], which was then utilized by many organizations and projects throughout the world. Subsequent research observed that assuming a constant Poisson's ratio of 0.5 for PyC during irradiation was likely inaccurate, so Miller generalized the solution to allow for time-dependent values [31]. This updated method, which serves as the basis for much of the current work in TRISO FPMs using closed-form solution approaches, is described in further detail in Boer's doctoral thesis [32]. Boer also includes matrix notation formulation of Miller's technique. A closed-form solution is limited to 1D effects and thus can only predict pressure vessel failure; 3D effects such as cracking or debonding must be accounted for in other ways, as will be discussed later when describing the PARFUME code.

Using numerical methods to solve the full 3D stress-strain-displacement equations for a TRISO particle has been demonstrated as an alternate approach to avoid the simplifications involving a closed-form solution. The ATLAS code developed by the Commissariat l'nergie Atomique (CEA) in France uses finite element analysis (FEA) to reach numerical solutions. Comparisons of ATLAS and PARFUME results show reasonable agreement [19].

The PARFUME code [19, 25, 33, 34, 35] developed at INL stands out as the state of the art TRISO FPM in the United States. PARFUME uses Miller's closed-form solution approach but incorporates multi-dimensional effects by using multidimensional ABAQUS calculations to aid the 1D model. As described more fully in Reference [19], a suite of ABAQUS calculations account for 3D effects such as shrinkage cracks in the IPyC or particle asphericity; these effects feed back into the overall fuel performance predictions by using correlations derived to show the impact on 1D symmetric particle calculations. PARFUME accounts for almost all of the known behavior and failure mechanisms in TRISO particles and allows the user to specify the stress boundary condition to model external stresses on a TRISO particle. Recent development efforts in the PARFUME code have involved modeling fission production transport across each layer.

TIMCOAT [28, 36] and PASTA [32, 37, 38] are extremely similar to PARFUME, since both were based upon the PARFUME code itself. TIMCOAT, developed at MIT, provides a particle/element model for pebble bed or prismatic block geometries and includes pebble

refueling effects such as temperature swings [28, 36, 39]. The PASTA code, developed by Boer during his doctoral thesis at TU Delft in The Netherlands, provides 1D stress analysis for TRISO fuels. It models the kernel and buffer as a single effective region and accounts for stresses due to particle-particle and particle-matrix interactions as well as the contributions of helium gas to internal gas pressure in the TRISO.

CEA's ATLAS code [19, 39, 40] represents the leading FPM using numerical 3D solutions. ATLAS provides a particle/element model that incorporates larger scale effects at the element level, explicitly represents and accounts for PyC and SiC layers, takes a thermomechanical approach to fuel performance modeling by tracking pressure and deformation effects, and uses an external stress boundary condition to model particle-matrix interaction effects [39]. As described above, an FEA numerical solver approach to fuel performance modeling explicitly accounts for 3D effects in the TRISO. ATLAS accounts for most of the known behavior and failure mechanisms of TRISO fuel, including pressure vessel failure of the SiC layer, IPyC cracking, debonding, and asphericity. One unique feature of ATLAS is that its fission gas release calculations explicitly account for changes to the microstructure of the fuel kernel at burnup levels above 10% FIMA.

STRESS3 [41], a U.K. TRISO FPM, focuses on stresses in the coating layers. It accounts for fission product and CO_2 gases, kernel swelling, residual stresses introduced by kernel sintering during fabrication, mismatches in coefficients of thermal expansion, dimensional changes due to irradiation, and particle-matrix surface effects [39]. STRESS3 addresses pressure vessel, IPyC cracking, and debonding failure mechanisms and uses an internal void volume that changes during irradiation.

Models built by FZJ in Germany [39] and JAERI in Japan [39, 42] both offer pressure vessel failure only models; the FZJ model only accounts for the SiC layer, while JAERI's model incorporates PyC shrinkage/swelling and independent failures for each PyC and SiC layer. The FZJ model is similar to the jointly-developed GA/KFA model [43], which offers a simple pressure vessel failure prediction without accounting for effects from the PyC layers. The GA/KFA model accounts for a shrinking void volume during irradiation while the JAERI model assumes a fixed void volume that does not change.

The HEISHI code [44] developed by Young at SNL used 1D finite difference calculations to estimate pressure vessel failure probabilities for pebble bed space reactors.

The HUPCCO model [45], developed at LLNL, uses a thermo-mechanical stress model with specific consideration given to extending or reformulating material property correlations so that they provide stable and reasonable results at the high neutron fluence levels likely to be achieved during operation of a fusion-fission hybrid system. The current version of HUPCCO exists as a stress analysis tool only; it does not provide any functionality for predicting failure fractions for populations of TRISO particles.

Table 1.2 summarizes key modeling approaches, capabilities, and other important information for these TRISO FPMs as found in the available literature; specific aspects of FPMs that are unknown or unclear are marked accordingly and details indicated by a source but with some ambiguity have a question mark after the item. It should be noted that the above descriptions of each code provide additional information that may not be captured

in the table. Furthermore, some of the terms used in this summary table may be defined in the Nomenclature section of this document or later descriptions of TRISO behavior and failure mechanisms (Section 2.1). Given the difficulty of collecting this data, some errors or inaccuracies may exist in the table; readers should consider examining the original source documents and contacting the model's development team to double-check any crucial details.

Table 1.2: Summary of several major TRISO fuel performance models.

Code	PARFUME	PASTA	ATLAS	Stress3	HUPCCO	GA/KFA
Developer	INL (US)	TU Delft (NL)	CEA (FR)	BNFL/NS (UK)	LLNL (US)	GA/KFA (US)/(DE)
Pressure Calc	R-K EOS	R-K EOS	R-K EOS	*unknown*	external calculation	R-K EOS
CO Production Method	HSC-based yield	Custom (Nabielek?)	*unknown*	Martin	external calculation	None, LEU, HEU
HT calc	1D finite difference with buffer-IPyC gap	THERMIX calculation with buffer-IPyC gap	Finite Element	*unknown*	external calculation	Single irr. temp used
Behaviors						
Pressure	Yes	Yes	Yes	Yes	Yes	Yes
PyC IIDC	Yes	Yes	Yes	Yes	Yes	Yes
PyC irr. creep	Yes	Yes	Yes	Yes	Yes	Yes
Thermal Expansion	Yes	Yes	*unknown*	*unknown*	Yes	*unknown*
FP Swelling	Solid FP	*unknown*	Solid+Gas FP	Solid FP	No	Solid FP
Failure Mechanisms						
Pressure Vessel	Yes	Yes	Yes	Yes	No	Yes
IPyC Cracking	Yes	*unclear*	Yes	Yes	No	No
Debonding	Yes	No	Yes	Yes	No	No
Asphericity	Yes	No	Yes	No	No	No
SiC thinning	Yes	No	No	No	No	No
Kernel migration	Yes	No	No	No	No	No
PyC Shrinkage	CEGA	FZJ	*unknown*	Custom	Custom	*unclear*
PyC Irr. Creep Coefficient [MPa*n*m^{-2}]$^{-1}$	User specified. Suggested: c=4x10^{-29} ν=0.4	3x10^{-29}	*unknown*	4.9x10^{-29}	3x10^{-29}	2x10^{-29}
Fission Gas Release Model(s)	Recoil + Booth	Modified Booth (cyclic situation)	*unknown*	*unknown*	external calculation	Booth
Displacement Calculations?	Yes	Yes	Yes	Yes	Yes	No

While these models provide a foundation for building upon, numerous challenges remain in TRISO fuel performance modeling including adequate benchmarks that reach the higher burnup levels proposed by projects such as Deep Burn [46], issues related to fundamental material properties and the phenomena exhibited by irradiated TRISO particles, quantifying and reducing manufacturing uncertainties, and modeling multidimensional effects.

While some data exists for TRISO fuel at high burnup levels [11, 29], the results vary significantly and have large uncertainties due to questions about the manufacturing processes used [24, 29]. Thus, little or no data exists with which to benchmark TRISO fuel performance models up to the burnup levels (50% FIMA or even higher) needed to support system designs targeting high burnup for actinide transmutation and/or efficient resource utilization.

Uncertainties and unknowns in fundamental material properties are also abundant, especially with regard to their functional dependence on temperature, fast fluence, and burnup. The response of SiC is understood fairly well for most properties up to radiation damage levels of about 10–30 displacements per atom (dpa), but the databases for dense PyC material properties need refinement and expansion. The properties of porous PyC are marginally known at best and contain large uncertainties, although these properties may be less important to the overall fuel performance assessment. Fuel properties may be the least well known due to the rapid nature in which fuel designs evolve (e.g., changing the fuel material from UO_2 to UCO or even TRU fuel kernels). Substantial work is required to improve the collective understanding of these materials in order to ensure high accuracy in fuel performance models, as investigated and detailed in Section 5.2.

Expanding models to incorporate additional phenomena offers opportunities for better agreement between computational predictions and experimental observations of irradiated TRISO fuel particles. Recent efforts at INL highlight the importance of partial and full debonding between the IPyC and SiC layers and its impact on predicted TRISO fuel performance, including accurate estimates for the interfacial bond strength between the IPyC and SiC layers and possible approaches to increase this bond strength [24, 47]. The use of fracture toughness based approaches to crack formation and propagation in TRISO coating layers, as implemented by MIT's TIMCOAT model, offers a potential path to incorporating fracture mechanics into TRISO fuel performance modeling to yield higher fidelity models that should produce more accurate predictions if the associated material properties and flaw sizes and distributions are accurately known [28].

Manufacturing uncertainties, quantified as acceptable tolerances around specified dimensions and specified material properties such as density and grain orientation, further complicate TRISO fuel performance modeling. To make matters worse, relatively little is known about the precise ways in which changes in manufacturing processes (e.g., coating rates and temperatures) affect the dimensions and properties of the TRISO particles produced or their performance under irradiation [24].

Lastly, modeling multidimensional effects such as cracking in coating layers, particle asphericity due to manufacturing, kernel migration, or other factors remains a substantial challenge in TRISO fuel performance modeling. While some approaches have been identified such as using finite element calculations to inform 1D calculations as in PARFUME [19] or

using a full finite element fuel performance calculation as in ATLAS [19], this remains one of the most challenging areas which requires additional research in the computational modeling of TRISO fuel performance.

1.1.3 Hybrid LIFE Engines

Laser Inertial Fusion-based Energy (LIFE) systems use laser-driven inertial confinement fusion (ICF) to produce energy and electricity [48]. Laser beams illuminate deuterium-tritium targets at the center of a spherical chamber with a repetition rate of about 13 Hz, igniting (D,T) fusion events that each produce 17.6 MeV of total energy including a 14.1 MeV neutron. Design options include pure fusion systems that directly harvest energy from the fusion events as well as hybrid fusion-fission systems that use high-energy fusion neutrons to drive a subcritical fission blanket wrapped around the chamber. Initial studies established a baseline design using depleted uranium (DU) as a fission blanket fuel [49, 50]. Subsequent studies further examined possibilities for hybrid LIFE engines [51, 52, 53, 54, 55]. These studies provided more detailed information in some cases than the summarized information below; however, some design assumptions and decisions have been changed for this current work compared to past studies, as will be explained later.

The National Ignition Facility (NIF) at LLNL should soon demonstrate the scientific feasibility of laser ICF ignition [56], a process illustrated in Figure 1.10.

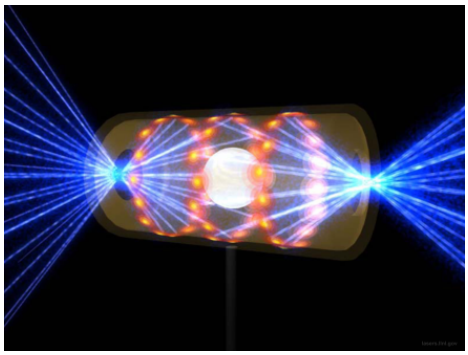

Figure 1.10: Illustration of a NIF fusion target holhraum illuminated by multiple lasers.

The LIFE concept builds upon NIF and provides a transition from demonstrating the scientific feasibility of ICF to developing commercial inertial fusion energy (IFE) systems. Possible reasons to pursue the development of hybrid fusion-fission LIFE engines include fission safety benefits from having a source-driven subcritical system, the ability to run a fission fuel cycle with no enrichment or reprocessing, and using the power gains of the fission blanket to achieve an economically attractive stepping stone technology that provides operational experience with fusion power plants before advances in driver technologies and target designs enable reasonable pure fusion plants.

Fusion (14.1 MeV) neutrons are born at the center of the LIFE engine, travel through a neutron multiplier layer, and then proceed into the fission blanket. The laser driver assumed in our current analyses provides NIF-like illumination and the target undergoes NIF-like indirectly-driven hot-spot ignition [48]. The fission blanket contains TRISO particles packed in graphite pebbles and flibe ($2\ LiF + BeF_2$) molten salt coolant [10, 57]. This work examines LIFE engine designs with 500 MW_{th} of fusion power and a total system power of about 2000 MW_{th}, and requires each LIFE engine to be tritium self-sufficient (i.e., each engine must breed enough tritium to fuel its fusion plant). While updated thermal-mechanical designs using modular construction design principles and non-spherical components exist, this work continues to utilize the original hybrid LIFE model of a set of concentric spherical shells separated structural walls shown in Figure 1.11 due to its simplicity and the fact that more recent designs have often very nearly approximated a set of concentric spheres. Figure 1.12 shows more recent models of possible designs for a LIFE chamber and plant, though the specific chamber pictured was designed for a cylindrical geometry rather than an approximately spherical geometry.

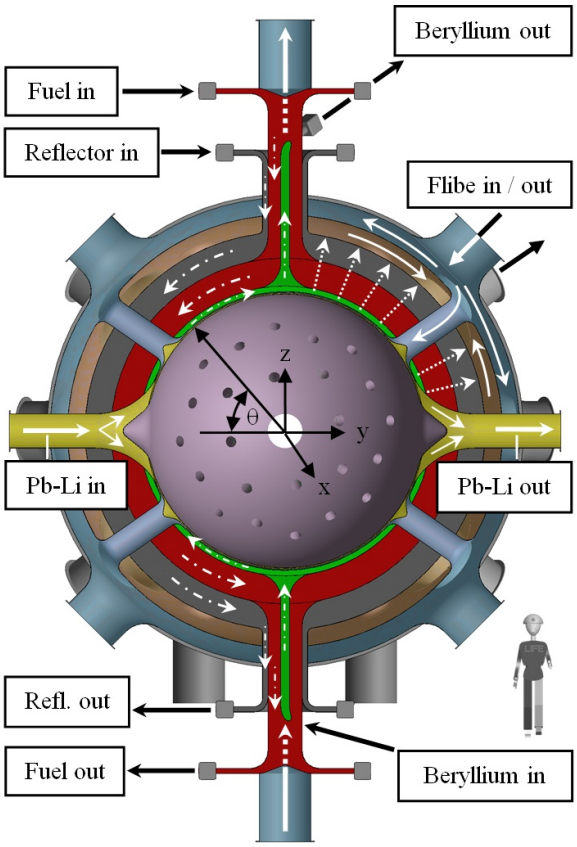

Figure 1.11: Cross-section view of a simple spherical geometry hybrid LIFE engine showing internal structures, coolant flows, and pebble flows [50].

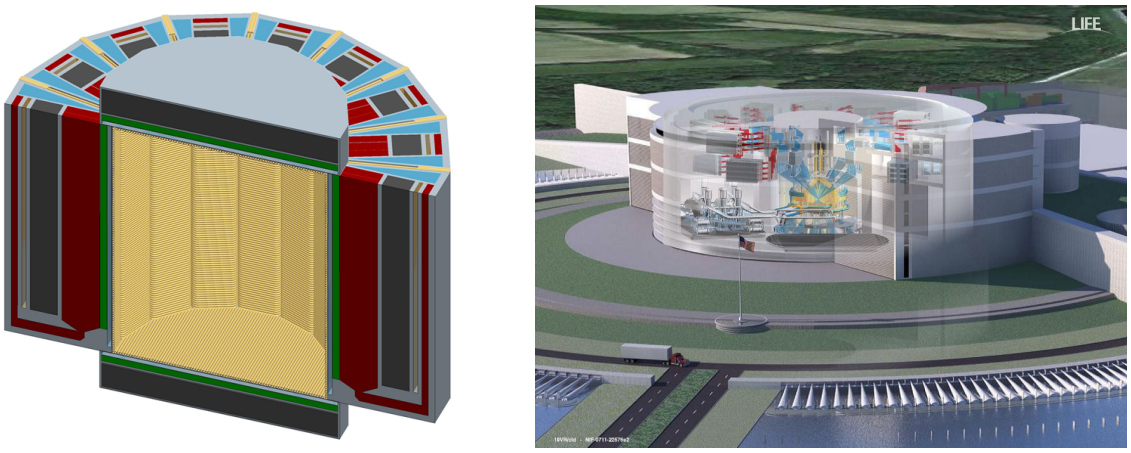

(a) (b)

Figure 1.12: Notional design possibilities for a LIFE (a) chamber design and (b) plant layout.

The inner sphere of the system serves as a fusion chamber; hohlraum targets are injected into this chamber and ignited at its center while the rest of the chamber is filled with xenon gas, or some other gas mixture if a more attractive option like a xenon-argon mixture is identified, to protect the chamber wall from ions and x-rays emitted from the fusion target. The fusion chamber wall (commonly referred to as the "first wall") consists of an oxide-dispersion strengthened (ODS) ferritic steel (this current work assumes the use of 12YWT) with a 250μm tungsten armor on the front of it facing the inside of the fusion chamber. A layer of lithium-lead surrounds the first wall and serves as a dedicated first wall coolant. These components are surrounded by a fission system. Its first layer consists of a flibe coolant injection plenum; from here, coolant flows radially outward through a neutron multiplication region loaded with beryllium pebbles, the fuel and reflector regions of the fission blanket loaded with fueled and unfueled graphite pebbles respectively, and then recollects in a coolant extraction plenum and leaves the LIFE engine. The pebble regions (neutron multiplier, fuel, and reflector regions) all consist of packed beds with 60% of their volume occupied by pebbles and the remaining 40% of their volume occupied by coolant. ODS steel structural walls separate each spherical shell of the chamber; use of a perforated wall is assumed wherever flibe flows through radially [50]. Further details, including dimensions of the radial build of the chamber and other information, are provided later in Section 3.1.2.

Figure 1.13 and Figure 1.14 show representative plots of total system power in a LIFE engine as a function of time and fuel burnup level, respectively. These curves, which were generated using an initial fuel load of 40 metric tons (MT), have previously been reported elsewhere but still provide a worthwhile example of the operation and evolution of a hybrid LIFE engine [54].

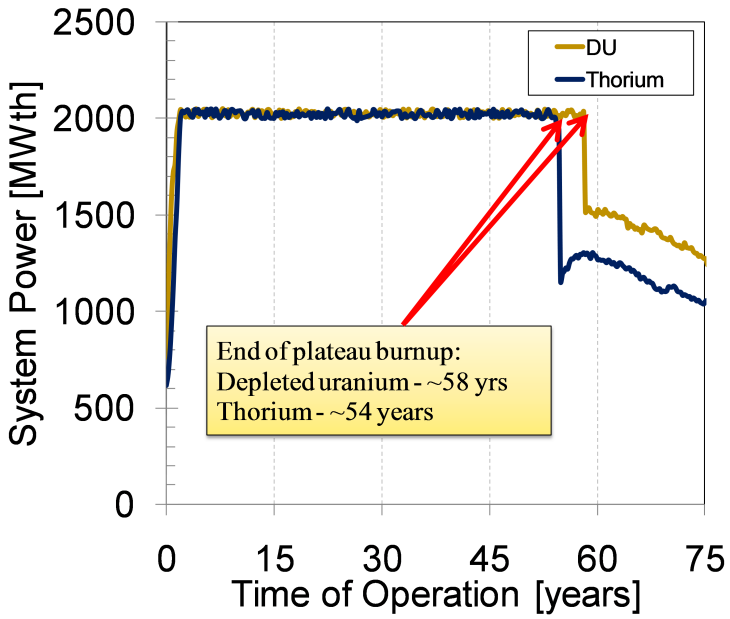

Figure 1.13: System power as a function of time for DU and Thorium hybrid LIFE engine designs with an initial fuel loading of 40MT.

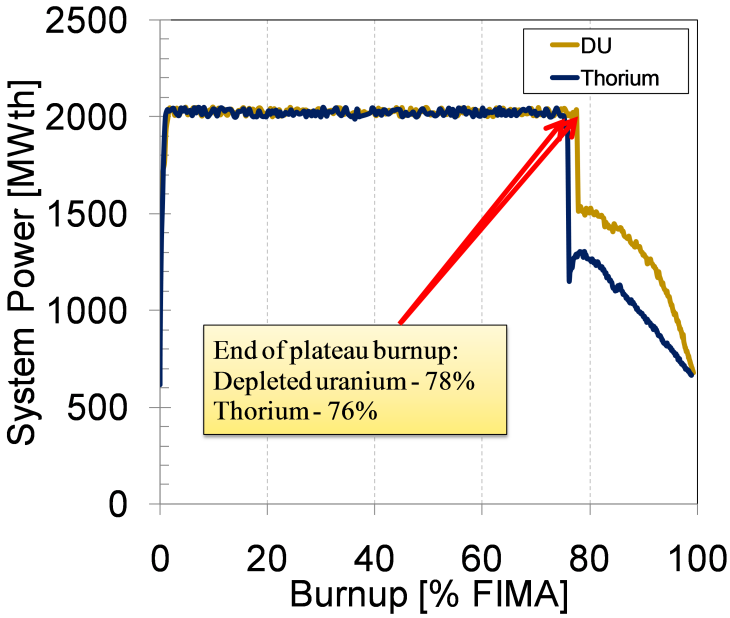

Figure 1.14: System power as a function of batch-averaged burnup value for DU and Thorium hybrid LIFE engine designs with an initial fuel loading of 40MT.

It is important to note that with the exception of a weapons-grade plutonium burning LIFE design [45], all previous hybrid LIFE design studies that utilized TRISO fuel particles assumed that either fuel failure would not be a limiting criterion or it would be a factor to be analyzed at some point in the future [54, 57]. This current work focuses on a thorium-fueled LIFE fission blanket as a relevant demonstration of the importance and impact of not only considering possible fuel failure but integrating TRISO fuel performance models into the design analysis process to help guide design optimization efforts. Early work on thorium LIFE engines looked at 40 metric ton fuel loads and provided a basic neutronics analysis and comparison to depleted uranium designs [54]; this work expands that by looking at smaller systems and provides both more detailed neutronics analysis as well as full fuel performance analysis.

1.2 Scope of Study

This study focuses on creating a new TRISO fuel performance model and demonstrating the integration of this model into an existing system of neutronics and heat transfer codes, offering a user-friendly option for obtaining fuel performance predictions to inform a broad range of calculations including design optimization and system-level trade-off studies. The end product enables both a deeper understanding and better overall system performance of nuclear energy systems limited or greatly impacted by TRISO fuel performance, which covers a broad range of systems being considered worldwide. A thorium-fueled fusion-fission LIFE blanket design provides a worthwhile application of this new capability and demonstrates both the importance of integrating fuel performance calculations into mainstream design studies and the impact that this new integrated analysis has on system-level design decisions.

The work involved in this study is loosely divided into four main areas. The first major effort involved the development, then verification and validation, of a new TRISO fuel performance model. This new model was developed entirely in MATLAB for the time being, due to convenient features of MATLAB that make it a good software prototyping platform and excellent engineering analysis tools such as easy data input and output along with robust visualization tools. While much of the underlying foundation of this new model was already available in the literature, some modifications and extensions were needed and numerous gaps in the development process were not covered anywhere in the literature. This model development effort resulted in approximately 5000 lines of MATLAB code for the final version of the model plus about 1000 lines more of code just to handle the specific intricacies of the benchmark suite used for verification and validation. The second major work effort involved integrating this new TRISO FPM into an existing package of neutronics and heat transfer codes, which necessitated creating and editing numerous Python scripts to parse data from output files on the Livermore Computing Center (LC) clusters as well as modifying the existing neutronics and heat transfer models to add new capabilities needed to support fuel performance analysis. This stage of work established the process to combine user-specified input with output data from the neutronics depletion runs to generate temperature

distributions using a heat transfer code and, then pull in these temperature distributions along with all of the necessary neutronics results to predict the expected performance of TRISO fuel particles during the irradiation history and conditions simulated in the neutronics calculations. Completing this integrated system of codes enabled the third major work effort, which involved performing Monte Carlo neutronics depletion simulations and subsequent self-consistent heat transfer and fuel performance calculations for each of a number of different combinations of design parameters. Performing this set of integrated and self-consistent neutronics, heat transfer, and fuel performance calculations for a full parametric study represents a new and novel capability of a type that has not been documented in the available literature. In addition, the fuel performance calculations use a novel technique to simulate a real lifetime history for a TRISO particle that does not appear to have been done anywhere else in the literature. The fourth stage of work consists of a number of side studies, which include comparing the predicted fuel performance from a depleted uranium LIFE blanket to the thorium LIFE blanket as well as a sensitivity study looking at the impact of material property correlation uncertainties on expected fuel performance for the recommended system design chosen from the thorium parametric study; this material property sensitivity study will help guide future experimental work by highlighting which important properties need additional measurements and allowing effective use of the finite amount of research funding allocated to such new experimental work. This guidance to future experimental work holds the promise of being one of the key items to come from this work.

This manuscript is organized into six chapters. This first chapter, Chapter 1, demonstrates the motivation and need for the work performed during this study and introduces background material on TRISO fuel particles and hybrid fusion-fission LIFE systems. Furthermore, it provides critical information setting the overall objectives and scope of the study. Chapter 2 describes the development of the TRIUNE fuel performance model, including all of the underlying TRISO particle behavior and failure mechanisms entailed as well as the formulation of the model itself and verification and validation efforts that were performed to ensure accurate results that adequately address the right issues. Chapter 3 explains the neutronics codes, methods, and assumptions used to perform neutronics depletions as well as the heat transfer code used and all of the methods needed to integrate the fuel performance model into this code package. The design variables, performance metrics, and results of the thorium-fueled LIFE engine design study application are shown in Chapter 4. Results from all side studies are documented in Chapter 5. The main portion of the manuscript concludes in Chapter 6 by discussing and analyzing the results, detailing recommendations and possible future work that surfaced during this work, and drawing conclusions where possible to demonstrate the fulfillment of all goals.

Chapter 2

Development of the TRIUNE FPM

This chapter documents the development of a new TRISO fuel performance model named TRIUNE (TRIso fUel in a Neutron Environment) and summarizes its subsequent verification and validation. The TRIUNE model makes use of many of the same approaches and material property correlations as the PARFUME model developed at INL [25]; the key features that set it apart are an overall code structure that allows it to flexibly meet emergent desires and needs that arise for the user while also integrating easily with existing neutronics depletion and heat transfer codes to provide integrated self-consistent neutronics and fuel performance analyses for a system in an expedient manner. In addition, design calculations for TRIUNE utilize updated and/or different material property correlations that enable reliable calculations at higher fast neutron fluence levels than PARFUME allows and that leverage recent advances in the understanding of TRISO fuel particles and associated material properties. TRIUNE is a one-dimensional (1D) thermomechanical model that uses a quasi-steady-state approach to handling time dependence.

2.1 TRISO Particle Behavior and Failure Mechanisms

Accurate fuel performance modeling for TRISO fuel particles requires a detailed and thorough understanding of their behavior and failure mechanisms. Several previous works have reviewed and summarized the overall state of the knowledge and modeling of TRISO fuel particle behavior and failure mechanisms, and Sections 1.1.1 and 1.1.2 provide brief summaries of these areas [10, 11, 19, 39]. This section contains a description of TRISO behavior and failure mechanisms that is by no means comparatively exhaustive but is considered sufficient for understanding the overall development and functionality of the TRIUNE model.

Particle behavior

A multitude of phenomena observed in TRISO fuel particles undergoing irradiation and fission have been identified as important aspects to understand and accurately model. In

particular, we will review the mechanisms of heat transfer, fission product production and transport, oxygen release from the fuel kernel, internal gas pressure buildup, irradiation effects on TRISO materials, and variability in TRISO particles due to manufacturing processes.

Heat transfer directly impacts any nuclear fuel due to the importance of conducting the heat generated by fission events out to the working coolant in the system. The resulting temperature distributions and gradients affect many other phenomena and material properties.

The simultaneous production, destruction (through radioactive decay or nuclear reactions with neutrons or gamma rays), and transport of fission products (FPs) represents another key behavior in TRISO fuel. Gaseous FPs, with Xe and Kr typically considered the dominant species, build up in the kernel and buffer of the particle and exert pressure on the PyC and SiC coatings. Some FPs migrate out of the kernel and can escape through the PyC and SiC layers to become radiological source terms in the matrix and coolant, impacting plant operational safety.

Oxygen atoms released from the fuel kernel to the buffer region, due to both thermal solubility and fission events consuming the heavy metal atoms in the kernel, can lead to the formation of CO or CO_2 gas via the reactions

$$O_2 + C = 2\ CO \tag{2.1}$$

and

$$2\ CO = CO_2 + C \tag{2.2}$$

and increase the internal pressure of the particle. The partial pressures or CO, CO_2, and O_2 are thermodynamically controlled and also impacted by the composition of the fuel.

Fission product, CO, and CO_2 gases accumulate in the buffer void volume and exert outward pressure on the coating layers. This internal gas pressure builds up over time and has traditionally been the dominant behavior suspected of causing TRISO fuel particle failures.

PyC initially shrinks, and then later swells, when irradiated with fast neutrons (defined in this manuscript as neutrons with energies above 0.18 MeV). The seminal 1993 Combustion Engineering-General Atomics (CEGA) report [58] defined this as Irradiation-Induced Dimensional Change (IIDC) and provided a reasonable description of the process. More detailed descriptions exist elsewhere [59, 60]. SiC undergoes a similar irradiation-induced volumetric change, though most FPMs ignore this because it is generally believed to be negligible compared to other degradation behavior in PyC and SiC [19]. Explicit investigation found SiC irradiation swelling to be a very minor factor in TRISO stress states [45].

Stresses and strains in the coating layers result from the phenomena described above, with additional contributions from irradiation creep and the differential thermal expansion of

each region. Displacements of the layer interfaces occur due to these strains and solid fission product swelling in the fuel kernel. These stress-strain-displacement relationships must be well understood for reliable TRISO fuel design and performance since they directly impact the maximum stress predicted in the SiC pressure boundary. A viscoelastic model is often used for the IPyC-SiC-OPyC system [31], with the SiC layer treated as an isotropic elastic material since SiC is a ceramic and thus undergoes very little (if any) plastic deformation before failure.

The material properties (e.g., thermal conductivity and Young's modulus) of each layer vary during operation. The properties should vary with temperature, porosity, accumulated fast fluence, and fuel burnup level. While fully accurate materials property calculations would incorporate all of these parameters and yield precise knowledge, the material property correlations currently available fall significantly short of this. The best known correlations should be used for each property in fuel models, with flexibility designed into the models to allow future revisions.

Lastly, the dimensions and densities of each layer of a TRISO particle vary from particle to particle due to variability in the manufacturing processes. The expected manufacturing tolerances for a TRISO particle of a particular design using specific manufacturing methods and processes can be identified and accounted for in fuel models. The calculated failure fraction of a set of "real" particles based upon nominal parameters and their manufacturing tolerances determines the predicted performance of the fuel; if it is too high then the fuel design or reactor design must be changed or, alternatively, the manufacturing tolerances can be tightened.

Failure mechanisms

Fuel performance modeling for any fuel form directly depends upon identifying the possible failure modes for the fuel and which modes are limiting. Once the limiting failure modes are known, computational models can be constructed to assess how the fuel behaves relative to these criteria. For example, if a fuel is limited by creep rupture then creep rate calculations determine fuel performance. Likewise, detailed stress calculations are necessary to model and assess performance of a fuel limited by through-clad cracking due to stresses. TRISO fuel particles have been experimentally observed to possess multiple possible failure modes, which are categorized as being driven by either 1-dimensional (1D) or 3-dimensional (3D) effects [19, 29].

The dominant 1D failure mechanism for TRISO fuel particles involves pressure vessel failure, where the SiC layer develops a through-thickness crack resulting from a tensile stress that exceeds the fracture strength of the material. This fracture stress for SiC varies significantly in the literature, with relevant recent estimates ranging from 330–650 MPa [26, 61]. The classic definition for this pressure vessel failure assumes that the SiC layer fails catastrophically once a crack initiates and that there is enough energy in the system released upon SiC cracking that the PyC layers crack as well. Other approaches to pressure vessel failure explicitly calculate separate through-layer crack probabilities for the SiC layer and

each PyC layer; models using this approach require that all three layers must fail for the particle to be considered "failed". The tangential stress at the IPyC/SiC interface usually represents the limiting stress in the SiC layer and depends upon multiple phenomena, as illustrated in Figure 2.1. More rigorous fracture mechanics approaches have generally not been undertaken in TRISO fuel performance modeling, though MIT's TIMCOAT code has pursued this fracture mechanics approach [28].

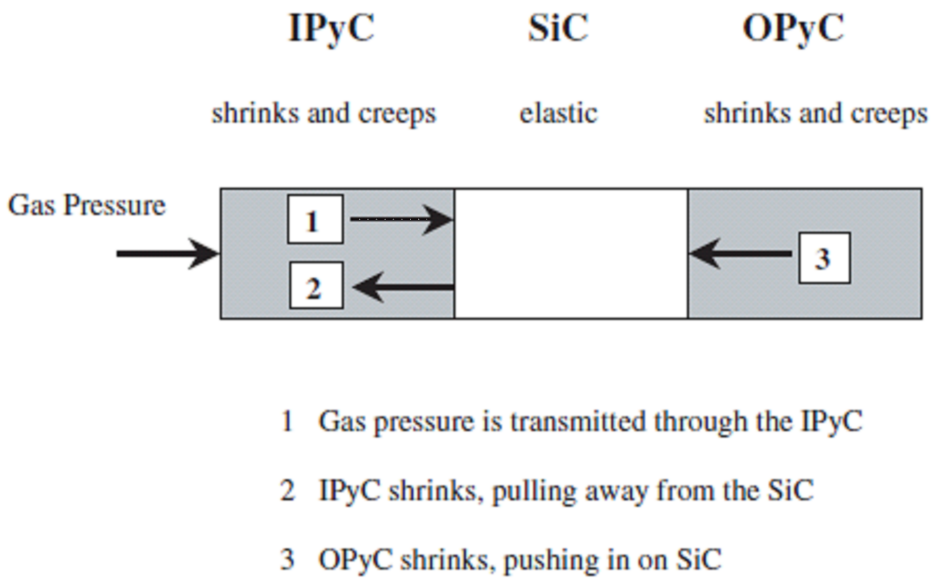

Figure 2.1: Illustration of the different fuel behaviors driving SiC stress, as reproduced from Ref. [19].

Both PyC layers initially experience irradiation-induced radial shrinkage; during this phase, the outward stress due to gas pressure is counteracted by an inward stress from PyC shrinkage. However, after an initial densification stage, PyC begins exhibiting irradiation-induced swelling. This produces a situation where internal gas pressure and PyC swelling both act outward on the coating layers. Thus, the maximum tangential stress in the SiC layer has a beginning of life (BOL) stress level determined by manufacturing and system stresses (usually assumed to be 0 MPa), decreases to a maximum compressive stress (nominally on the order of 100 MPa at a fast fluence of roughly 0.5×10^{25} [n-m^{-2}]), and then increases until end of life (EOL). Usually the stress becomes tensile (positive) before EOL, and may lead to failure of the SiC. Figure 2.2 shows micrographs of an intact TRISO particle and a TRISO particle that experienced catastrophic pressure vessel failure.

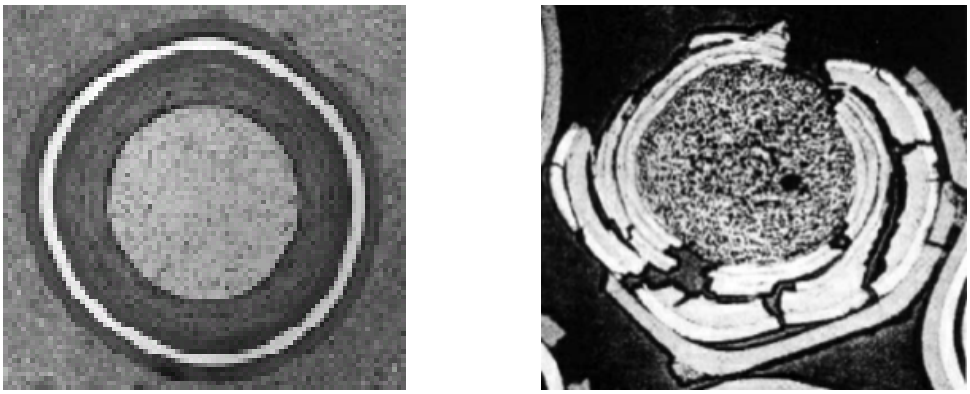

(a) (b)

Figure 2.2: Micrographs showing (a) an intact TRISO particle [19], and (b) a TRISO particle that has undergone catastrophic pressure vessel failure [24].

3D failure modes observed in TRISO fuel particles include shrinkage cracks within the IPyC layer, IPyC/SiC debonding, particle asphericity, kernel migration and SiC coating thinning. A brief description of each mechanism is given below, while References [19] and [29] each provide more detailed information.

Irradiation-induced shrinkage of the IPyC can cause a partial or through-coating crack to form in the IPyC [28, 62]. Partial or full debonding of the IPyC and SiC layers at their interface can occur if the differential radial stress exceeds the IPyC/SiC interfacial bond strength [47]. Particle asphericity refers to a TRISO particle's geometric deviation from a perfect sphere [19, 47]. Kernel migration, the movement of the center of mass of the fuel kernel away from the center of the TRISO particle, results from CO gas migration down the thermal gradient in a TRISO toward the cold side of the particle and subsequent formation of CO_2 and solid-phase carbon due to the combination of two CO molecules. Over time, solid carbon builds up on the cold side of the buffer and "pushes" the kernel to migrate toward the hot side of the TRISO particle, as shown in Figure 2.3(c). Each of these mechanisms lead to changes in temperature or stress distributions and may lead to particle failure.

Lastly, experimental observations indicate that chemical attack of the SiC by species such as palladium (Pd) can thin the coating. Erosion rates are low but can be appreciable for high stress environments or long irradiation times [24, 63]. Chemical attack rates have been shown to accelerate in the presence of defects such as cracks in the IPyC layer or IPyC/SiC debonding.

Figure 2.3 shows micrographs of real TRISO particles exhibiting these behaviors and failure mechanisms.

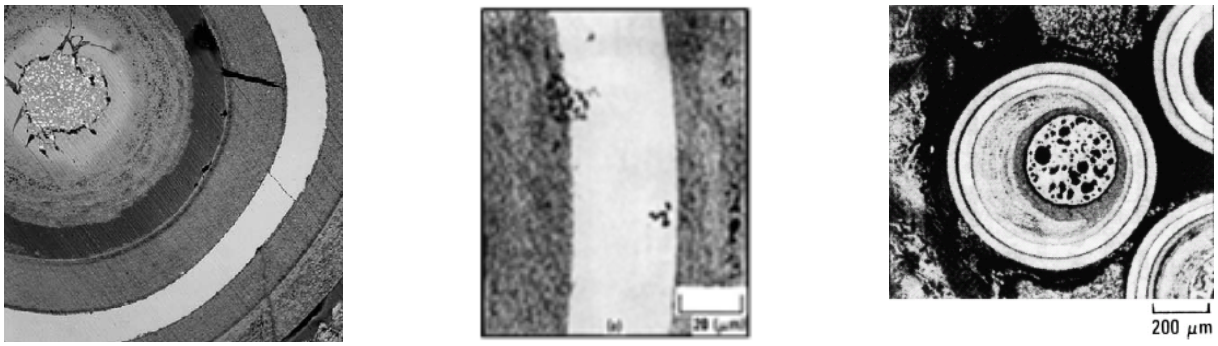

(a) (b) (c)

Figure 2.3: Micrographs showing (a) IPyC shrinkage cracking, (b) fission product attack of SiC, and (c) kernel migration in a TRISO particle, all as reproduced from Ref. [24].

It should be noted that while the above failure mechanisms represent the dominant known failure modes for TRISO fuel particles, additional failure mechanisms likely exist.

2.2 Material Properties

Several literature reviews and other articles have identified and discussed the best available correlations and values for material properties to model fuel [10, 19, 25, 64, 65], PyC [10, 19, 25, 45, 58, 66], and SiC [10, 19, 25, 26, 45, 58, 66] in TRISO FPMs. In particular, Snead [26] provides a review and handbook of SiC properties for fuel performance modeling containing especially useful information and further resources and DeMange and Marian examine the issue of recasting PyC IIDC correlations to extend them to higher neutron fast fluence levels [45]. A summary of the important findings can be found below, but the interested reader can find more details in the references cited throughout this section. It is also worth noting that there may be a PyC Handbook coming soon from ORNL reviewing experimental material property data for PyC and giving recommendations on correlations and properties to use for PyC in fuel performance modeling, similar to Snead's SiC Handbook [26]; further details on when this PyC Handbook would be released are currently unavailable to the best of this author's knowledge.

Table 2.1 summarizes the key material properties for a UO_2 fuel kernel. τ represents the fuel burnup in units of %FIMA and P is the fractional porosity of the fuel kernel. Though not included in the table below, it is important to note that the effective Booth diffusion coefficient for Xe and Kr in the fuel kernel as a function of temperature is being taken from Appendix 1 of Reference [67]. Modifications or additions to these properties would be necessary for hypostoichiometric fuel forms (e.g., $UO_{1.7}$) or non-uranium fuels (e.g., PuO_2); however, as noted elsewhere [19, 25], there is a general lack of material property correlations and experimental data for any fuel other than UO_2. Some data for ThO_2 fuel should exist

but is generally unavailable in the open literature and is likely to be far less robust than the UO_2 data. For these reasons, TRIUNE currently relies upon these largely UO_2 fuel properties for all fuel forms, even the thorium oxycarbide (ThCO) fuel assumed for the design applications in this document. This simplification represents a major challenge in TRISO fuel performance modeling not only for TRIUNE but for all of the other TRISO FPMs previously discussed as well.

Table 2.1: Summary of recommended material properties for TRISO fuel kernels.

Parameter [Units]	**Recommended Correlation or Value**	**Source and Notes**
Thermal conductivity, k[W/m-K]	$k_{fuel} = K_{1d}K_{1p}K_{2p}K_{4r}k_{0,fuel}$ $K_{1d} = \left(\frac{1.09}{\tau^{3.265}} + \frac{0.0643}{\sqrt{\tau}}\sqrt{T_{kern}}\right) \times \arctan\left(\frac{1}{\frac{1.09}{\tau^{3.265}} + \frac{0.0643}{\sqrt{\tau}}\sqrt{T_{kern}}}\right)$ $K_{1p} = 1 + \frac{0.019}{3 - 0.019\tau}\left(\frac{1}{\left(1 + \exp\left(-\frac{T_{kern} - 1200}{100}\right)\right)}\right)$ $K_{2p} = \frac{1 - P}{1 + 2P}$ $K_{4r} = 1 - \left(\frac{0.2}{1 + \exp\left(\frac{T_{kern} - 900}{80}\right)}\right)(1 - \exp(-\tau))$ for $T_{kern} < 1650$ [℃] $k_{0,fuel} = 0.0132\exp(1.88 \times 10^{-3}T_{kern}[℃]) + \frac{4040}{464 + T_{kern}[℃]}$ for $T_{kern} \geq 1650$ [℃] $k_{0,fuel} = \frac{17885}{T_{kern}[K]}$	Unirradiated $k_{0,fuel}$ from Reference [25]. Adjustments for irradiation based on UO_2 work from Reference [19]
Solid FP swelling rate, $\dot{S}_s$ [% / GWd/t_{HM}]	$\dot{S}_s = \frac{d\left(\frac{\Delta V}{V}\right)}{d\tau}$	References [19] and [60]

Recommended correlations and values for the key material properties of PyC are summarized in Table 2.2. P is the fractional porosity of the PyC layer being analyzed, Φ represents the fast neutron fluence in units of 10^{25} n-m^{-2} ($E_n > 0.18$ MeV), and BAF_0 is a measure of the as-manufactured anisotropic grain orientation (nominally 1.02–1.05 [19] and chosen to be 1.03 for LIFE fuel performance calculations). The buffer PyC is assumed to have isotropic grain orientation. The tangential (normal) and radial (parallel) directions are sometimes denoted by the subscripts 1 and 3, respectively. $M_{Irr.Creep}$ is a user-specified PyC irradiation creep constant multiplier with a value of 2.0 based upon Idaho National Laboratory (INL) recommendations [19].

Several properties in this table, such as the PyC IIDC correlation and the thermal conductivity correlation, needed to be modified from those used by PARFUME and other fuel performance models. The reworked PyC IIDC (irradiation shrinkage/swelling) correlation formulated by DeMange and Marian for use in high fluence applications has been adopted for use in TRIUNE for dense PyC layers; further details on the reasoning behind this and the methods used to formulate this new version are available in the source paper [45]. Though not employed in this model, it should be noted that the CEGA correlation for PyC IIDC is generally considered the best available correlation for lower levels of fast neutron fluence [25, 58]. The PyC thermal conductivity shown below is a reworked version of a UK correlation [19] that has been modified to yield thermal conductivities more in line with PARFUME and other recommendations while still containing a direct functional dependence on porosity in the PyC; since the magnitude of the temperature gradient across a TRISO fuel particle largely determined by the temperature drop across the buffer layer, this could have a significant impact on fuel performance calculations. Figure 2.4 compares several different correlations and data sets for PyC thermal conductivity that are recommended in the literature along with the version being used in TRIUNE. The "UK dense" and "UK buff" data comes from Reference [19], while the "PARFUME" correlation comes from Reference [25]. None of these were found to be acceptable for direct use in TRIUNE, due to the desire to have PyC thermal conductivity as a function of porosity instead of just fixed data points for dense and buffer PyC while also having values for thermal conductivity that compare reasonably against the well-known thermal conductivity data points given by the PARFUME data set. "TRIUNE1" and "TRIUNE2" show simple attempts at recasting the UK correlation by adjusting the prefactor of the correlation; these attempts kept a functional dependence and each matched up well against one of the PARFUME data points but missed the other by a considerable margin. "TRIUNE3", the correlation shown in Table 2.2, had its prefactor adjusted and also had its porosity factor adjusted to get a different slope; this results in a single correlation that maintains functional dependence of PyC thermal conductivity on porosity while also matching up well to the PARFUME data points.

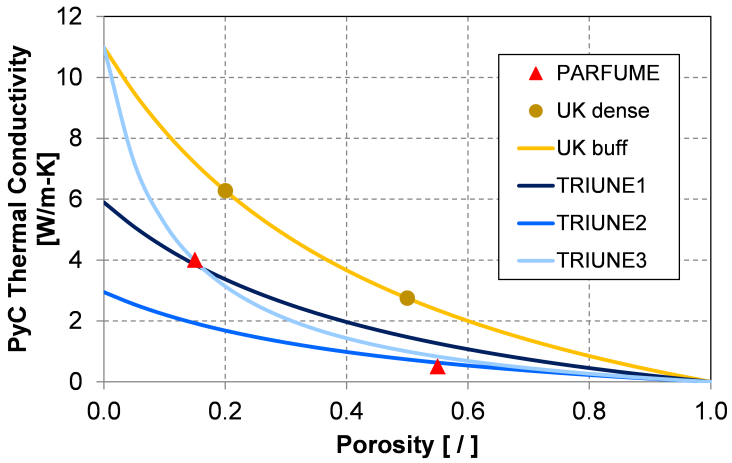

Figure 2.4: PyC Thermal Conductivity as a function of porosity for according to several different correlations and data sets [19, 25].

In addition to these new correlations for thermal conductivity and IIDC, TRIUNE allows the user to specify that the PyC anisotropy factor (BAF) should vary as a function of neutron fast fluence following the relationship established in Table 7-5 of Reference [25]. Lastly, the user can also request that the value for Poisson's ratio in PyC Irradiation Creep (ν) be set to a fixed value of either 0.4 or 0.5 or a value that is a function of fast fluence and starts at 0.5 but becomes 0.4; this fluence-dependent definition is the recommended option [25, 28].

Table 2.2: Summary of recommended material properties for buffer and dense PyC.

Parameter [Units]	**Recommended Correlation or Value**	**Source and Notes**
Thermal conductivity, k[W/m-K]	$k_{PyC} = 10.98666\dfrac{1-P}{1+9P}$	Custom reformulation (see text).
Anisotropy Parameters	$R_3 = \frac{2}{2+\mathrm{BAF}}, \quad R_1 = \frac{1-R_3}{2}, \quad R_{buff} = \frac{2}{3}$	Reference [58]
Young's Modulus, E[MPa]	*Buffer:* $E = 34500\exp(-2.03P)k_\phi k_T$ *Dense PyC:* $E_1 = E_{01}k_\rho k_{\mathrm{Lc}} k_\Phi k_T k_{\mathrm{BAF}_{01}}$ $E_3 = E_{03}k_\rho k_{\mathrm{Lc}} k_\Phi k_T k_{\mathrm{BAF}_{03}}$ E_{01}=E_{03}=25500 k_ρ=0.384+0.324ρ k_{Lc}=2.985−0.0662Lc k_Φ=1+0.23Φ k_T=1+0.00015(T[℃]−20) $k_{\mathrm{BAF}_{01}}$=0.481+0.519BAF$_0$ $k_{\mathrm{BAF}_{03}}$=1.463−0.463BAF$_0$	Reference [25]. Lc is the crystallite size; Reference [25] suggests a value of 30 Angstroms, which results in $k_{\mathrm{Lc}} = 1.0$.
Poisson's Ratio, μ [/]	*Buffer:* $\mu = 0.23$ *Dense PyC:* $\mu_{12} = 0.766R_3 - 0.275$ $\mu_{13} = -0.844R_3 + 0.825$ $\mu_{31} = \frac{\mu_{13}E_3}{E_1}$	US Correlations from Table 1-12 of [19].
Coefficient of thermal expansion, $\alpha[10^{-6}\ ℃^{-1}]$	$\alpha_r = A(-37.5R_3+30), \quad \alpha_t = A(36(R_1-1)^2+1)$ $A = 1 + 0.11\frac{(T[℃]-400)}{700}$	Reference [25].
IIDC rates, $\dot{\varepsilon}$ $[10^{25}n-m^{-2}]^{-1}$	*Buffer:* $\dot{\varepsilon}_r = \dot{\varepsilon}_t = -0.176\exp(0.175\Phi)$ *Dense PyC:* $\dot{\varepsilon}_r = 0.01 \times (-1.066 + 0.362\Phi)$ $\dot{\varepsilon}_t = 0.01 \times (-1.324 + 0.280\Phi)$	Buffer: German correlations, Reference [19]. Dense PyC: Reference [45]
Irradiation Creep Parameters, K $[10^{25}n-m^{-2}]^{-1}$ ν[/]	$\mathrm{K} = \mathrm{K}_0\,(1 + 2.38(1.9-\rho))\,\mathrm{M}_{\mathrm{Irr.Creep}}$ $\mathrm{K}_0 = 2.193\times10^{-4} - 4.85\times10^{-7}(T[℃])$ $+ 4.0147\times10^{-10}(T[℃])^2$ $\nu = 0.4 - 0.5$	Reference [25]. $\mathrm{M}_{\mathrm{Irr.Creep}}$ is a user-specified input variable.

The recommended material properties for SiC (β-CVD SiC in particular) are summarized in Table 2.3. P represents the fractional porosity and Young's modulus has units of GPa instead of MPa. More detailed information, as well as experimentally measured material property data, can be found in Snead's SiC Handbook [26] and the PARFUME documentation [25]. Though the temperature dependence is accounted for, the effects of irradiation and porosity are currently not explicitly captured in the SiC thermal conductivity correlation being used; despite this shortcoming, this correlation yields results that are considered more reasonable than the correlations suggested in Snead's SiC Handbook that yield significantly higher thermal conductivity values. If the correlations in suggested by Snead in fact turn out to be true then heat transfer through the SiC layer should improve. It should be noted that there is typically a very small temperature rise across the SiC layer in a TRISO particle, so changes to SiC thermal conductivity are expected to have minimal impacts on overall fuel performance. The user can select the Snead correlation in the current version of TRIUNE with some minimal effort but the default correlation used is the correlation listed below.

Table 2.3: Recommended material properties for SiC.

Parameter [Units]	**Recommended Correlation or Value**	**Source and Notes**
Thermal conductivity, k[W/m-K]	$k_{SiC} = \dfrac{17885}{T_SiC + 2}$	Reference [25].
Young's Modulus, E[GPa]	$E_1 = E_0 \exp(-3.57P) - 0.04\, T_{SiC} \exp\left(\dfrac{-962}{T_{SiC}}\right)$ $E_0 = 460$	Reference [26].
Coefficient of thermal expansion, α[10^{-6} ℃$^{-1}$]	*if* $T_{SiC} \leq 1273K$ $\alpha = -1.876 + 0.0178\, T_{SiC} - 1.5544 \times 10^{-5}\, T_{SiC}^2 + 4.5246 \times 10^{-9}\, T_{SiC}^3$ *if* $T_{SiC} \leq 1273K$ $\alpha = 5.0$	Reference [26].

Finally, in addition to the above material properties, TRIUNE requires PyC and SiC Weibull parameters in order to calculate predicted failure fractions within populations of TRISO particles. As described later in Section 2.3.7, the Weibull calculations performed in TRIUNE require two parameters for each material (PyC and SiC): the mean strength and the Weibull modulus. Several recommendations are available in the literature for PyC [19, 25, 58, 68] and SiC [19, 25, 26, 61, 68]. Table 2.4 summarizes the Weibull parameters currently used in TRIUNE. Section 5.2 examines some of the implications of the wide ranges in recommendations values for Weibull parameters.

Table 2.4: PyC and SiC Weibull parameters currently used in TRIUNE.

Parameter [Units]	**Recommended Correlation or Value**	**Source and Notes**
Weibull mean strength, σ_{ms} [MPa]	PyC: $\sigma_{ms} = 200$ SiC: $\sigma_{ms} = 650$	References [25] and [61].
Weibull modulus, m [MPa]	PyC: $m = 5.0$ SiC: $m = 7.25$	References [25] and [61].

2.3 Model Formulation

The formulation and structure of the TRIUNE fuel performance model is best understood by breaking it down into a summary overview of the full model followed by detailed descriptions of the various functional modules.

The TRIUNE model has been developed to both analyze the expected behavior of the various components of a TRISO particle undergoing irradiation as well as provide true fuel performance capabilities by predicting fuel failures. The user supplies input data that covers neutronics and thermal aspects of an irradiation environment and history that a TRISO particle has been or is expected to be subjected to along with some user-specified assumptions about the particle itself and some of its properties (e.g., densities and dimensions); in return, TRIUNE calculates temperature distributions and material properties that evolve during burnup and uses them to solve stress-strain-displacement equations that model the particle's behavior. The calculated stresses enable fuel performance calculations that predict the probability that the TRISO particle would fail as a function of time or burnup or fast fluence.

Similar to other FPMs, TRIUNE uses a quasi-steady-state methodology for progressing through the lifetime of a TRISO particle. Steady-state calculations performed at distinct points in time, synchronized to the neutronics depletion analysis, track the changes in properties and behaviors of the layers, layer interfaces, and materials. Between time steps (and their corresponding steady-state calculations), neutronics input parameters are updated along with particle geometry and material properties. The total number of time steps used in TRIUNE calculations varies directly with the number of time steps used in the neutronics analysis, which should have been chosen to minimize unnecessary calculations while ensuring that effects such as decay and transmutation are captured accurately. Each steady-state calculation in TRIUNE involves a series of coupled modules to perform the required tasks and handle input and output data. The material properties and fuel behavior at a given time step are assumed to remain constant since the time step represents a single moment in time with an infinitesimally small duration; in general, the time periods between the steady-state calculations are handled by averaging the properties at the neighboring time steps.

Fuel performance assessment in TRIUNE utilizes a Monte Carlo approach to predicting failure fractions for a batch of fuel particles in a given system that combines failure probabilities from calculations performed on a user-specified number of simulated "real" particles that are constructed based upon a set of manufacturing assumptions (e.g., mean dimensions and distribution functions for the fuel kernel and coating layers).

Figure 2.5 shows a schematic flow chart of the calculation process used in TRIUNE, which has been briefly outlined above and will be more finely detailed below.

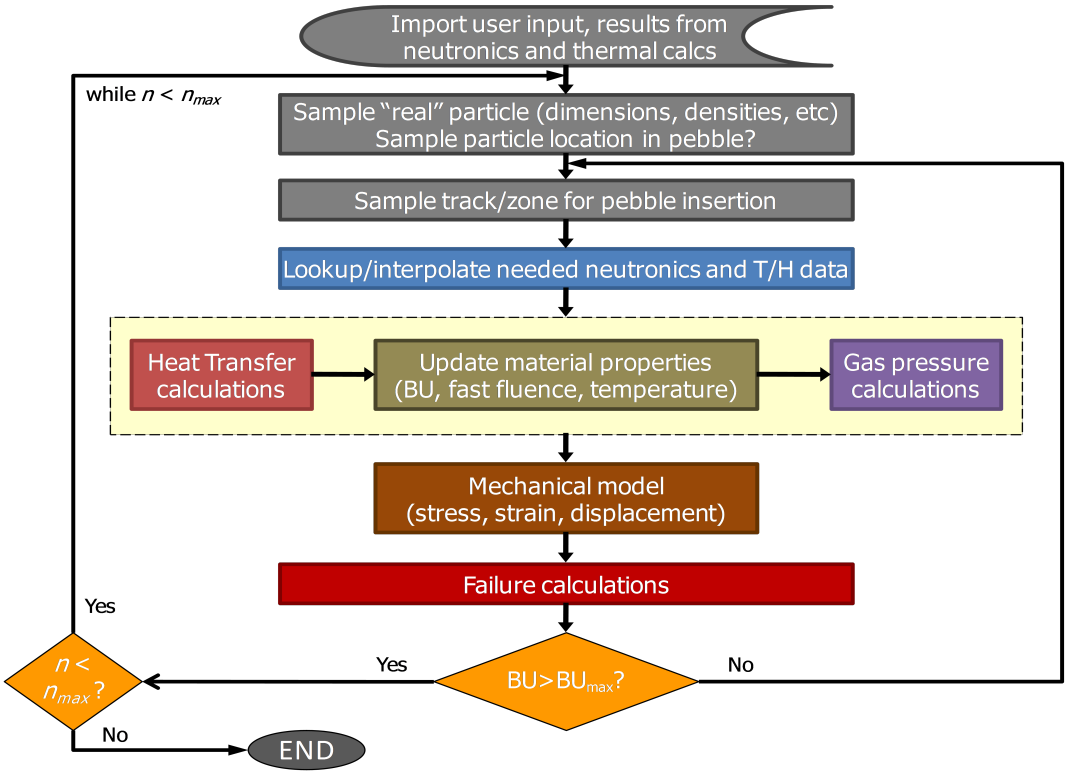

Figure 2.5: Schematic flow chart of the calculation process used in the TRIUNE model.

Subsequent subsections contain detailed descriptions of most of the major computational modules. User-specified modeling assumptions include choosing which correlation or value to use for some material properties, the desired convergence level for heat transfer calculations, gas production model options and assumptions, and fission gas release module assumptions. The geometry calculations listed involve adjusting layer thicknesses and volumes, as well as covariant properties such as porosity and density, to account for displacements of the interfaces between layers. The neutronics input consists of data vectors for numerous parameters that are inputs or outputs from the neutronics depletion analysis.

In summary, the steady-state calculation at each time step begins with reading in the appropriate neutronics and thermal inputs as well as the updated geometry parameters calculated at the end of the previous time step based upon initial values and subsequent

layer interface displacements. Heat transfer calculations, which include an iterative solver to determine the thermal conductivity of each zone, determine the layer interface temperatures and bulk material temperatures. These temperatures, along with neutronics input and updated porosities and densities, enable all of the materials properties to be calculated for the time step. Gas pressure calculations follow, including fission gas release and possible CO gas generation, yielding the total gas pressure. TRIUNE currently reads in data parsed directly from the neutronics analyses to provide the fission product (Xe and Kr) inventories at each time step rather than estimate fission gas production on its own; this ensures that any energy-dependent or isotope-dependent variations in fission product yield caused by the neutron spectrum and fuel in the system are accurately reflected in the fuel performance calculations. Void volume calculations are included in the gas pressure module. With the internal gas pressure, material properties, and temperatures all known, the stress-strain-displacement equations can be solved for that time increment. Finally, updated values for the volume, thickness, porosity, and density of each layer are calculated as input values for the next time step.

2.3.1 Neutronics and Thermal Input

The neutronics input for all of the TRIUNE calculations provided in this document came from depletion analysis performed as a part of this study. A full description of the methods and models for the neutronics depletion analysis can be found in Chapter 3. Scripts used to parse the input and output files from this neutronics analysis, to prepare and reformat the data for heat transfer and fuel performance calculations, are described in Section 3.4. Key output parameters of the neutronics analysis needed for TRIUNE include volumetric heating rates in the TRISO particles in units of Watts per cubic meter), the burnup level of the fuel expressed as the number of fissions per initial heavy metal atom (FIMA), and the accumulated fast fluence in the particle. In TRIUNE calculations, this fast fluence is converted to units of neutrons per square meter (or 10^{25} n-m^{-2} as appropriate) and used as a representative average fast fluence for the entire particle; this is a reasonable approximation since there is minimal self-shielding of fast neutrons within the TRISO particle.

Explicit thermal input must be provided to TRIUNE in the form of a data vector containing the temperature at the OPyC outer surface at each time step for the particle. This parameter, referred to as T_{bound}, provides a required boundary condition for heat transfer solutions. As currently formulated, and detailed more explicitly in Section 3.4, this thermal input is currently provided in the form of temperatures at the fuel pebble surface and center. TRIUNE calculates the resultant particle boundary temperature by either calculating an average temperature within that fuel pebble for a nominal particle calculation or calculating the expected particle boundary temperature at the sampled radial position of the particle within the pebble for a Monte Carlo batch particle fuel performance calculation. The reader is directed to Section 3.4 for further details of the implementation used during this work; in summary, however, TRIUNE requires that the user or an outside

code provides the temperature at the outer surface of the OPyC. Heat transfer calculations within the TRISO particle are handled by TRIUNE itself.

2.3.2 Material Properties

TRIUNE utilizes the best available correlations identified in literature for each required material property and in some cases these correlations have been reworked to address inconsistencies or gaps that were identified. Section 2.2 details the material property correlations currently used in TRIUNE.

2.3.3 Heat Transfer Model

TRIUNE uses 1D heat transfer calculations to determine layer interface temperatures and bulk temperatures of each layer. Since the material property correlation for thermal conductivity is a function of the temperature of the region for both SiC and the fuel kernel, an iterative solver was developed that uses initial guesses at the bulk average temperatures of the SiC (T_{SiC}) and fuel kernel (T_{kern}) based upon the thermal input for T_{bound}. The heat transfer solver converges on a solution based upon the user-specified maximum deviation allowed for the bulk temperature in the fuel kernel or SiC between consecutive iterations.

The temperature difference across zone i with volumetric heat generation and no incident heat flux (i.e., a fuel kernel zone) is given by

$$\Delta T_i = \frac{q_i''' \times (r_b^2 - r_a^2)}{6k_i} \tag{2.3}$$

where:

$\mathbf{q}_i'''$ is the volumetric heat generation rate in zone i,

k_i is the thermal conductivity of zone i [W/m-K], and

r_a, r_b are the inner and outer radii (respectively) of zone i [m]

while the temperature difference across zone i without volumetric heat generation but with an incident heat flux is

$$\Delta T_i = \frac{q_{incident} \times (r_b - r_a)}{4\pi k_i r_b r_a} \tag{2.4}$$

where:

$\mathbf{q}_{incident}$ is the total heating incident upon zone i,

k_i is the thermal conductivity of zone i [W/m-K], and

r_a, r_b are the inner and outer radii (respectively) of zone i [m]

since it simply depends on spherical heat conduction without an internal source term. In typical heat transfer models for TRISO fuel particles, it is assumed that all heat production occurs in the fuel kernel and thus Equation 2.3 is applied to the central fuel kernel with q_i''' set equal to q_{kernel}''' and Equation 2.4 is applied to each of the coating layers with $q_{incident}$ set equal to $q_{particle}$. The heat transfer model implemented in TRIUNE allows for a more finely detailed analysis by incorporating the possibility of a volumetric heat source in the coating layers of the particle in addition to the heat flux incident upon these layers; this is envisioned to be potentially important for application to LIFE systems due to neutron and photon heating in the coating layers being an appreciable heat source during some foreseeable operating regimes (e.g., low power operation when fertile materials are being converted to fissile and fissionable nuclides). With this in mind, the fuel kernel in the TRIUNE particle heat transfer model still uses Equation 2.3 with q_i''' set equal to q_{kernel}''' but the temperature difference across a coating layer is calculated as

$$\Delta T_i = \frac{q_i''' \times (r_b^2 - r_a^2)}{6k_i} + \frac{q_{incident} \times (r_b - r_a)}{4\pi k_i r_b r_a} \tag{2.5}$$

where:

$\mathbf{q}_i'''$ is the volumetric heat generation rate in zone i,

$\mathbf{q}_{incident}$ is the total heating incident upon zone i,

k_i is the thermal conductivity of zone i [W/m-K], and

r_a, r_b are the inner and outer radii (respectively) of zone i [m]

which incorporate both the heat generated within the coating layer of interest as well as the heat deposited interior to that coating layer that must pass through it.

2.3.4 Internal Gas Pressure

Gas pressure builds up inside a TRISO particle due to gaseous fission products (predominantly Xe and Kr) released from the fuel kernel, and possibly carbon monoxide (CO) as well, accumulating in the interior void volume formed in the buffer and the gap that forms between the buffer and IPyC. Gas pressure calculations in TRIUNE thus involve quantifying the amount of gaseous FPs produced that subsequently undergo fission gas release (FGR) from the kernel to the void volume, quantifying the amount of CO gas produced in the buffer if there is any, and then performing calculations to determine the internal pressure due to released gaseous FPs and CO gas.

TRIUNE currently utilizes Xe and Kr inventories that are directly parsed from the self-consistent neutronics depletion analysis to ensure that the fission gas inventories include precise energy and nuclide dependence in their production terms and also account for fission gas destruction due to both radioactive decay and transmutation. Furthermore, this approach guarantees consistency between neutronics and TRIUNE calculations, which

supports one of the fundamental goals of this work: integrated self-consistent neutronics and fuel performance analyses.

Fractional release calculations, due to both recoil release and Booth diffusive release, are performed to determine the amount of fission gas released to the particle's void volume. Recoil release accounts for the direct kinetic release of fission fragments from the kernel into the buffer region. It is governed by the equation

$$(\mathrm{FR})_{\mathrm{recoil}} = 0.25\frac{r_{\mathrm{k}}^3 - (r_{\mathrm{k}} - \mathrm{d})^3}{r_{\mathrm{k}}^3} \tag{2.6}$$

where:

$(\mathrm{FR})_{\mathrm{recoil}}$ is the fractional release due to recoil,

r_{k} is the radius of the fuel kernel [m], and

d is the average fission fragment range [m]

and is currently assumed to vary only with the fuel kernel's geometry rather than its composition or material properties. Nominal values of recoil release for kernel diameters of 350μm and 500μm are roughly 2% and 1.5%, respectively [19]. The Booth FGR model assumes diffusive release to grain boundaries from an "equivalent sphere" representing a single grain of fuel (e.g., UO_2). Booth model calculations in TRIUNE follow the PARFUME approach given as

$$(\mathrm{FR})_{\mathrm{Booth}} = 1 - \left(\frac{6}{\mathrm{D}'t}\right)\sum_{n=1}^{\infty}\left[\frac{1 - \exp(-n^2\pi^2\mathrm{D}'t)}{n^4\pi^4}\right] \tag{2.7}$$

where:

$(\mathrm{FR})_{\mathrm{Booth}}$ is the Booth model fractional release,

$\mathrm{D}' = \dfrac{D}{a^2}$,

D is the diffusion coefficient [m_2/s],

a is the diffusion coefficient [m_2/s], and

t is time [s]

with the series approximation to the integral truncated at n_{max} terms (a user-specified number currently set to $n_{max} = 50$). The user-specified Booth radius has been assigned a value of 15μm in current TRIUNE calculations based upon INL documentation [19]. TRIUNE currently calculates effective diffusion coefficients for Xe and Kr as a function of kernel temperature ($\mathrm{T}_{\mathrm{kern}}$) by interpolating on data reported for diffusion of Xe and Kr in a UO_2 kernel shown below in Figure 2.6 [67].

The data used for interpolation in TRIUNE follows the upper (continuous) curve branch for "I, Kr, Xe" in Figure 2.6, such that the diffusion coefficient is approximately equal to

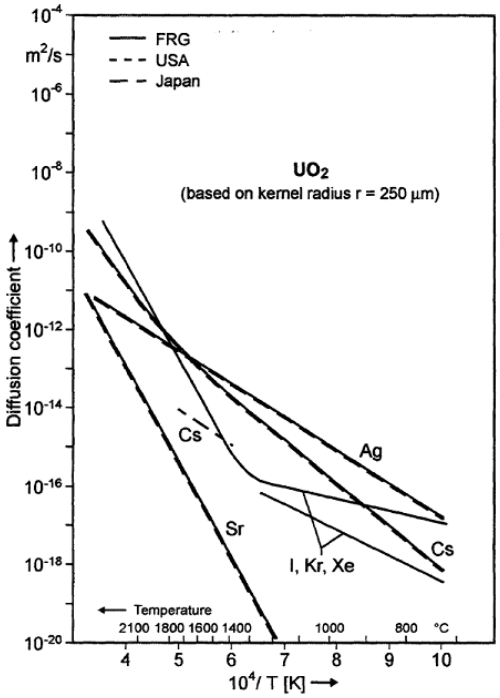

Figure 2.6: Diffusion coefficients of fission product species in UO_2 as a function of temperature, as reproduced from Fig. A-1 of Reference [67].

10^{-17} m^2/s at a temperature of about 700°C (corresponding to 10^4/T[K] about equal to 10). Given this source data, the diffusion coefficients for Xe and Kr are assumed to be identical.

For fuel systems where oxygen release from the fuel kernel is expected to be appreciable, TRISO FPMs must be able to adequately predict CO gas generation because the resulting pressure often represents the majority of internal gas pressure. The simple approach to CO production taken by many TRISO fuel performance models has been to use a correlation to calculate the number of free oxygen atoms released from the fuel kernel per fission event [19]. Common correlations include the Homan formulation [19]

$$\begin{aligned} \mathrm{O/f} &= 1.64 \exp(-3311/T) \\ \mathrm{O/f_{max}} &= 0.61 \end{aligned} \tag{2.8}$$

where:

O/f is the number of oxygen atoms released per fission event, and

T is the temperature [K]

for LEU (^{235}U < 20 wt%) UO_2 fuels, the Proksch model [19]

$$\log_{10}\left[\frac{\mathrm{O/f}}{t^2}\right] = -0.21 + (-8500/T) \tag{2.9}$$
$$\mathrm{O/f_{max}} = 0.4\,\mathrm{f_U} + 0.85\,\mathrm{f_{Pu}}$$
$$\mathrm{O/f_{upper\ limit}} = 0.625$$

where:

O/f is the number of oxygen atoms released per fission event,

t is the irradiation time [EFPD],

T is the particle surface temperature [K],

$\mathbf{f_U}$ is the fraction of fissions from U [/], and

$\mathbf{f_{Pu}}$ is the fraction of fissions from Pu [/]

which accounts for both U and Pu fission contributions but is limited to the ranges of $950 < T[\mathrm{°C}] < 1525$ and $66 < t[EFPD] < 550$, and Martin's STRESS3 model [19]

$$\mathrm{O/f_{Pu}} = 1.641\exp(-3311/T) \tag{2.10}$$

where:

$\mathbf{O/f_{Pu}}$ is the number of oxygen atoms released per fission event, and

T is the temperature [K]

which assumes oxygen release is proportional only to plutonium fission rates. These approaches are likely not representative for fuel systems that use hypostoichiometric fuel kernels (e.g., $UO_{1.7}$), systems that involve significant fission events in TRU elements, or thorium fuel systems. Furthermore, computational thermochemistry codes that predict CO production rates based upon the chemical composition of the fuel kernel along with the temperature and partial gas pressures in the system yield oxygen release rates significantly different than the correlations lists above. This has been demonstrated by comparing the resultant gas pressures predicted using these correlations in TRIUNE and other TRISO fuel performance models to the CO gas pressures predicted by PARFUME which employs the HSC thermochemistry code [25]; Reference [69] shows these gas pressure differences for the IAEA TRISO benchmark cases and they are also shown and discussed in Appendix D of this document. Oxygen release from the fuel kernel, and subsequent CO gas generation in the buffer, thus poses a serious challenge for fuel performance modeling. Demonstrated approaches to mitigating CO production, including the use of oxycarbide fuel kernels (e.g., UCO) or using an oxygen getter in the fuel kernel (e.g., SiC), reduce the internal gas pressure in the TRISO and largely eliminate potential kernel migration issues [29]. For situations such as these, it can be assumed that there is negligible CO production in the buffer and thus the TRISO fuel performance model can bypass oxygen release calculations. TRIUNE allows

the user to request either the Proksch or Homan correlation for use in CO gas generation calculations or the user can specify that there is no oxygen release at all. For the purposes of this study, it is assumed that oxycarbide fuel forms would be used in LIFE applications, so TRIUNE has been set to assume negligible CO production. The calculated quantities of fission product and CO gases released to the void volume feed into subsequent calculations for internal gas pressure, which can be calculated through various means. The simplest method is the Ideal Gas Law (IGL) which gives the pressure as

$$P_{gas} = \frac{RT_{buffer}}{n_{tot} V_{void}} \tag{2.11}$$

where:

$\mathbf{P_{gas}}$ is the internal gas pressure [Pa],

$\mathbf{R}$ is the ideal gas constant (8.31441 [J/K-mol]),

$\mathbf{T_{buffer}}$ is the average temperature in the buffer region [K],

$\mathbf{n_{tot}}$ is the total quantity of gas [moles], and

$\mathbf{V_{void}}$ is the void volume the gas occupies [m^3]

but most TRISO FPMs use the Redlich-Kwong Equation of State (R-K EOS), which defines the internal gas pressure as

$$P_{gas} = \frac{RT_{buffer}}{\nu - \overline{b}} - \frac{\overline{a}}{(T_{buffer})^{0.5}\nu(\nu + \overline{b})} \tag{2.12}$$

where:

$\mathbf{P_{gas}}$ is the internal gas pressure [Pa],

$\mathbf{R}$ is the ideal gas constant (8.31441 [J/K-mol]),

$\mathbf{T_{buffer}}$ is the average temperature in the buffer region [K],

ν is the void volume per mole of gas [m^3/mol], and

$\overline{a}$**,** $\overline{b}$ are averaged gas constants

with the averaged gas constants calculated via

$$\overline{a} = \left[\sum_{i=1}^{n} x_i a_i^{0.5}\right]^2 \tag{2.13}$$

$$\overline{b} = \sum_{i=1}^{n} x_i b_i$$

where:

x_i is the mole fraction of species i in the total gas,

a_i is gas constant a for species i,

b_i is gas constant b for species i, and

n is the total number of gas species

as in PARFUME. Table 2.5 provides the gas constants needed for R-K EOS calculations.

Table 2.5: Gas constants for R-K EOS calculations, as reproduced from Ref. [19].

Gas	$\mathbf{T_C}$ **[K]**	$\mathbf{P_C}$ **[MPa]**	**a** **[N m^4 K$^{0.5}$/mol^2]**	**b** **[m^3/mol]**
CO	132.91	3.5	1.72	2.736×10^{-5}
CO_2	304.14	7.38	6.46	2.969×10^{-5}
Kr	209.45	5.5	3.411	2.743×10^{-5}
Xe	289.75	5.9	7.158	3.538×10^{-5}

Reference [19] demonstrated that IGL calculations can yield significantly lower internal gas pressures compared to R-K EOS results because the IGL does not consider the volume occupied by the gas molecules themselves whereas the R-K EOS adjusts the void volume to take this factor into account.

2.3.5 Stress-Strain-Displacement Analysis

TRIUNE uses the updated closed-form solution to stress-strain-displacement relationships within a spherical pressure vessel described by Miller [31] and Boer [32], which was based upon earlier work by Miller [30]. The governing equations for this approach start with the radial and tangential strain derivatives with respect to neutron fluence given by

$$\frac{\partial \varepsilon_r}{\partial t} = \frac{1}{E}\left[\frac{\partial \sigma_r}{\partial t} - 2\mu\frac{\partial \sigma_t}{\partial t}\right] + c\left[\sigma_r - 2\nu\sigma_t\right] + \dot{S}_r + \alpha_r\dot{T} \tag{2.14}$$

$$\frac{\partial \varepsilon_t}{\partial t} = \frac{1}{E}\left[(1-\mu)\frac{\partial \sigma_t}{\partial t} - \mu\frac{\partial \sigma_r}{\partial t}\right] + c\left[(1-\nu)\sigma_t - \nu\sigma_r\right] + \dot{S}_r + \alpha_r\dot{T} \tag{2.15}$$

using the notation documented in the Nomenclature section of this document. The terms in these derivatives account for elastic effects, irradiation creep, irradiation-induced shrinkage and/or swelling, and thermal expansion respectively. It must be noted at this time that in the above equations, and in all subsequent equations, one must pay particular attention to the units of the notation used (e.g., the PyC irradiation creep constants given as c are in units of 10^{25} n-m^{-2}) and to the fact that t represents fast neutron fluence rather than time in these equations. The second section of the governing equations defines the strain-displacement relationships and the equilibrium requirement imposed on the system, written as

$$\varepsilon_r = \frac{\partial u}{\partial r} \tag{2.16}$$

$$\varepsilon_t = \frac{u}{r} \tag{2.17}$$

$$\frac{\partial \sigma_r}{\partial r} + \frac{2}{r}(\sigma_r - \sigma_t) = 0 \tag{2.18}$$

where the notation defined in the Nomenclature section is again used. Figure 2.7 shows the spherical geometry of a typical TRISO fuel particle and the numbering scheme for the radial positions of the various layer interfaces.

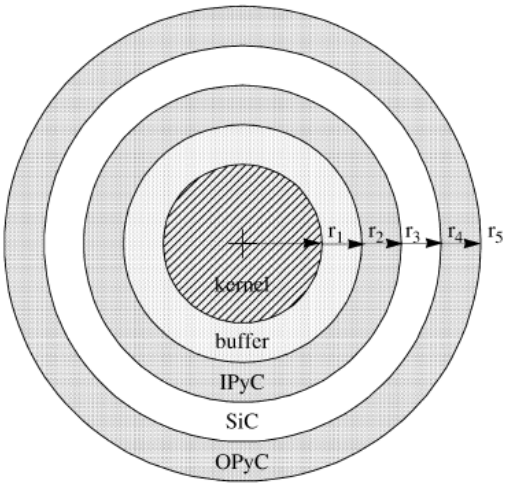

Figure 2.7: TRISO particle geometry numbering scheme, as reproduced from Reference [31].

Following the procedure of both Miller [25] and Boer [32], the radial displacement and radial and tangential stresses in the governing equations are assumed to be well-represented by polynomial series of the form

$$u(r,t) = \sum_{i,n=0}^{\infty} u_i(r) t^n \tag{2.19}$$

$$\sigma_r = \sum_{i,n=0}^{\infty} \sigma_{r,i}(r) t^n \tag{2.20}$$

$$\sigma_t = \sum_{i,n=0}^{\infty} \sigma_{t,i}(r) t^n \tag{2.21}$$

which are then truncated at the $n = 1$ terms to provide first-order polynomial expansions. Combining Equations (2.14) through (2.21) yields an incremental solution for the displacement

$$\frac{d^2u_i}{dt^2} + \frac{2}{r}\frac{d^2u_i}{dr^2} - \frac{2}{r^2}u_i = \frac{2}{Er}(1-2\mu)f_i + \frac{2}{r}c(1-2\nu)\frac{f_{i-1}}{i} \tag{2.22}$$

where

$$f_{i+1} = -\frac{cE(1-\nu)}{(1-\mu)}\frac{f_i}{(i+1)} + \frac{E\left(\dot{S_{r,i}} - \dot{S_{t,i}} + \alpha_{r,i}\dot{T_i} - \alpha_{t,i}\dot{T_i}\right)}{(1-\mu)(i+1)} \tag{2.23}$$

with $f_0 = 0$. Using these terms, a function $F(t)$ can be defined as

$$F(t) = \sum_{i,n=1}^{\infty} f_i t^n \tag{2.24}$$

and is used later to calculate stresses within a given coating layer. The incremental solution for the displacement can thus be written as

$$u_i = A_i r + \frac{B_i}{r^2} + \left[\frac{2(1-2\mu)}{3E}f_i + \frac{2c(1-2\nu)}{3i}f_{i-1}\right] r\ln(r) \tag{2.25}$$

with A_i and B_i being coefficients which will be calculated later. The subsequent stress equation of Reference [30] remains unchanged in Reference [31]:

$$\sigma_{t,i}(r) - \sigma_{r,i}(r) = \frac{3(r_a r_b)^3}{r^3(r_a^3 - r_b^3)}\left[p_i - q_i - \frac{2}{3}f_i \ln\left(\frac{r_a}{r_b}\right)\right] + \frac{f_i}{3}. \tag{2.26}$$

Equations (2.25) and (2.26) allow the development of a general equation for radial displacement as a function of both radial position and time given by

$$\begin{aligned} u(r,t) =& K_1 p + K_2 q + K_3 \int p c\, dt + K_4 \int q c\, dt + K_5 \int \left(\dot{S}_r + \alpha_r \dot{T}\right) dt \\ &+ K_6 \int \left(\dot{S}_t + \alpha_t \dot{T}\right) dt + K_7 F(t) \end{aligned} \tag{2.27}$$

where coefficients K_i are dependent upon the geometry and properties of a layer and are calculated using Equations (B.2)–(B.7) of Appendix B. K_7 goes to 0 at the layer surfaces/interfaces. The internal and external pressures, $p(t)$ and $q(t)$, are applied as boundary conditions at the inner and outer surfaces of the coating layer being considered and use a sign convention wherein pressure is positive outward away from the center of the TRISO particle. As noted by Miller [31], the contribution to overall displacement due to the integral terms of Equation (2.27) can grow significantly with time due to cumulative energy deposition in the layer.

By applying Equation (2.27) to the layer interfaces of a TRISO particle, a set of radial displacements at the layer inner and outer surfaces of the coating layer interfaces ($r = r_3, r_4$)

can be found as shown below. The PyC layers are assumed to undergo irradiation creep and IIDC, and the PyC and SiC layers are assumed to undergo anisotropic thermal expansion.

IPyC outer surface:

$$\begin{aligned} u_I =& a_1 p + a_2 \sigma_{rI} + a_3 \int p c_I \, dt + a_4 \int \sigma_{rI} c_I \, dt \\ &+ a_5 \int \left(\dot{S}_{rI} + \alpha_{rI} \dot{T}_I \right) dt + a_6 \int \left(\dot{S}_{tI} + \alpha_{tI} \dot{T}_I \right) dt \end{aligned} \tag{2.28}$$

SiC inner and outer surfaces:

$$u_I = b_1 \sigma_{rI} + b_2 \sigma_{rO} + b_5 \int \alpha_{rS} \dot{T}_S \, dt + b_6 \int \alpha_{tS} \dot{T}_S \, dt \tag{2.29}$$

$$u_O = c_1 \sigma_{rI} + c_2 \sigma_{rO} + c_5 \int \alpha_{rS} \dot{T}_S \, dt + c_6 \int \alpha_{tS} \dot{T}_S \, dt \tag{2.30}$$

OPyC inner surface:

$$\begin{aligned} u_O =& d_1 \sigma_{rO} + d_2 q + d_3 \int \sigma_{rO} c_O \, dt + d_4 \int q c_O \, dt \\ &+ d_5 \int \left(\dot{S}_{rO} + \alpha_{rO} \dot{T}_O \right) dt + d_6 \int \left(\dot{S}_{tO} + \alpha_{tO} \dot{T}_O \right) dt \end{aligned} \tag{2.31}$$

The coefficients a_j, b_j, c_j, and d_j are determined using the appropriate radii and material properties in the corresponding K_j expressions. If swelling or thermal expansion in a given layer is isotropic then the radial and tangential components of that behavior can be set equal to each other.

The radial stresses at the layer interfaces can now be determined by setting the displacements in the neighboring surfaces equal at the radial position of the interface (e.g., setting Equations (2.28) and (2.29) equal at $r = r_3$) and then differentiating with respect to t. The result is a set of two simultaneous differential equations

$$\frac{d\sigma_{rO}}{dt} - B_2 \sigma_{rO} - B_1 \sigma_{rI} = x(t) \tag{2.32}$$

$$\frac{d\sigma_{rI}}{dt} - B_3 \sigma_{rI} - B_4 \sigma_{rO} = y(t) \tag{2.33}$$

with the quantities B_i calculated using Equations (B.8)–(B.12) in Appendix B. The functions $x(t)$ and $y(t)$ are assumed to be well-represented by the linear functions

$$x(t) = x_0 + x_1 t \tag{2.34}$$

and

$$y(t) = y_0 + y_1 t \tag{2.35}$$

over a given time increment. The solution to Equations (2.32) and (2.33) thus becomes

$$\sigma_{rO} = D_1 e^{m_1 t} + D_2 e^{m_2 t} + v_0 + v_1 t \tag{2.36}$$

$$\sigma_{rI} = \frac{m_1 - B_2}{B_1} D_1 e^{m_1 t} + \frac{m_2 - B_2}{B_1} D_2 e^{m_2 t} + w_0 + w_1 t \tag{2.37}$$

where the terms x_0, x_1, y_0, y_1, m_1, m_2, v_0, v_1, w_0, and w_1 are given by Equations (B.13)–(B.21) and are constant during a time increment but change between subsequent increments. This solution assumes a spherical system with three coating layers where m1 and m2 are the eigenvalues for a two-equation matrix form of Equations (2.32) and (2.33). Boer shows much more detail about the matrix form and solution approach [32], while Miller's simpler approach [31] is used in TRIUNE; both approaches are accurate and identical but the Boer documentation provides a more rigorous mathematical technique.

The stress-strain-displacement relationships are thus solved over a series of time increments, with D_1 and D_2 determined for each increment using the initial conditions of that specific time increment. The initial values for internal and external pressure, p and q, are applied at the beginning of irradiation ($t = 0$) to determine the initial radial stresses at the layer interfaces. Since all of the integral terms of Equations (2.28) through (2.31) vanish at $t = 0$, this gives

$$\sigma_{rO}(0) = \frac{a_1 c_1 p - d_2 (b_1 - a_2) q}{b_2 c_1 - (c_2 - d_1)(b_1 - a_2)} \tag{2.38}$$

$$\sigma_{rI}(0) = \frac{a_1 (c_2 - d_1) p - d_2 b_2 q}{(b_1 - a_2)(c_2 - d_1) - c_1 b_2} \tag{2.39}$$

for the layer interfaces at r_3 and r_4, which are then used as the initial conditions for finding D_1 and D_2 in the first time increment. Thus, using Equations (2.36) and (2.37) over a general time increment n, D_1 and D_2 are found to be

$$D_1 = \frac{(m_2 - B_2)X - B_1 Y}{m_2 - m_1} e^{-m_1 t_{n-1}} \tag{2.40}$$

$$D_2 = \frac{(m_1 - B_2)X - B_1 Y}{m_1 - m_2} e^{-m_2 t_{n-1}} \tag{2.41}$$

where

$$X = \sigma_{rO}(t_{n-1}) - v_0 - v_1 t \tag{2.42}$$

$$Y = \sigma_{rI}(t_{n-1}) - w_0 - w_1 t \tag{2.43}$$

and t_{n-1} is the time t at the end of the time increment $n - 1$. All material properties, strain rates due to IIDC and thermal expansion, and internal and external pressures are approximated as constant values averaged over the increment.

The function $F(t)$ used in the above equations, after substituting Equation (2.23) into (2.24) and differentiating with respect to t, becomes

$$\frac{dF}{dt} + \frac{cE(1-\nu)}{(1-\mu)}F = \frac{E}{(1-\mu)}\left(\overline{\dot{S}_r} + \overline{\alpha_r}\overline{\dot{T}} - \overline{\dot{S}_r} - \overline{\alpha_r}\overline{\dot{T}}\right) \tag{2.44}$$

where the bars over the variables denote that they are averaged over the increment and then held constant in TRIUNE calculations for the time increment. As provided by Miller et. al [31], the general solution to this equation is

$$F(t) = \left[F(t_{n-1}) - a_0\right] e^{-\frac{cE(1-\nu)}{(1-\mu)}(t-t_{n-1})} + a_0 \tag{2.45}$$

where a_0 for the time increment n is given by:

$$a_0 = \frac{\left(\overline{\dot{S}_r} + \overline{\alpha_r}\overline{\dot{T}} - \overline{\dot{S}_r} - \overline{\alpha_r}\overline{\dot{T}}\right)}{c(1-\nu)}. \tag{2.46}$$

Each PyC layer has its own function $F(t)$; the SiC layer's $F(t)$ becomes zero if SiC is treated as an isotropic elastic medium.

Combining the radial interface stresses calculated by Equations (2.36) and (2.37) with $F(t)$ from Equation (2.45) allows the calculation of radial or tangential stress at any radial location in the coating layers using the general stress equations

$$\begin{aligned}\sigma_r(r,t) =& \frac{r_a^3\left(r_b^3 - r^3\right)}{r^3\left(r_b^3 - r_a^3\right)}p - \frac{r_b^3\left(r_a^3 - r^3\right)}{r^3\left(r_b^3 - r_a^3\right)}q \\ &- \frac{2}{3}\left[\frac{r_a^3\left(r_b^3 - r^3\right)\ln r_a - r_b^3\left(r_a^3 - r^3\right)\ln r_b}{r^3\left(r_b^3 - r_a^3\right)} - \ln r\right]F(t) \end{aligned} \tag{2.47}$$

$$\begin{aligned}\sigma_t(r,t) =& -\frac{r_a^3\left(r_b^3 + 2r^3\right)}{2r^3\left(r_b^3 - r_a^3\right)}p + \frac{r_b^3\left(r_a^3 + 2r^3\right)}{2r^3\left(r_b^3 - r_a^3\right)}q \\ &+ \frac{1}{3}\left[\frac{r_a^3\left(r_b^3 + 2r^3\right)\ln r_a - r_b^3\left(r_a^3 + 2r^3\right)\ln r_b}{r^3\left(r_b^3 - r_a^3\right)} + 2\ln r + 1\right]F(t) \end{aligned} \tag{2.48}$$

where r_a and r_b are the inner and outer radii of the layer and p and q are the radial stresses at the inner and outer surfaces of the layer. It should be noted that the tangential stresses determine whether or not a coating layer fails and that although the maximum tangential stress usually occur at the inner surface there are circumstances for which the maximum tangential stress in a PyC layer could instead be at the outer surface [31]. To determine tangential stresses at the SiC layer boundaries, Equation (2.48) is used with $F(t)$ set to zero since TRIUNE currently treats SiC as an isotropic elastic material.

With radial and tangential stresses known at the layer interfaces, displacement calculations can be performed to determine the new radii for the interfaces at the end of the increment which are then used to update the geometry for the next time increment. These updated radii greatly affect heat transport, fission product transport, and can affect future stress-strain-displacement calculations [31]. The radial stresses and Equations (2.28)–(2.31) enable incremental solutions to interface radii (r_2, r_3, r_4, and r_5) displacements. As an example, Equation (2.29) becomes

$$\Delta u_I = b_1 \Delta\sigma_{rI} + b_2 \Delta\sigma_{rO} + b_5 \alpha_{rS} \dot{T}_S \Delta t + b_6 \alpha_{tS} \dot{T}_S \Delta t \tag{2.49}$$

in its incremental form [31]. Determining the displacements at r_2 and r_5 requires modifying Equations (2.28) and (2.31) to take the form

$$\begin{aligned} \Delta u_2 =& a'_1 \Delta p + a'_2 \Delta\sigma_{rI} + \left(a'_3 p + a'_4 \sigma_{rI}\right) c_I \Delta t \\ &+ a'_5 \left(\dot{S}_{rI} + \alpha_{rI} \dot{T}_I\right) \Delta t + a'_6 \left(\dot{S}_{tI} + \alpha_{tI} \dot{T}_I\right) \Delta t \end{aligned} \tag{2.50}$$

and

$$\begin{aligned} \Delta u_5 =& d'_1 \Delta\sigma_{rO} + d'_2 \Delta q + \left(d'_3 \sigma_{rO} + d'_4 q\right) c_O \Delta t \\ &+ d'_5 \left(\dot{S}_{rO} + \alpha_{rO} \dot{T}_O\right) \Delta t + d'_6 \left(\dot{S}_{tO} + \alpha_{tO} \dot{T}_O\right) \Delta t \end{aligned} \tag{2.51}$$

where the coefficients a'_i and d'_i are calculated using Equations (B.1)–(B.6) with the dimensions appropriate for the inner IPyC and outer OPyC surfaces, respectively.

The current version of TRIUNE accounts for the development of a gap between the buffer and IPyC layers during irradiation; Miller et al. [31] provide a description of this behavior and how to account for it in displacement calculations, including additional pressure calculations needed for the buffer layer. Most of the formulation described above remains the same but some additional stress coefficients are calculated and a separate displacement equation is used for the buffer outer surface in addition to the one used for the inner surface of the IPyC. The difference between those two surface locations determines the size of the gap. Also, TRIUNE calculations of the displacement of the interface between the fuel kernel and the buffer at $r = r_1$ currently directly follow the solid FP swelling of the kernel; the buffer pressure calculations would affect this as well, but it is widely assumed no gap will form [31, 32].

The standard version of TRIUNE does not currently allow for one-layer or two-layer solutions for TRISO particles with failed coating layers, though specific variants of TRIUNE were developed and used for to handle one-layer and two-layer solutions for the IAEA benchmark cases. Reference [31] provides the additional formulations needed to handle one-layer and two-layer calculations as well as a comparison of PARFUME calculations of this type to FEA calculations performed by ABAQUS for the same inputs.

2.3.6 Model Parameter Updates

After determining the radial displacement of each layer interface location over a given time increment, TRIUNE updates parameters for the next time step. The new radii most significantly affect the volumes, porosities, and densities of each shell. In addition, the void volume in the buffer changes with buffer volume and porosity. After determining the new shell volumes (V) at time step $t+1$, the density (ρ) and porosity (P) of a particular layer at time step n are updated according to

$$\rho_{t+1} = \rho_t \left(\frac{\mathrm{V}_t}{\mathrm{V}_{t+1}} \right) \tag{2.52}$$

and

$$\mathrm{P}_{t+1} = 1 - \left(\frac{\rho_{t+1}}{\rho_{\mathrm{TD}}} \right) \tag{2.53}$$

where ρ_{TD} is the theoretical density of the material (e.g., 3.21 g/cm^3 for SiC). TRIUNE currently calculates the updated void volume for time step $t+1$ as

$$\mathrm{V}_{\mathrm{void}}^{t+1} = \mathrm{V}_{\mathrm{buff}}^{t+1} \times \mathrm{P}_{\mathrm{buff}}^{t+1} + \mathrm{V}_{\mathrm{buffer/IPyC\ gap}}^{t+1} \tag{2.54}$$

which accounts for the void volume in the buffer as well as the gap between the buffer and IPyC; alternate approaches, such as the one used in ATLAS, may assume that voids in the kernel impact the void volume that internal gas generation fills [19].

2.3.7 Fuel Failure Model

TRIUNE currently assumes the dominant failure mode expected for TRISO particles in future systems will be pressure vessel failure of the SiC. As with other TRISO fuel performance models [19, 25], TRIUNE uses Weibull theory for predicting failure probabilities. Miller [25] and Wang [36], among others, provide specific detailed discussion of the application of Weibull theory to TRISO fuel performance modeling; for the purposes of this document, it is sufficient to note that Weibull statistical strength theory "represents a distribution of SiC strengths" within a population of TRISO particles and allows failure probability predictions for this population [11]. The specific failure probability equation used in TRIUNE for the SiC layer of a particle, similar to the one provided in Reference [11], is given as

$$P_f = 1 - \exp\left[-\ln 2 \left(\frac{\sigma_{t,SiC\_calc}}{\sigma_{t,SiC\_ms}} \right)^m \right] \tag{2.55}$$

where:

P_f is the failure probability of the SiC layer [/],

σ_{t,SiC_calc} is the maximum calculated tangential stress in SiC [MPa],

σ_{t,SiC_ms} is the SiC Weibull mean strength [MPa], and

m is the SiC Weibull modulus

with σ_{t,SiC_calc} usually equal to the tangential stress at the inner surface of the SiC ($\sigma_{t,SI}$).

Failure fraction predictions for a batch of particles are made within TRIUNE by first simulating a user-specified number of "real" particles that are constructed based upon a set of manufacturing assumptions; TRIUNE currently allows for as-manufactured variations in the kernel diameter and coating thicknesses of TRISO particles, with the user specifying the mean values, and assumes that the manufacturing results for each parameter follow a truncated Gaussian distribution with user-specified values for the standard deviation and upper and lower truncation bounds. After sampling particles dimensions to build "real" TRISO particles, and possibly sampling items like the radial position of the particle within a fuel pebble, TRIUNE simulates the lifetime history of each particle. At each time step, after the stress-strain-displacement calculations are completed, Weibull failure probabilities are calculated for each particle. The effective predicted batch failure fraction (Batch FF) for the full population of particles is then calculated as

$$\text{Batch FF} = \frac{\sum_{n=1}^{N} P_f^n}{N} \tag{2.56}$$

where:

Batch FF is the total predicted failure fraction for a batch of N particles [/],

P_f^n is the Weibull failure probability of particle n [/],

n is the particle number, and

N is the total number of simulated particles requested by the TRIUNE user

at each timestep, which results in TRIUNE producing a predicted failure fraction as a function of time, burnup, or fast fluence.

For the purposes of this currently study, a failure fraction limit of 10^{-4} will be assumed, in keeping with failure fraction limits for NGNP and mentioned elsewhere [19]. The fuel burnup level at which TRIUNE calculations predict that 10^{-4} failures occur (1 in 10,000 particles) will thus be taken as the maximum credible burnup for that case. Given that this 10^{-4} failure limit appears to be set to ensure that radiation source terms for radiation getting out of the particles and through the pebbles into the coolant does not exceed a certain level, sound arguments could likely be made that a thorium LIFE system might be able to accept higher failure fractions for several reasons: reduced fission product diffusion coefficients due to lower temperatures in LIFE than in NGNP, increased attenuation of fission products in

the coolant itself given the affinity of flibe molten salt for fission products, and likely different diffusion coefficients of fission products in the particle kernels due to thorium being the fuel material of interest rather than uranium.

TRIUNE currently assumes that pressure vessel failure of the SiC layer will be the dominant failure mechanism of interest; in its present form, TRIUNE does not handle any multidimensional failure mechanisms described in Section 2.1 such as IPyC cracking or Pd attack of the SiC. These multidimensional failure mechanisms have been important historically; however, it is believed that improved manufacturing techniques are eliminating or at least partially mitigating several of these mechanisms. For example, carefully controlled coating environments and coating rates during IPyC coating have yielded IPyC layers with significantly reduced cracking. Another good example is that new coating techniques that result in SiC penetrating down into the IPyC layer have resulted in significantly stronger radial bond strength between IPyC and SiC, thus reducing IPyC/SiC debonding issues, while simultaneously addressing concerns about SiC thinning due to Pd attack because the SiC "fingers" act as sacrificial getters before Pd can reach and attack the bulk SiC.

2.4 Verification and Validation Efforts

In addition to comparing the output of individual material property correlations and fuel behavior models against comparable results available in the literature, some of which was previously documented in Reference [70], an extensive verification and validation (V&V) effort was conducted for the TRIUNE model using the IAEA Normal Operation Steady-State TRISO-Coated Particle Fuel Performance Benchmark Cases [68, 69]. Detailed results from this verification and validation effort, including relevant tables and/or figures for each benchmark case with TRIUNE results compared to PARFUME results, can be found in Appendix D. In summary, the V&V efforts proved useful for debugging and demonstrated that TRIUNE performs acceptably for all benchmark cases. Differences between PARFUME and TRIUNE results were generally small and could be attributed to known differences in CO gas generation rates and likely differences in fission product diffusion coefficients.

Putting the results into the larger code comparison context of Reference [69], TRIUNE appears to reliably produce results that are well within the bounds of what is considered acceptable; furthermore, TRIUNE produces results that may be better than several of the other codes being compared.

It should be noted that quite a bit of this V&V work falls into the category of "verification", which focuses on ensuring that the intended equations are being correctly solved in the model. The IAEA benchmark suite consists largely of computational benchmarks (Cases 1–8) or planned irradiations (Cases 13 and 14); relevant and reliable benchmark quality experimental results (Cases 9–12) make up a small portion of the overall benchmark suite. True "validation" is confined to these few cases that can be compared to experimental results and even for these cases the only result that can be reasonably validated is the integral result of the fraction of fuel particles that failed. Put differently,

verification asks "Did we answer the question correctly?" while validation asks "Did we ask the right question?" The lack of extensive, relevant, and reliable experimental data with which to benchmark TRISO fuel performance models up to the burnup and fast fluence levels expected in emerging nuclear energy systems presents a major challenge to validating such models. In addition, the information provided as part of the IAEA TRISO fuel performance benchmark suite is relatively limited; additional information for each case, such as actual fission product inventories and void volumes and other intermediate parameters that are calculated in fuel performance models, should be reported to simplify debugging efforts for new fuel performance models and enable better comparisons between existing fuel performance models to carefully identify differences and deficiencies.

Chapter 3

Neutronics Models and Methodologies

Neutronic depletion analysis in this work was carried out using a combination of two primary computational tools: the MONTEBURNS 2.0 Monte Carlo depletion analysis code package [71], which couples the MCNP5 Monte Carlo steady-state radiation transport code [72] to the time-dependent isotopic depletion analysis code ORIGEN-2.2 [73], and the LIFE Neutronics Control (LNC) code package developed by Kevin Kramer and others at LLNL [57]. The LNC package acts as a control agent for MONTEBURNS depletion analyses by tracking and controlling the LIFE operational parameters, such as Tritium Breeding Ratio (TBR) and tritium mass as well as system power level, and then modifies the ratio of ^{6}Li to ^{7}Li in the coolants in order to change how neutrons in the system are utilized and thus adjust the LIFE operational parameters within their desired ranges. The results of the neutronics depletion analysis of thorium-fueled LIFE engines were then passed through a heat transfer code to generate temperature distributions in the fuel blanket and then both of these information sources were integrated into TRIUNE to perform fuel performance calculations.

This chapter describes in detail the design features of a thorium-fueled LIFE engine, including reviewing specific benefits and challenges associated with using thorium as a nuclear fuel as well as explaining the operational approach used to control power and govern plant operations for LIFE engines in this study. Specific details of the MCNP radiation transport models are given, with particular emphasis on describing what levels of geometric heterogeneity are modeled in the various blanket regions. The depletion methodologies used in MONTEBURNS are then briefly outlined. Finally, details are provided as to how the neutronic analysis performed during this work was integrated with a heat transfer code and the TRIUNE fuel performance model. This last section documents the heat transfer methods and assumptions used to produce temperature distributions for pebbles in the fuel blanket based upon neutronics results and then describes the modeling assumptions made to simulate real pebble and particle lifetime histories.

3.1 Thorium LIFE Design Features

3.1.1 Thorium as a Nuclear Fuel

Recent years have demonstrated a resurgence of interest in the current and future use of nuclear power, brought on by many factors including a progressive improvement in the operating performance of existing reactors over the past couple decades and a growing concern about the risk and potential of anthropogenic global climate change due to greenhouse gas emissions, that has been accompanied by renewed interest in examining a thorium nuclear fuel cycle. The motivations for possible utilization of thorium as a nuclear fuel vary between nations but the broad international interest in the topic speaks to the widespread advantages thorium may offer [74, 75, 76, 77, 78, 79, 80].

Thorium occurs naturally in various forms but is currently most commonly extracted from monazite, a phosphate mineral that contains rare earth elements and thorium [79]. Table 3.1 summarizes the known thorium reserves in the world; it should be noted that the USGS only reports the reserves to two significant digits and that the fractions may not sum to 100% due to rounding errors and significant digit issues. These numbers represent the latest data from the 2010 USGS report and include both an increase in thorium reserves in the United States and the deletion of reserves previously listed for Norway, in light of recent survey data [79].

Table 3.1: Known thorium reserves in the world, from 2010 USGS report [79].

Location	**Known Thorium Reserves [MT]**	**Fraction of Known Thorium Reserves**
Australia	300,000	25.0%
Brazil	16,000	1.3%
Canada	100,000	8.3%
India	290,000	24.2%
Malaysia	4,500	0.4%
United States	440,000	36.7%
South Africa	35,000	2.9%
Other Countries	90,000	7.5%
Total	**1,300,000**	**-**

Thorium exists in nature as nearly 100% ^{232}Th with small amounts of other thorium isotopes that come from actinide decay chains. As a nuclear fuel, thorium serves as a fertile material that converts into fissile ^{233}U via the reaction

$$^{232}_{90}\mathrm{Th} \xrightarrow{(\mathrm{n},\gamma)} {}^{233}_{90}\mathrm{Th} \xrightarrow[\beta^-, t_{1/2}=21.83m]{} {}^{233}_{91}\mathrm{Pa} \xrightarrow[\beta^-, t_{1/2}=26.97d]{} {}^{233}_{92}\mathrm{U} \tag{3.1}$$

when irradiated with neutrons. These external neutrons generally come from other "driver" fuel elements that contain fissile fuels but could also come from an accelerator-driven system (ADS) or fusion reactions. Like uranium, thorium is pyrophoric when in powdered metallic form and thus must be handled carefully. Thorium oxide nuclear fuels are generally more chemically stable than uranium oxide fuels, which results in lower fission product release rates and reduced long-term storage and disposal risks [80].

Motivations for using thorium vary between nations but generally include resource utilization, neutronic performance, and possible reductions in waste storage and nonproliferation risks. Thorium offers potential resource utilization advantages due to the fact that it is roughly three times more abundant than uranium and offers an alternative to uranium-based fuel cycles, in case uranium reserves deplete sufficiently that economic costs of extracting further uranium outweigh its usefulness [74, 75]. Nations such as India that have very little uranium but have a relative abundance of thorium are particularly interested in thorium fuel cycles in order to avoid being dependent upon outside sources. The ^{233}U produced by thorium tends to yield superior neutronic performance in thermal reactors than other fuels because it tends to release a higher number of neutrons per fission event; this provides a second general motivation for thorium fuel cycles [74]. Thorium may reduce or mitigate risks associated with long-term waste storage and nonproliferation. The actinides produced in a thorium fuel cycle may be better for long-term storage than those that come from a uranium fuel cycle, the thorium fuel cycle may offer enhanced proliferation resistance due to strong gamma emitters from the ^{232}U decay chain that make waste handling and separations more radiologically difficult than low-enriched uranium (LEU) fuel cycle waste, and thorium fuel cycles may enable unique options for burning excess plutonium from weapons and the uranium fuel cycle [74, 75, 81]. Lastly, with specific regard to the use of thorium in a TRISO fuel form, ^{233}U has a fission yield for Pd that is significantly lower than the yield for Pd from ^{235}U or ^{239}Pu ; this provides a direct benefit to TRISO fuel performance because chemical attack on the SiC pressure vessel by Pd fission products is a known issue.

Thorium fuel cycles involve serious challenges as well. The intermediate nuclide in the process that converts ^{232}Th to ^{233}U is ^{233}Pa and has a 26.97 day half-life; this leads to a much higher likelihood of parasitic neutron absorption in the intermediate nuclide before it can decay to the fissile product when compared to the 2.36 day half-life of ^{239}Np, which is the intermediate nuclide in the process that converts ^{238}U to ^{239}Pu. Higher parasitic neutron capture, and thus less efficient fissile isotope production, can lead to a less efficient neutron economy and reactor design. In addition, there are still proliferation risks from thorium fuels despite the nonproliferation benefits of ^{232}U content in the fuel [82] and the ^{232}U can also cause radiological problems for handling spent fuel in thorium fuel cycles due to the hard gamma rays in the decay chain.

While a multitude of specific configurations exist for thorium fuel cycle options, they can generally be sorted into two broad categories: open fuel cycles and closed fuel cycles. Open thorium cycles, which involve the irradiation of thorium with in-situ fission of ^{233}U, are the simplest options to envision [76]. One possible open thorium cycle involves once-through burning of plutonium reprocessed from commercial spent nuclear fuel (CSNF) to produce

^{233}U which can then be denatured by adding depleted uranium (DU) [74]. Closed thorium cycles reprocess irradiated thorium and used ^{233}U fuel and then refabricate new fuel using the recovered ^{233}U. Thorium, DU, or reprocessed uranium could be mixed with the ^{233}U from the reprocessed fuels [76]. Once-through, partial, and full recycle modes have all been studied for ^{233}U, ^{235}U, and ^{239}Pu driven thorium fuel cycles. Notably, the International Fuel Cycle Evaluation (INFCE) program found that once-through LEU/Th fuel cycles were preferred over straight LEU cycles both in terms of resource efficiency and fuel cycle economics [74].

Uranium fuel cycles dominate the global nuclear energy industry but interest in thorium fuel cycles over the past 50 years has nonetheless generated a fairly large operational experience base for thorium-fueled nuclear reactors [74, 76, 80]. Table 3.2 summarizes the available data and information from this experience base, collapsing together multiple sources to yield a single concise reference [74, 75, 76, 77, 78, 79, 80].

Table 3.2: Summary of operational experience with thorium fuels [74, 75, 76, 77, 78, 79, 80].

Country	Reactor	Type	Dates of Operation	Power Level	Fuel	Notes
US	Peach Bottom	HTGR	1967 - 1974	40 MWe	Th+^{235}U TRISO	Th/HEU fuel
	Fort St Vrain	HTGR	1976 - 1989	330 MWe	Th+^{235}U TRISO	842 MWth, Th and Th/HEU (4:1 atom ratio) carbide TRISO, almost 25 MT of thorium fuel manufactured
	MSRE	MSBR	1964 - 1969	7.5 MWth	^{233}U molten fluoride salt	-
	Shippingport	LWBR PWR	1977 - 1982	100 MWe	Th+^{233}U pellets	HEU and Pu drivers investigated for ^{233}U production, Th/^{233}U seed/blanket operation demonstrated
	Indian Point 1	LWBR PWR	1962 - 1980	285 MWe	Th+^{233}U pellets	-
	Borax IV	BWR	1963 - 1968	2.4 MWe	Th+^{235}U pellets	-
	Elk River	BWR	1963 - 1968	24 MWe	Th+^{235}U pellets	-
India	KAMINI	MTR	In Operation	30 kWth	(Th+^{233}U)Al rod	-
	CIRUS	MTR	In Operation	40 MWth	(Th+^{233}U)Al rod	Th and Th/Pu test fuel rods irradiated up to 18000 MWd/t
	DHRUVA	MTR	In Operation	100 MWth	(Th+^{233}U)Al rod	-
	KAPS 1&2	PHWR	In Operation	220 MWe	ThO_2 pellets	-
	KGS 1&2	PHWR	Planned (Future)	220 MWe	ThO_2 pellets	-
	RAPS 2,3,4	PHWR	Planned (Future)	220 MWe	ThO_2 pellets	-
	FBTR	LMFBR	In Operation	40 MWth	ThO_2 blanket	-
UK	Dragon	HTGR	1966 - 1973	20 MWth	Th+^{235}U TRISO	Thorium fuel elements with a 10:1 Th:HEU ratio, 741 EFPD at 240 MWth (950 Celsius helium outlet temperature)
Germany	AVR	HTGR	1967 - 1988	15 MWe	Th+^{235}U TRISO	~121000 hours of operation with Th-based fuel, ~300000 fuel pebbles containing 1360 kg of Th, maximum burnup achieved ~150 GWd/t
	THTR	HTGR	1985 - 1989	300 MWe	Th+^{235}U TRISO	675000 fuel pebbles containing Th/HEU fuel, shut down after 3 years for non-technical reasons, demonstrated industrial-scale fuel fabrication
	Lingen	BWR	1970 - 1973	60 MWe	Th+Pu test pellets	-
Canada	NRU & NRX	MTR	-	-	Th+^{235}U test fuel	-

While further irradiation testing would be needed to examine specific temperature ranges and burnup or fluence levels of interest, the experiences above seem to indicate reliable and sufficient performance for thorium fuels in the operational regimes for those reactors.

The possible advantages offered by a thorium fuel cycle, some of which have been demonstrated to various levels while others remain entirely conjecture at this point, seem to warrant additional research into whether thorium should be utilized as a nuclear fuel and how best to do so. Numerous challenges related to thorium fuel cycles exist, with many known questions unanswered and many new questions yet unasked, but the possible rewards for a successful effort to more extensively utilize thorium for energy production appear to significantly outweigh the risks of ignoring this option.

3.1.2 System Description

The basic description of a thorium-fueled hybrid LIFE engine has already been given in Section 1.1.3; a spherical fusion chamber is surrounded and cooled by a lead-lithium first wall coolant, which is in turn surround by a fission blanket containing a packed bed of graphite pebbles containing TRISO fuel particles that is cooled by flibe flowing radially outward through the region.

Table 3.3 provides details for the composition, densities, and physical dimensions of each region for a typical thorium-fueled hybrid LIFE engine. Previous work describes more explicitly the reasons for some of the choices of materials and densities [49, 50]. Tritium breeding in a LIFE engine occurs primarily through (n,T) reactions with ^{6}Li in the flibe and LiPb coolants. Controlling the isotopic ratio of ^{6}Li to ^{7}Li in each coolant governs the production rate of tritium and the resulting Tritium Breeding Ratio (TBR), which expresses the ratio of tritium production divided by tritium consumed by fusion, and the fission power.

Table 3.3: Radial Build for a Representative Thorium-fueled Hybrid LIFE Engine.

Component	**Material**	**Density [g/cm^3]**	**Thickness [cm]**
Fusion Chamber	Xe Fill Gas	6.5×10^{-6}	250 (radius)
Armor	Tungsten	19.3	0.025
First Wall (FW)	ODS steel	8.0	0.275
FW Coolant	LiPb	9.4	3
Injection Plenum	FLiBe	2.0	3
Multiplier	60% Be 40% FLiBe	1.94 2.0	20
Fission Blanket	60% Fuel 40% FLiBe	- 2.0	104.9
Reflector	60% Graphite 40% FLiBe	- 2.0	125

The multiplier region consists of beryllium (Be) pebbles in flibe coolant and accomplishes both tritium breeding and neutron multiplication through (n,2n) reactions of fast neutrons (mostly E > 2.7 MeV) and ^{9}Be. The fission blanket uses TRISO fuel particles randomly packed into 2cm diameter graphite pebbles at a 15% packing fraction with design parameters as specified by Table 3.4. TRISO particles themselves have already been described in detail in Section 1.1.1 as well as Section 2.1. It should be noted that multiple values for TRISO packing fraction and beryllium multiplier layer thickness are used during the course of this work and at times values are well outside the range of parameter values considering during previous thorium LIFE design studies.

Table 3.4: Design Parameters for Thorium-fueled LIFE TRISO Particles.

Layer	**Density** [**g/cm^3**]	**Thickness** [μ**m**]
Kernel (ThCO)	10.0	600 (diameter)
Buffer	1.0	100
IPyC	1.9	40
SiC	3.2	45
OPyC	1.9	40
Matrix (graphite)	1.7	-

Existing analyses assume the graphite pebbles to be pure graphite with a fueled radius of 0.99cm and a 0.01cm pure graphite shell on the outside. Future analyses may examine whether a different coating or shell would have to be put on the fuel and reflector pebbles to mitigate possible corrosion or mechanical erosion issues, and time-dependent buoyancy concerns may need to be addressed in the future by looking at adding weigh to the center of pebbles or pebble coatings.

This work focuses exclusively upon the fission blanket aspects of a hybrid LIFE engine; the fusion part of the engine acts as a high energy neutron source and provides some of the overall system power but no design studies are being performed varying any of the parameters of the fusion system. In addition, the material selection and component sizing studies performed in the past are generally being left untouched [48, 49, 50]; this means that parameters such as the operating temperature of the engine, fusion and overall system power levels, fuel pebble sizing, initial lithium enrichments, and selection of materials such as lithium-lead and flibe as the coolants are not going to be re-evaluated. While good arguments can and have been made regarding revisiting some of these decisions as other design features and mission objectives shift, such considerations are outside of the scope of this work.

3.1.3 Operational Approach

Previous publications describing the neutronic design of hybrid LIFE engines with fertile fuels characterized in great detail the three main phases of operation: ramp-up, plateau, and

incineration [49, 51, 57]. During ramp-up, fertile fuels are transformed into fissile fuels (e.g., ^{232}Th becomes ^{233}U or ^{238}U becomes ^{239}Pu) and total system power increases from a value just above the fusion power (500 MW_{th}) to full system power (2000 MW_{th}). The plateau phase involves continued conversion of fertile fuels into fissile fuels and sustained operation within the plateau power range; system power level is controlled using ^{6}Li as a neutron poison early in life and then using excess tritium to maintain system power later in life. The incineration phase involves operation at a reduced power level so that fusion neutrons can be used more extensively for tritium production and heavy metal transmutation. Figure 3.1 provides an illustration of how operational controls can be used in a LIFE engine to flatten the power profile of the system over time and thus enable better performance for the balance of plant (BOP) systems, which are largely designed and sized for the peak temperatures and power levels they will experience [51]. The "rep rate" control scheme shown reduces system power at time of peak power by reducing the repetition rate at which fusion targets are injected into the system, thus reducing fusion power and reducing the neutron source rate in the fission blanket. As illustrated in the figure, Lithium control was found to be superior to rep rate control.

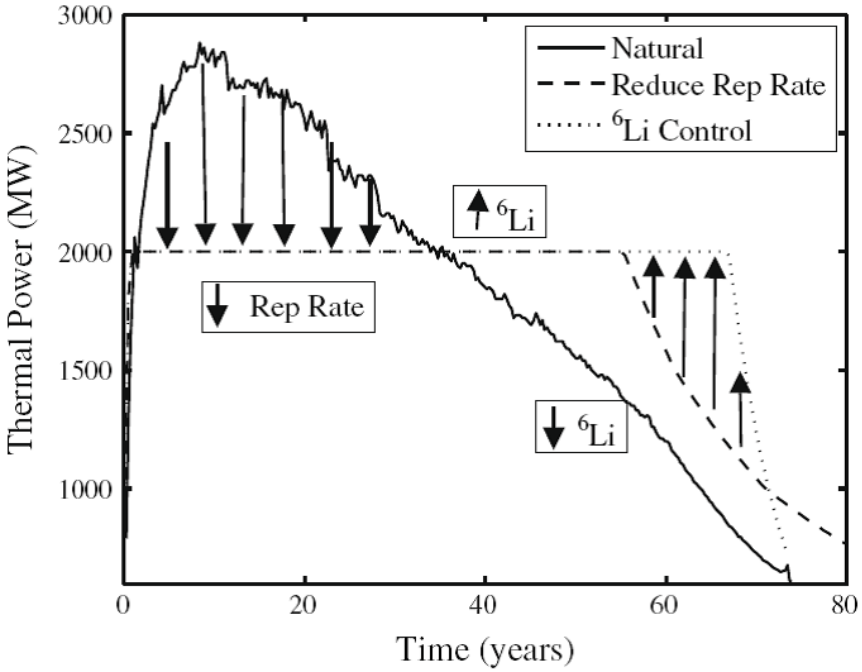

Figure 3.1: Illustration of operational approach for a depleted uranium (DU) LIFE engine requiring TBR >1.0, as reproduced from Reference [51].

For the purposes of this current work, it is assumed that lithium control is used to maintain plateau power level. The lithium used for reactivity, and thus power level, control is found in both the lead-lithium first wall coolant and the flibe molten salt coolant in the fission

blanket. The LNC control parameters used to govern LIFE operations in this study include requiring a positive tritium mass at all times (each engine must be tritium self-sufficient), maintaining a plateau power level between 2000 MW_{th} and 2020 MW_{th}, and allowing TBR to go anywhere in the range of 0.2–3.0 as long as the minimum tritium mass requirement is met.

Neutronics depletion calculations will be stopped shortly after plateau operation ends and incineration phase operation begins, on the basis that continued operation past the end of plateau (EOP) point would be unlikely to prove economically attractive for merchant generators.

3.2 MCNP Models

All radiation transport calculations in this work were performed using version 1.42.2 of MCNP5 [72] with ENDF/B-VII.0 neutron cross section source data [83]. All calculations were performed using a full blanket geometry model of concentric spheres with angled beam ports at the sides of the model to account for laser entrance [49, 52, 57].

The materials used in the MCNP model have been previously listed in Table 3.3. Structural components generally assumed the use of 12YWT ODS steel, lithium-lead was used as a first wall coolant, flibe molten salt coolant flows radially through the fission blanket region of the engine, the neutron multiplier region contains a packed bed of beryllium pebbles, and a packed bed of graphite pebbles is used in the fuel and reflector regions with TRISO particles loaded in them in the fuel region but just pure carbon pebbles used in the reflector region. Openings in ODS structural walls needed to allow radial flow of flibe coolant were accounted for by adjusting the density of the 12YWT steel from 8 g/cm^3 to 6 g/cm^3. The MCNP models assume that the materials in the system are at their actual expected operating temperatures and densities with corresponding cross sections and Doppler broadening. Scattering kernels for thermal elastic scattering were applied to carbon in all graphite pebble regions and to beryllium in the neutron multiplier region.

The burnup analyses in this study utilize an MCNP input with double-heterogeneous fuel modeling: lattice geometry is used to pack pebbles into the fuel blanket region and TRISO fuel particle kernels into each pebble. Multiple independent studies available in the literature demonstrate the importance of modeling the double-heterogeneous nature of TRISO fuel kernels in pebbles and that using a regular lattice in MCNP5 to place fuel pebbles and kernels adequately captures physics effects [84, 85]. Homogenous modeling was used for all other regions, including the neutron multiplier and reflector regions which respectively contain beryllium and graphite pebbles; previous LIFE studies investigating the effects of treating the multiplier and reflector regions as homogenous zones found the net effect in the DU system to be less than 1% difference in reaction rates. Figure 3.2 depicts the MCNP modeling used for homogenizing the neutron multiplier ("Be/Flibe") zone as well as the heterogeneity of the fuel region, with magnified views of a single pebble surrounded by flibe and kernels in the pebble matrix.

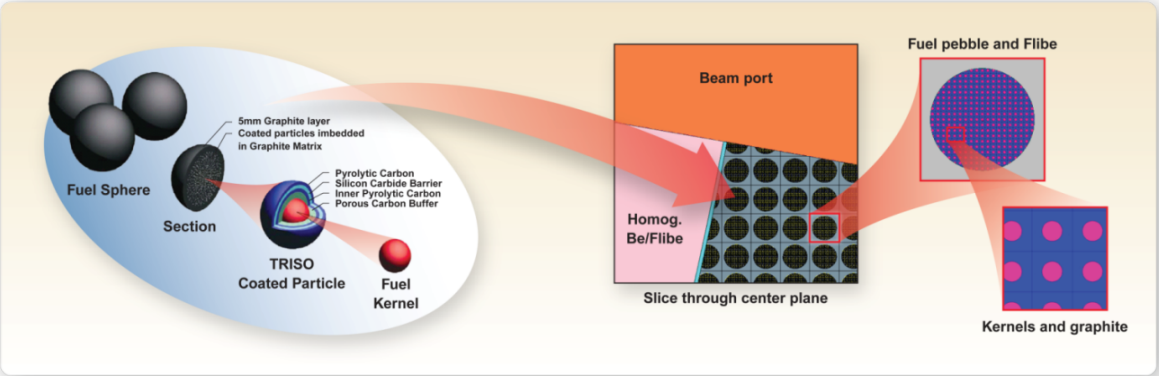

Figure 3.2: Illustration of MCNP lattice models used for fuel kernels in a pebble and pebbles in a bed in a hybrid LIFE fission blanket.

3.3 Depletion Methodologies

Past thorium LIFE analyses assumed a single burnup zone [54]; this represents a fair approximation if fuel pebbles have a short residence time during each pass in the fission blanket and are randomly mixed before being reinserted. The fuel pebble blanket region in the MNCP models used for this work was broken up into multiple flux zones for radiation transport purposes. Each of these flux regions, sized such that the maximum thickness of any one flux zone was no more than about 9cm, was modeled as a regular lattice of fuel pebbles each with a regular lattice array of fuel kernels. All of these flux regions were defined as having the same depletion material in them however, meaning that all of the fuel in the full blanket was still modeled as a single burnup zone. The end result of this approach is that detailed variations in neutron flux magnitude and spectrum and other parameters that vary with radial position in the system are captured for use in heat transfer and fuel performance modeling purposes but the effects are averaged out when running ORIGEN within MONTEBURNS to track the time-dependent composition of the fuel material. This remains a fair approximation of a system that uses relatively short pebble residence times with fully-randomized reinsertion probabilities with respect to radial position in the blanket. This system models a single fuel batch that is initially loaded and then irradiated until discharge; there is no refueling during the operation of the single batch and thus there is no equilibrium state ever reached in the system.

Careful attention was paid to how MONTEBURNS handled the depletion of a fuel material specified in the manner described above and it was confirmed that MONTEBURNS depleted a single material composition using averaged flux and cross-section values from the various MCNP flux regions.

All neutronics depletion analyses in this document were performed using a time step of 20 days in MONTEBURNS. This time step length was chosen to be short enough to

adequately capture transmutation and decay effects while being long enough to avoid large numbers of unnecessary radiation transport calculations. Variable time step schemes have been developed for use in with LNC and MONTEBURNS in hybrid LIFE blanket depletion analysis to minimize the number of radiation transport calculations needed [57] but fixed time steps were kept for the calculations in this document to simplify integration with the fuel performance model.

3.4 Integration with Fuel Performance Calculations

Some of the fundamental contributions of this work involve the development and demonstration of new methods, both conceptually and mechanically, for integrating fuel performance calculations with neutronics and heat transfer codes to help shape design processes. While other fuel performance models may have been used in the past in some capacity to guide design decisions, the focus in this work is on developing and implementing methods that enable fuel performance calculations to be routinely executed as part of a suite of analysis tools. New capabilities and conceptual understanding could be unleashed if fuel performance calculations were efficient and easy enough to be employed in such ordinary, or "mainstream", design analyses on a regular basis.

In the past, most nuclear engineering projects have operated as a collection of somewhat segregated and distinct disciplines (e.g., neutronics or reactor physics, thermal-hydraulics, and materials). This "stove-piped" organizational structure, which has often been dominated by a single discipline such as neutronics, has led to design optimization studies which are likewise segmented and only give full weight to one discipline's interests. This method of design process, referred to as "Method 1", is illustrated below in Figure 3.3.

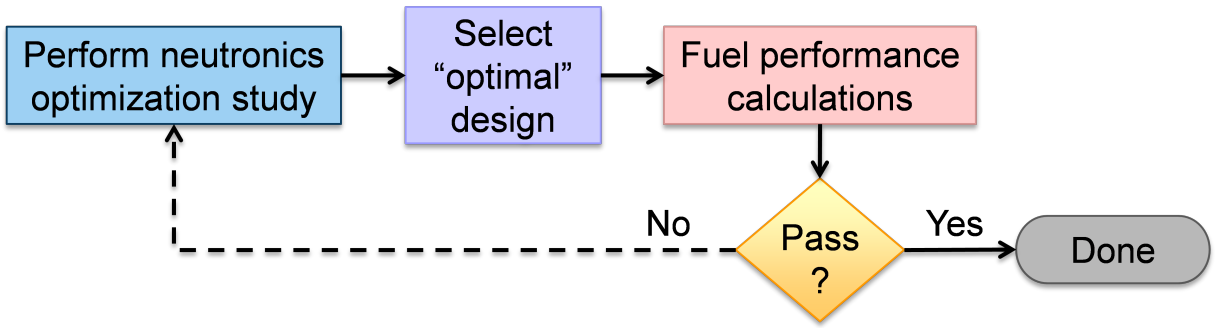

Figure 3.3: Flow diagram illustrating a design optimization process that follows Method 1.

As shown, the "Method 1" design optimization process begins with a full neutronics optimization study during which there is likely some limited iteration to ensure that thermal-hydraulics concerns are adequately addressed. The results of this neutronics optimization study are then fed into fuel performance calculations, which are largely performed to simply answer the question of whether or not the existing design meets any defined fuel performance

constraints. If the answer is no, then some additional neutronics work will be done with some attention to how the fuel performance shortcomings might be addressed. If the answer is yes, however, it is likely that the design would simply be accepted as is with no thought given to any performance margin that may have existed. While this satisfies the requirement to understand the expected fuel performance of the chosen concept, it does not provide feedback to the design process on ways the design could be changed to increase system performance while maintaining acceptable fuel performance. This "post-processing only" approach of Method 1 can be improved by integrating a TRISO FPM into a code package to allow for comprehensive use of fuel performance calculations in a broader range of calculations as part of a parametric or optimization study. This integrated approach, referred to as "Method 2", offers a path to significant improvements in the understanding and overall design performance of advanced nuclear energy systems where the performance of TRISO fuel fundamentally impacts the overall system design. Hybrid LIFE engines offer a very relevant and worthwhile application for a Method 2 design process, with Figure 3.4 illustrating a possible benefit of this integrated approach to parametric or optimization studies.

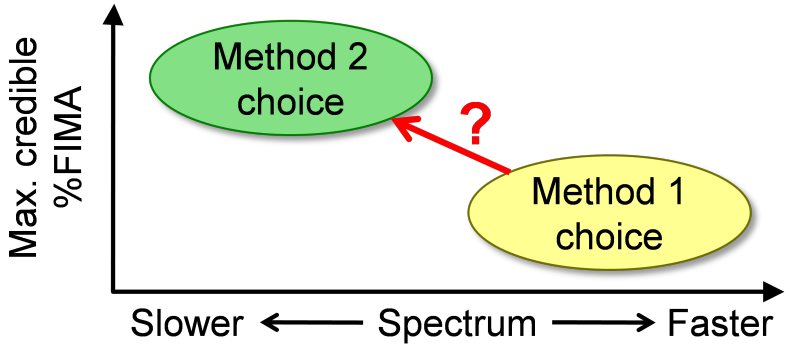

Figure 3.4: An illustration of possible benefits of integrating fuel performance calculations into the design process.

This improved, integrated approach better supports systems-level approaches to design optimization by providing design performance metrics and results from more than one discipline for consideration in trade-off studies. While this current work includes neutronics and fuel performance, other factors such as economic factors (e.g., Levelized Capital Costs [$/kW] or projected Cost of Electricity [¢/kWh]) or safety goals could also be included. The overall shift, then, is from a Method 1 approach of optimizing a system design based upon a single discipline's perspective to a Method 2 approach which could incorporate and balance multiple competing criteria when searching for an optimal system design.

3.4.1 Heat Transfer Analysis

Python scripts were created and modified to extract output parameters from the results of neutronics depletion analysis; parameters including cell volumes and masses, MCNP tallies tracking zone-dependent fission rates and neutron fluxes, Xe and Kr fission product inventories, and MCNP neutron and photon energy deposition tallies in various cells of interest all needed to be parsed from the various neutronics input and output files.

After parsing all of the required data from the neutronics results, energy deposition tallies and cell volumes were combined to estimate volumetric heating [W/cm^3] in the neutron multiplier and reflector regions and as a function of radius within the fuel blanket region. A MathCAD model created by Abbott [50] to perform heat transfer calculations in a LIFE blanket, using these volumetric heating terms along with blanket geometry information, produced zone-averaged temperatures for the fuel pebble surface and center in each of the flux regions defined in the MCNP neutronics model.

3.4.2 Simulating lifetime irradiation histories for a batch of particles

Different types of expected irradiation environments and operational modes require different methods for simulating the conditions a batch of TRISO particle would be expected to see during their lifetime. Irradiation experiments, pebble bed systems which simulate an equilibrium condition with continuous fuel mixing and refueling, and pebble bed systems which assume a single batch of fuel irradiated with continuous mixing but no refueling all require very different modeling approaches for fuel performance predictions.

Irradiation experiments generally have very simple and clear specifications for parameters such as particle power levels, fast fluence accumulation, irradiation temperature, and other parameters needed as input data for fuel performance calculations [68, 69]. In many such cases, the conditions that specific particles in a population are exposed to during irradiation may vary for certain parameters (e.g., internal heat generation will vary according to the sampled fuel kernel diameter) while remaining constant for others (e.g., irradiation temperature and fast fluence). This simplifies fuel performance modeling by limiting the number of off-nominal variations from the nominal specified conditions.

Pebble bed systems which simulate an equilibrium operation condition due to continuous fuel mixing and refueling represent a higher level of complexity in fuel performance modeling. Parameters such as particle power that vary in an irradiation experiment will again likely vary, but new variations will occur as well, such as particle power and fast neutron flux varying due to changes in axial position during pebble flow [28, 36]. The equilibrium operation assumptions still simplify matters, however, by generally removing any burnup or time dependence from parameters such as the neutron flux level and spectrum. Once the equilibrium condition is determined, a single neutronics calculation can yield the expected neutronics input parameter values that particles would then experience at all times and in most locations in the system.

Pebble bed systems which assume a single batch of fuel irradiated with continuous mixing but no refueling, such as the thorium LIFE system in this study, add multiple new levels of complexity. In addition to variations in particle-specific parameters such as particle power due to a distribution of kernel diameters and position-dependent variations in parameters such as particle power and fast neutron flux, many parameters such as fast neutron flux and fission rate will also begin to vary according to the batch-average burnup level of the fuel material itself. The LIFE system brings specific additional complexities, given that it is a source-driven subcritical system with strong dependencies on radial position within the fuel blanket for parameters such as fission rate, fast neutron flux, and temperatures that far exceed the variations seen in most large critical fission reactor systems.

In an effort to address all of these issues and ensure the highest possible accuracy in simulating TRISO particle lifetime histories for fuel performance calculations, a module has been developed and integrated into TRIUNE that samples the geometry and composition of a TRISO particle along with its radial position in a fuel pebble and then builds a lifetime history for that particle that simulates repeated passes through a LIFE fission blanket from BOL conditions until the end of the available data read in from neutronics depletion analysis. The LIFE blanket is represented in the resultant fuel performance calculations by a blanket segmented into a number of "tracks" or zones which match the number of fuel blanket flux regions in the neutronics models. Conceptually, this overall lifetime simulation process can be thought of as a simple process of randomly inserting a fuel pebble into the LIFE blanket and then, using track-dependent information from the neutronics analysis along with a user-specified residence time (t_{res}) that states how long it takes the pebble to transit from insertion into the blanket to extraction from the blanket, tracking the accumulation and changes in relevant input parameters needed for fuel performance calculations. Some of these parameters vary more directly with time (e.g., fast flux) while others (e.g., fission product inventories) vary more directly with burnup level. This insertion and parameter update process is repeated for a single simulated TRISO particle inside a fuel pebble until the irradiation time matches the time simulated in the neutronics analysis, and then is repeated for each simulated TRISO particle requested for TRIUNE fuel performance calculations.

The computational procedure used to simulate TRISO particle lifetime histories is detailed in Appendix A. This particle lifetime history simulation procedure in TRIUNE currently assumes an instantaneous reinsertion of a fuel pebble back into the fuel blanket upon discharge; in reality, there might be a "cooling period" where the pebble is exposed to lower boundary temperatures and no irradiation due to in-service inspections or operational constraints such as pebble transportation and insertion/discharge limitations. The procedure defined above could easily be modified to include cooling periods after each pass through the blanket or even on regular or random intervals if it is thought that blanket operations would pull a pebble on fixed intervals or randomly select pebbles for inspection or other processes as they go through.

Chapter 4

Design Study Application

This chapter defines the goals and approach of the integrated self-consistent thorium LIFE engine design studies, defines the performance metrics used to assess the results of neutronics and fuel performance analyses in the study, and then provides the results of the study with some discussion of how to interpret them. Chapter 6 provides a more detailed analysis of the results and states conclusions that arise from the parametric study.

4.1 Goals and Approach

The primary goal of this parametric design study lies in providing a proof-of-principle demonstration of the importance and impact of integrating fuel performance calculations into LIFE blanket design optimization and system-level trade-off studies. This specific parametric study covered a broad possible design space for a thorium-fueled LIFE engine and thus accomplished the second goal of identifying a reasonable recommended design for a thorium-fueled hybrid LIFE engine. The first goal represents a more fundamental conceptual and methodological accomplishment while the second goal offers specific benefit to the LIFE project at LLNL but with perhaps some aspects that could be extrapolated to other source-driven systems or thorium-fueled systems.

Figure 4.1 illustrates the integrated design and analysis process used during this work. For each desired set of design parameters, a neutronics depletion analysis was performed using the MONTEBURNS and LNC codes. The results from the neutronics depletion were fed into heat transfer calculations and, combined with temperature distributions from the heat transfer code, enabled the fuel performance calculations. After mapping the full design space of interest with regard to both neutronics performance and fuel performance, an "optimal" case was selected from the cases analyzed to serve as a baseline recommended thorium LIFE design in subsequent sensitivity ("design") studies. It is important to note that the recommended design is not truly "optimal" in the mathematical sense of the word; rather, it represents the best choice of the particular parameter sets evaluated in this study.

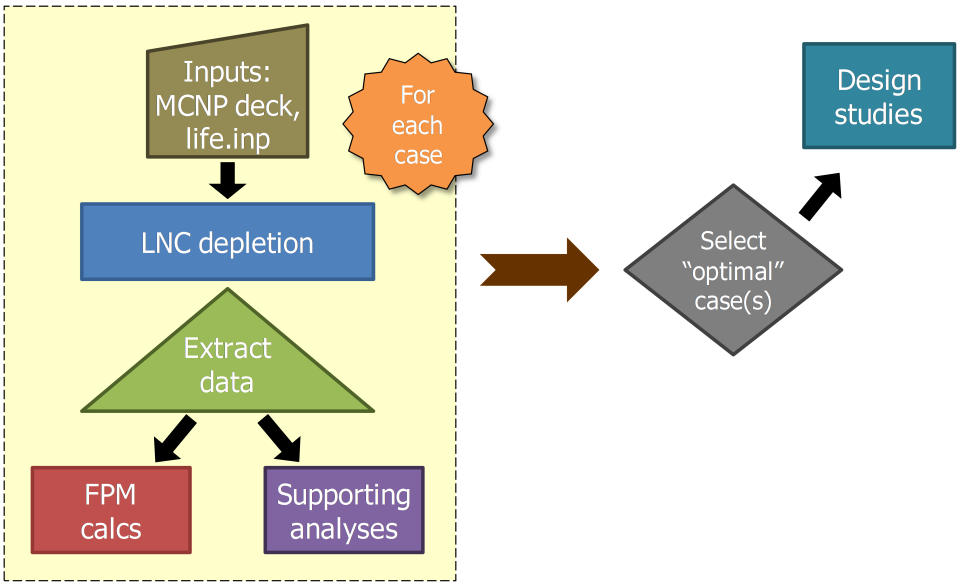

Figure 4.1: An illustration outlining the integrated process used for this work.

The parametric study was performed assuming a 500 MW_{th} fusion engine with a total system power of 2000 MW_{th} during plateau operation and the LIFE engine was required to be tritium self-sufficient. Past efforts in both depleted uranium (DU) and thorium LIFE systems examined the sensitivity of the design performance to various parameters [51, 53, 54]; this study focused on varying the TRISO packing fraction within fuel pebbles along with the beryllium neutron multiplier layer thickness. The TRISO packing fraction was evaluated over the range of 5% to 40% in 5% increments while the beryllium neutron multiplier layer will be evaluated over the range of 5cm to 30cm in 5cm increments with an extra 8cm thickness option added due to the system sensitivity in that range of multiplier thickness. While past studies focused on large 40 metric ton fuel loadings [54], this study evaluated 10 metric ton and 20 metric ton design options. These smaller system sizes reach discharge burnup within more reasonable time frames than the extremely long irradiation times found in the larger systems, which is desirable because shorter irradiation times should enable faster and cheaper fuel qualification.

Establishing the number of particles to simulate for fuel performance calculations

One of the most important input variables in TRISO fuel performance models that use Monte Carlo techniques to predict a failure fraction of a batch of TRISO particles undergoing irradiation is the number of particles to simulate during the calculations. Increasing the number of simulated particles decreases stochastic uncertainty and allows for a more complete sampling of the effects of as-manufactured parameters (e.g., manufacturing variations in kernel diameter or SiC thickness) and possible combinations of variations in as-manufactured

parameters; however, increasing the number of simulated particles also proportionally increases the overall number of calculations that must be performed, which leads to longer calculation times and increased memory requirements to store larger arrays. Given this important balance of getting worthwhile results while also ensuring reasonable run times and memory requirements, a high priority was given to establishing a reference value for the number of particles to simulate during TRIUNE fuel performance calculations performed for this work before performing the calculations needed to examine the parametric system design study. In order to select a reference value for the number of particles to simulate, fuel performance calculations were run using various numbers of simulated particles for a representative case with an initial loading of 20MT of thorium, a multiplier layer thickness of 20cm, and a TRISO packing fraction of 15%. The resulting curves for predicted TRISO particle failure fraction as a function of batch average burnup in the blanket are shown in Figure 4.2 for several different numbers of simulated particles. It must be noted that these curves were generated using Weibull parameter values significantly different than the Weibull parameter values established as the default values for TRIUNE and thus the predicted failure fractions do not match those found in the main results from the parametric study.

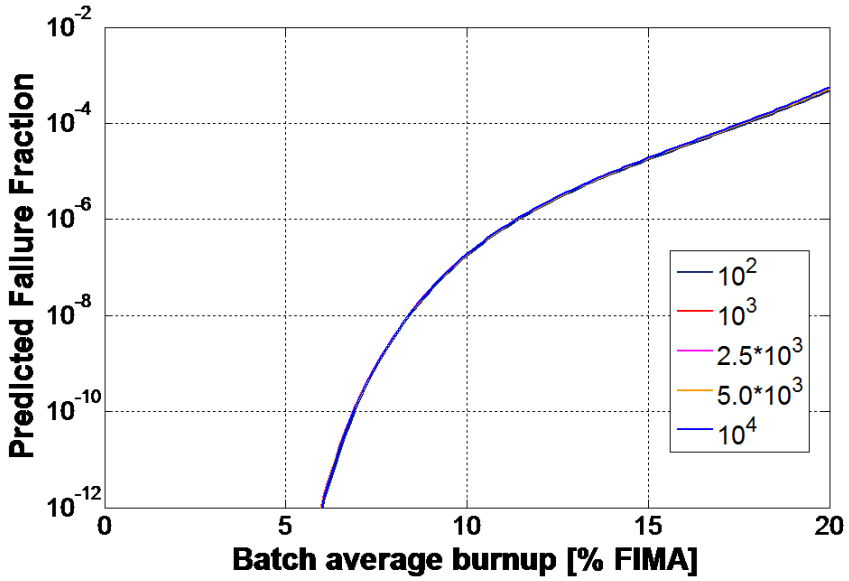

Figure 4.2: Predicted failure fraction as a function of batch average burnup for fuel performance calculations using several different numbers of simulated particles.

It is hard to distinguish between the different curves because they all lie nearly on top of one another. While this seems to indicate very little difference between the different results, a more precise measure can be used for a detailed analysis of the impact that the number of simulated particles has on the achievable burnup. Direct estimations of the achievable burnup of the system can be made by using MATLAB to interpolate on the vectors that contain batch average burnup and predicted failure fraction and estimate the burnup value at

which the curves cross the 10^{-4} failure limit. Table 4.1 shows both the estimated achievable burnup value and the time required for the full fuel performance calculation using each number of simulated particles.

Table 4.1: Calculation time requirements and calculated burnup values for different numbers of simulated particles.

Number of Particles	**Time [min]**	**Burnup [% FIMA]**	**Fractional Run Time**	**Relative Burnup Difference**
1.0×10^2	1.20	17.7827	0.9%	1.0%
1.0×10^3	11.94	17.5166	8.5%	-0.5%
2.5×10^3	30.79	17.5453	21.8%	-0.4%
5.0×10^3	65.86	17.5906	46.7%	-0.1%
1.0×10^4	141.03	17.6097	100.0%	0.0%

These burnup values show some actual differences brought about by varying the number of simulated particles but also contain stochastic noise. To investigate the amount of stochastic noise in the calculations, a simple study was performed wherein the achievable burnup was estimated eight separate times using fuel performance calculations with 2.5×10^3 particles. The resulting population statistics look reasonable in that the mean estimated achievable burnup was 17.60% FIMA with a relatively low standard deviation of 0.03% FIMA, which represents a standard deviation that is only 0.18% of the mean value. It should be noted that the estimated burnup value does not need to be incredibly precise because uncertainties in material properties and neutronics input and other sources of error overshadow small differences in estimated achievable burnup, so the low standard deviation of this study should be sufficiently small to produce statistically meaningful differences between estimated achievable burnup values from cases that used different system design parameter values.

Overall, given the results shown in Table 4.1 and the population statistics discussed in the previous paragraph, using 2.5×10^3 as the reference number of simulated particles in TRIUNE fuel performance calculations appears to provide a good balance of speed and accuracy for the calculations involved in this current work. Lower numbers of particles (e.g., 1.0×10^3) might also be reasonable, and higher numbers of particles would certainly be good because it would cut down on stochastic noise and allow for sampling more combinations of random variables, but the half hour run time of 2.5×10^3 particles is reasonable and the results appear stable enough to use. Any future studies using a significantly different system design that the TRISO particles are irradiated in, or significantly different estimates for manufacturing parameters such as mean values and standard deviations, should consider repeating this type of study to determine the number of simulated particles needed for reliable and efficient TRIUNE fuel performance calculations for their own application.

Heat transfer calculations

The temperature at the outer boundary of the TRISO particle (T_{bound}) is determined by the pebble surface temperature, the pebble center temperature, and the radial position of the TRISO particle within the pebble along with the radial temperature distribution within the pebble. Variations in T_{bound} due to burnup and $r_{blanket}$ needed to investigated and quantified in order to properly model temperatures for fuel performance calculations. Temperature distributions were calculated using the neutronics results from a representative thorium LIFE engine at the time of peak fissile mass and end of plateau (EOP) as input for the MathCAD model described in Section 3.4.2. Using 25 W/m-K as the effective thermal conductivity of the fuel pebbles yields Figure 4.3, which shows the temperature distributions at time of peak fissile content (19.2 %FIMA) and EOP (61.5 %FIMA). Using 35 W/m-K as the effective thermal conductivity of the fuel pebbles yields Figure 4.4, which shows the resulting temperature distributions of the system at the time of peak fissile content and EOP.

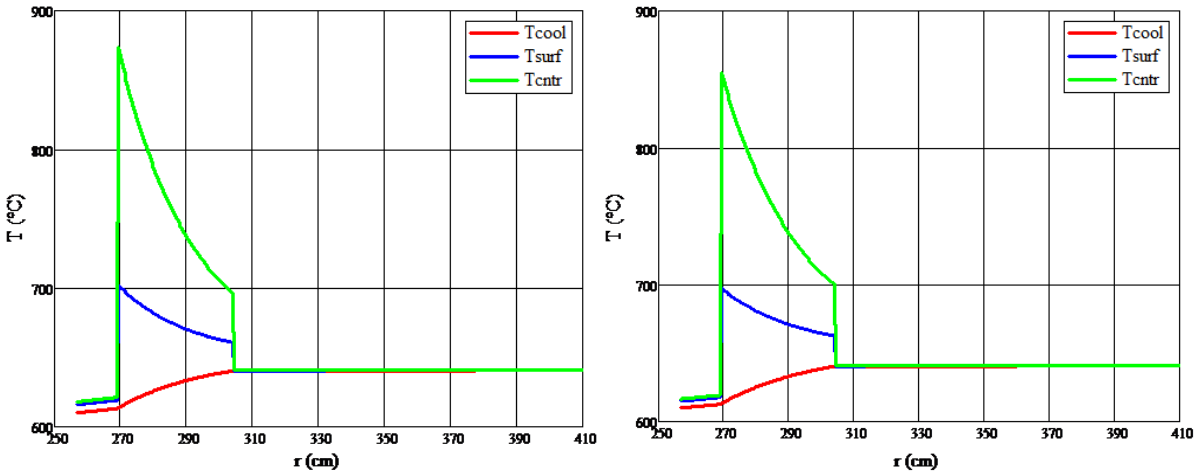

(a) (b)

Figure 4.3: Temperature of pebble center (Tcntr), pebble surface (Tsurf), and flibe coolant (Tcool) as a function of blanket radius for a representative system with k_{pebble}=25 W/m-K at (a) time of peak fissile content, and (b) end of plateau (EOP).

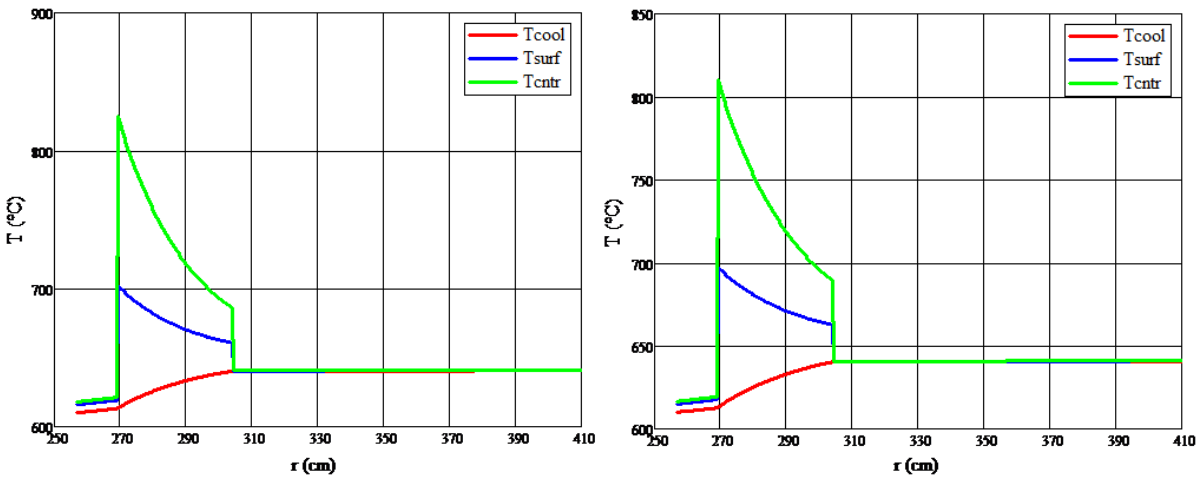

(a) (b)

Figure 4.4: Temperature of pebble center (Tcntr), pebble surface (Tsurf), and flibe coolant (Tcool) as a function of blanket radius for a representative system with k_{pebble}=35 W/m-K at (a) time of peak fissile content, and (b) end of plateau (EOP).

Table 4.2 and Table 4.3 show the results using k_{pebble}=25 W/m-K and k_{pebble}=35 W/m-K, respectively. They focus on specific effects arising from time/burnup dependence and radial position, while Table 4.4 focuses on the effect that using different assumed values for pebble thermal conductivity has on the fuel pebble center temperature.

Table 4.2: Summary of key temperature calculation results at the time of peak fissile material ("peak") and end of plateau ("EOP") for the inner and outer radius of the fueled region of the blanket with k_{pebble}=25 W/m-K.

Radial Position	**$T_{coolant}$ [°C]**	**$T_{pebsurface}$ [°C]**	**$T_{pebcenter}$ [°C]**
r=269.2cm	613.3 (peak)	702.5 (peak)	873.9 (peak)
(inner)	612.8 (EOP)	697.4 (EOP)	855.0 (EOP)
r=303.685 cm	640.1 (peak)	660.7 (peak)	696.5 (peak)
(outer)	640.2 (EOP)	662.6 (EOP)	700.3 (EOP)

Table 4.3: Summary of key temperature calculation results at the time of peak fissile material ("peak") and end of plateau ("EOP") for the inner and outer radius of the fueled region of the blanket with k_{pebble}=35 W/m-K.

Radial Position	$\mathbf{T_{coolant}}$ [℃]	$\mathbf{T_{pebsurface}}$ [℃]	$\mathbf{T_{pebcenter}}$ [℃]
r=269.2cm	613.3 (peak)	702.5 (peak)	824.9 (peak)
(inner)	612.8 (EOP)	697.4 (EOP)	810.0 (EOP)
r=303.685 cm	640.1 (peak)	660.7 (peak)	686.3 (peak)
(outer)	640.2 (EOP)	662.6 (EOP)	689.5 (EOP)

Table 4.4: Summary of key temperature calculation results highlighting variations due to different values for graphite thermal conductivity.

Radial Position	$\mathbf{k_{pebble}}$**=25 W/m-K** $\mathbf{T_{pebcenter}}$[℃]	$\mathbf{k_{pebble}}$**=35 W/m-K** $\mathbf{T_{pebcenter}}$[℃]
r=269.2cm	873.9 (peak)	824.9 (peak)
(inner)	855.0 (EOP)	810.0 (EOP)
r=303.685 cm	696.5 (peak)	686.3 (peak)
(outer)	700.3 (EOP)	689.5 (EOP)

An analysis of these results yields several important conclusions. First, as illustrated in Table 4.2, there exists only a very weak burnup-dependence of the temperature distributions during plateau power operation; for example, results for k_{pebble}=25 W/m-K show changes of only 0.5℃, 5.1℃ and 18.9℃ for the coolant and pebble surface and center temperatures at the inner radius of the fueled region of the fission blanket. Second, Table 4.2 also shows that the temperatures vary drastically with radial position. The corresponding differences in coolant and pebble surface and center temperatures going from the inner radius to the outer radius of the fueled region of the blanket at the time of peak fissile mass are 26.8℃, 41.8℃, and 177.4℃. Finally, Table 4.4 indicates a clear sensitivity of system temperatures to the value assumed for pebble thermal conductivity; 25 W/m-K and 35 W/m-K are both reasonable values for the effective thermal conductivity of the pebble but result in a difference in predicted pebble center temperature at the inner fuel blanket radius of 49℃ at the time of peak fissile mass and 45℃ at EOP.

Based upon the results and conclusions described above, fuel performance calculations described in this work will use temperatures derived from a single radial temperature distribution generated at the time of peak fissile mass (using k_{pebble}=25 W/m-K) for all burnup values unless otherwise stated. This approach captures the dominant radial dependence of blanket temperatures while neglecting the contributions from burnup dependence, which should have a negligible impact on fuel performance calculations given that the burnup-dependent temperature variations were on the order of 1–10℃. Each

system design option (i.e., each unique neutronics depletion analysis) will have its own heat transfer calculation performed to generate temperature distributions specific to that particular geometry and layout.

4.2 Performance Metrics

The main performance metrics used for analyzing the results of this parametric study include the time to plateau (TTP) and End of Plateau (EOP) burnup calculated during neutronics depletion analysis. In addition, the "maximum credible burnup" from the fuel performance calculations, defined as the batch average burnup level at which the predicted failure fraction crosses the 10^{-4} design limit, will also be used. These performance metrics will be mapped over the full design space to allow for discussion and understanding of the results along with the selection of a recommended blanket design, with specific emphasis on contrasting the EOP burnup from neutronics analysis and the maximum credible burnup from fuel performance analyses.

4.3 Results

This section reports the results obtained from the parametric study performed for a thorium-fueled LIFE blanket. Neutronics depletion analyses are reported as well as corresponding TRIUNE fuel performance predictions. Chapter 6 provides a more detailed analysis and discussion of the results.

The first results shown are for a thorium-fueled LIFE blanket design with an initial fuel load of 20 metric tons (MT). The results are formatted as contour maps showing a performance metric (e.g., EOP burnup) as a function of two variables (neutron multiplier thickness and TRISO packing fraction). Regions that are shaded gray indicate that plateau operation was never achieved in that region of the design space, as is indicated by the simple annotation "No plateau operation". Figure 4.5 displays the TTP (the number of years needed to reach plateau power) as a function of TRISO packing fraction and multiplier layer thickness. Large values of time to plateau (TTP greater than 5 years or so) indicate a design never reached plateau. Figure 4.6 displays the EOP burnup calculated using the LNC and MONTEBURNS codes. Finally, Figure 4.7 displays the maximum credible burnup calculated by the TRIUNE fuel performance model for each set of design parameters.

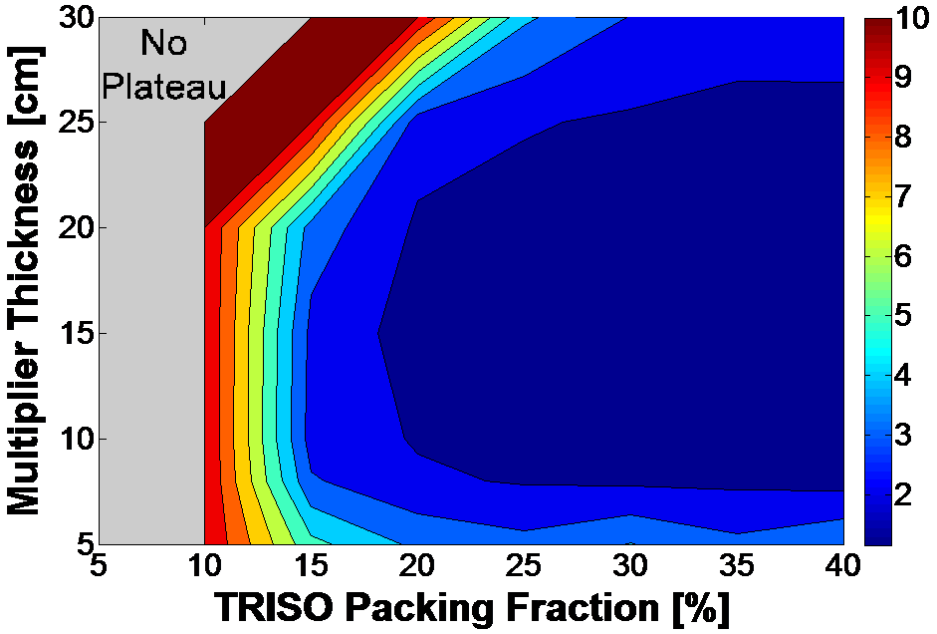

Figure 4.5: Time to Plateau (TTP) [years] as a function of TRISO packing fraction and neutron multiplier thickness for an initial fuel loading of 20MT of thorium.

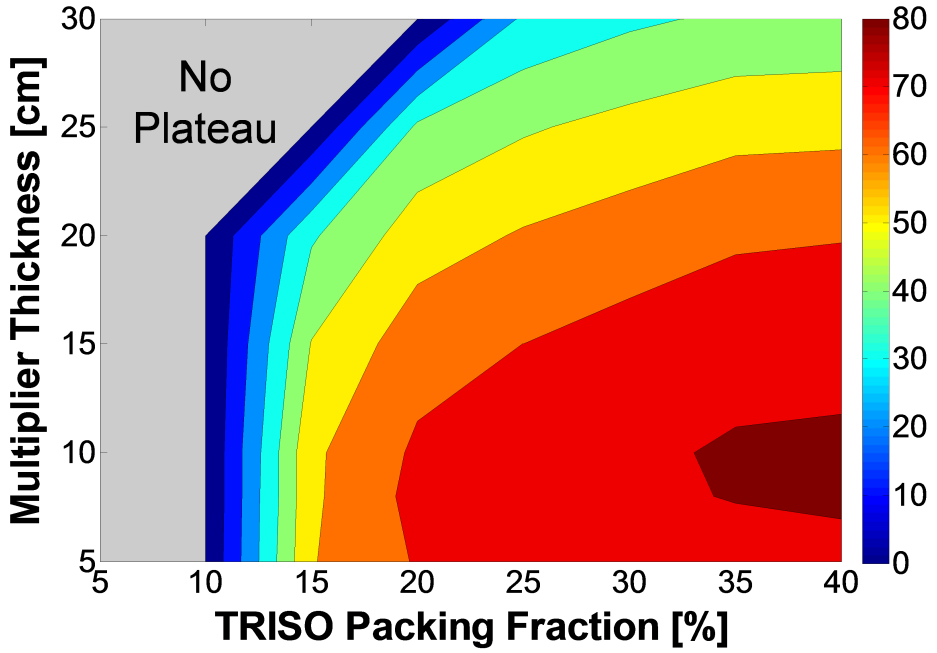

Figure 4.6: EOP burnup [%FIMA] from neutronics analysis as a function of TRISO packing fraction and neutron multiplier thickness for a 20MT initial thorium load.

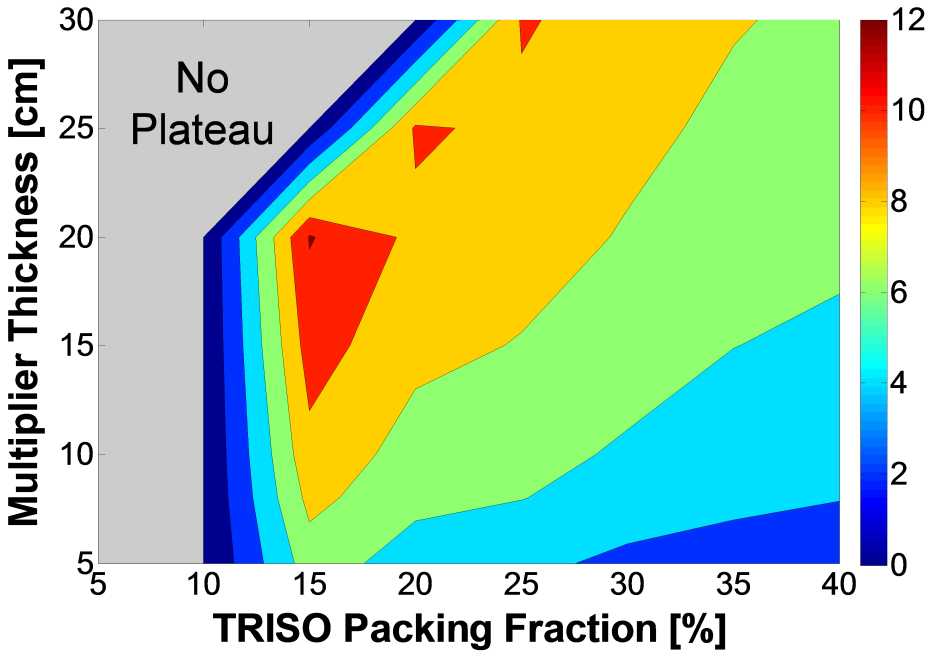

Figure 4.7: Maximum credible burnup [%FIMA] predicted by TRIUNE fuel performance calculations as a function of TRISO packing fraction and neutron multiplier thickness for a 20MT initial thorium load.

The same process performed for the 20MT thorium study was repeated for a 10MT system. Figure 4.8 and Figure 4.9 display the neutronics depletion results for time to plateau (TTP) and end of plateau (EOP) burnup for each case. Figure 4.10 presents the maximum credible burnup calculated by TRIUNE for each 10MT system design possibility considered.

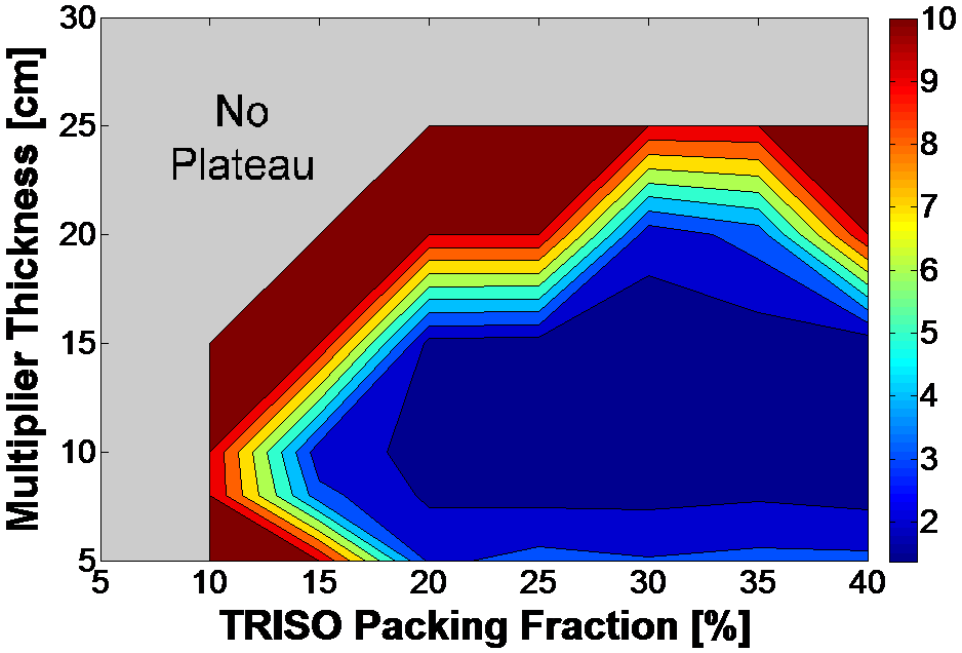

Figure 4.8: TTP [years] as a function of TRISO packing fraction and neutron multiplier thickness for a 10MT initial thorium load.

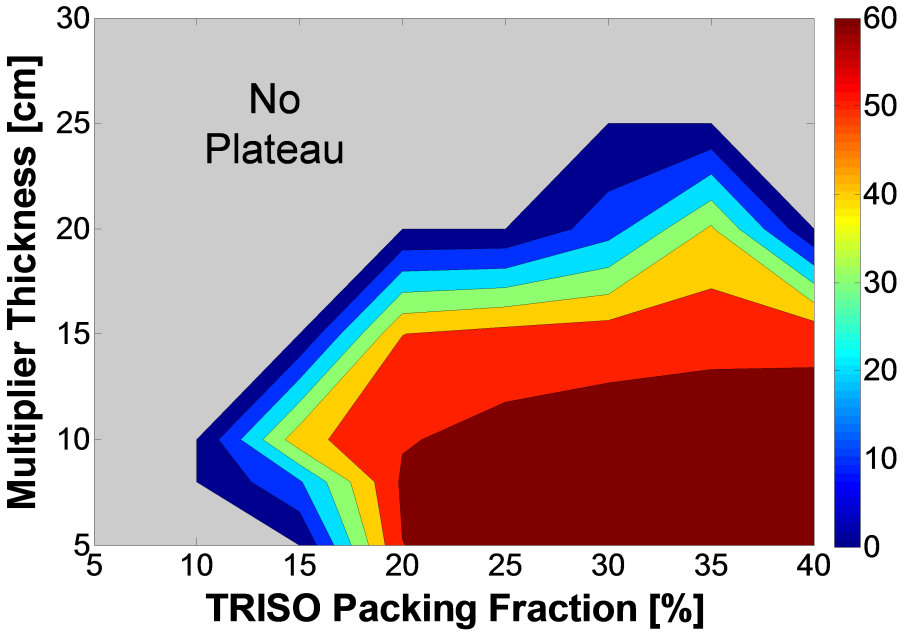

Figure 4.9: EOP burnup [%FIMA] from neutronics analysis as a function of TRISO packing fraction and neutron multiplier thickness for a 10MT initial thorium load.

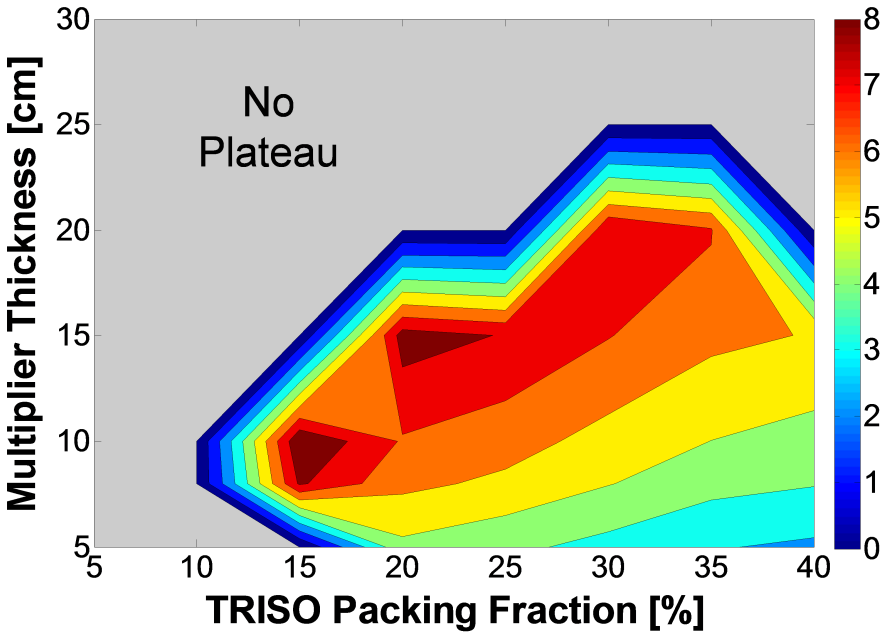

Figure 4.10: Maximum credible burnup [%FIMA] predicted by TRIUNE fuel performance calculations as a function of TRISO packing fraction and neutron multiplier thickness for a 10MT initial thorium load.

A quick comparison of the 10MT and 20MT design options indicates that the 20MT system appears superior in both end of plateau burnup level in the neutronics analyses (69 %FIMA for the 10MT system and 81 %FIMA for the 20MT system) and maximum achievable burnup in the fuel performance analyses (just over 8 %FIMA for the 10MT system compared to just over 12 %FIMA for the 20MT system). This mass-dependence indicates that future studies should consider larger (30–40MT) system sizes; however, for the purposes of the rest of this work the 20MT thorium LIFE system will be used as a reference point because it demonstrated more flexibility in workable design space and achieved higher end of plateau burnup values as well as higher maximum credible burnup values from TRIUNE predictions. It is worth noting that the 10MT system had significantly shorter service lifetimes for fuel, which could help simplify fuel qualification processes, and the 10 MT system also demonstrated fairly short values for time to plateau over a wide range of its design space; however, these factors will be set aside in light of burnup capabilities of the 20MT system for now.

After identifying two cases of interest within the 20MT study, a design with an 8cm multiplier and 40% TRISO packing fraction ("Case 1") and a design with a 20cm multiplier layer thickness and 15% TRISO packing ("Case 2"), the calculated neutron flux per unit lethargy can be extracted from the MCNP results for the Beginning of Plateau (BOP) timestep for each of these cases. Figure 4.11 shows the results of the neutron flux spectra. These cases were chosen because "Case 1" represents the best case for EOP burnup from

neutronics depletion (80.9 %FIMA) while "Case 2" represents the best case for maximum credible burnup predicted by TRIUNE (12.1 %FIMA). Comparing these two cases should help explain why the design parameter values optimize differently for neutronic performance and fuel performance.

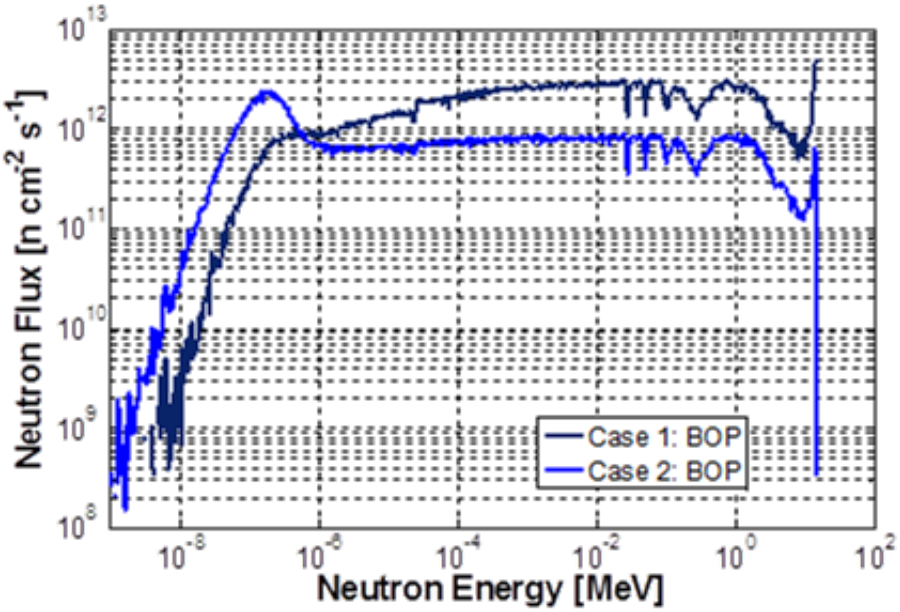

Figure 4.11: A plot showing the neutron flux per unit lethargy for two design cases of interest from the 20MT thorium-fueled LIFE blanket parametric study.

Figure 4.11 illustrates some of the same points that arise when looking at the End of Plateau burnup results (Figure 4.6) and the maximum credible burnup results (Figure 4.7). The combination of these three figures shows that the neutronic performance of the system generally optimizes for a high TRISO packing fraction (40 % or even higher) and a low neutron multiplier thickness (around 8–10cm), the maximum achievable burnup optimizes for lower TRISO packing fractions (around 15 %) and a thicker neutron multplier layer (about 20cm), and that differences in neutron flux spectra seem to be the primary underlying reason for why neutronics and fuel performance optimize for different areas of the design space. The neutron cross sections in the thorium system yield more efficient use of neutrons in a harder spectrum, as shown by the fast neutron flux for Case 1 being three times higher than the fast flux of Case 2 in Figure 4.11. This higher fast flux leads to more rapid accumulation of fast neutron fluence, which in turn means that the TRISO particles experience more radiation damage effects such as volumetric changes in the PyC layers. Figure 4.7 seems to indicate that the effects of reduced neutron efficiency due to neutron moderation in Case 2 are more than offset by the improved material performance due to the lower fast flux in Case 2, making a softer neutron spectrum better for the overall system design.

Chapter 6 contains further discussion and analysis of the results displayed above but enough analysis has already been done to establish a recommended system design. A 20MT system with a 20cm multiplier layer thickness and 15% TRISO packing fraction has been chosen as the recommended thorium-fueled hybrid LIFE blanket design because it achieved the highest maximum credible burnup (12.1 %FIMA). It operated at a system power level of 2000 MW_{th}, had a relatively soft (epithermal) neutron flux spectrum compared to design options with higher TRISO packing and thinner multiplier layers, took about 3.5 years to reach full plateau power, and was capable of an End of Plateau burnup of 38.7 %FIMA if considering just the neutronic constraints in the system design but yielded a TRIUNE-predicted maximum credible burnup of 12.1 %FIMA due to a combination of internal gas pressure and irradiation effects on the TRISO materials (especially PyC) leading to SiC pressure vessel failures. This recommended design provides a fundamental basis for subsequent work.

Chapter 5

Side Studies

A number of side studies were performed as part of this work. The first side study (Section 5.1) compared the predicted fuel performance of a depleted uranium LIFE blanket to the recommended design for a thorium LIFE blanket identified at the end of Section 4.3. The second side study (Section 5.2) involved an important sensitivity study looking at the impact of material property correlation uncertainties on expected fuel performance for the recommended thorium LIFE blanket design; this material property sensitivity study will help guide future experimental work by highlighting which important properties need additional measurements and allowing effective use of the finite amount of research funding allocated to such new experimental work. This guidance to future experimental work holds the promise of being one of the key contributions of this study. The final side study (Section 5.3) examined the sensitivity of the recommended design to changes to the user-specified pebble residence time.

5.1 Depleted Uranium (DU)-fueled LIFE Engine

Depleted uranium fuel is similar to thorium fuel, in that it is mostly a fertile material, but it contains some initial fissile content that pure thorium does not. In addition, key nuclides in DU and thorium systems have different neutron cross sections and yield different numbers of neutrons from fission reactions and thus exhibit slightly different performance [52, 53, 54]. Figure 5.1 displays some of the most important capture cross sections related to breeding fissile material from thorium and DU feed fuel. The capture cross section for ^{238}U substantially exceeds the cross section for ^{232}Th in the resonance region, which encompasses a large fraction of the neutrons in the LIFE blankets being analyzed.

Due to these factors, a study was performed to compare the recommended thorium-fueled hybrid LIFE blanket design to a variant fueled with depleted uranium that starts with 0.3% ^{235}U. The DU system used the same 20cm multiplier thickness and 15% TRISO packing fraction as the recommended thorium design but the fuel blanket volume decreased slightly because UCO fuel has a slightly higher density than ThCO and thus needs less value to load

the same 20MT of initial fuel. The performance metrics used to facilitate this comparison are the same ones used for the thorium parametric study: time to plateau, end of plateau burnup as calculated by neutronics analysis, and then the maximum credible burnup predicted by TRIUNE. Table 5.1 summarizes the neutronics and fuel performance results of this DU comparison study while Figure 5.2.displays the predicted failure fractions as a function of fuel burnup level for thorium and DU LIFE engines.

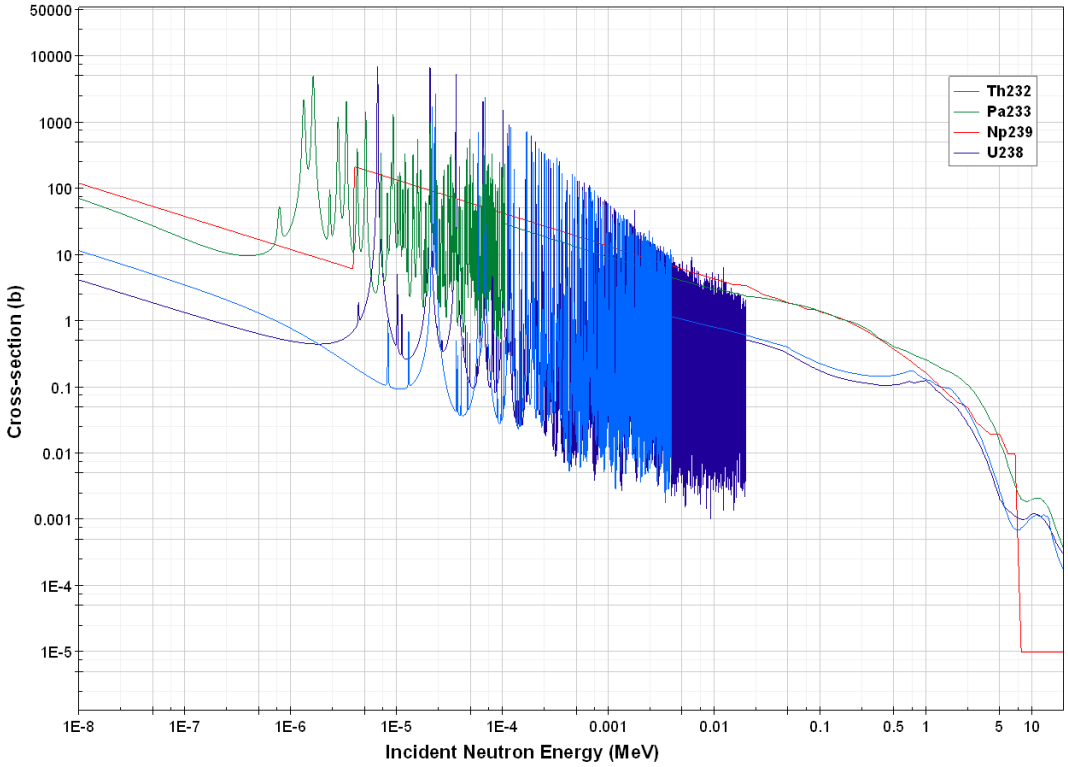

Figure 5.1: Important cross sections for fissile material breeding in DU and thorium fertile systems.

Table 5.1: Summary of results comparing 20MT DU and thorium systems.

Fuel	**Time to Plateau [years]**	**EOP Burnup [% FIMA]**	**Max. Credible Burnup [% FIMA]**
Thorium	3.56	38.71	12.14
DU	1.04	67.42	12.27

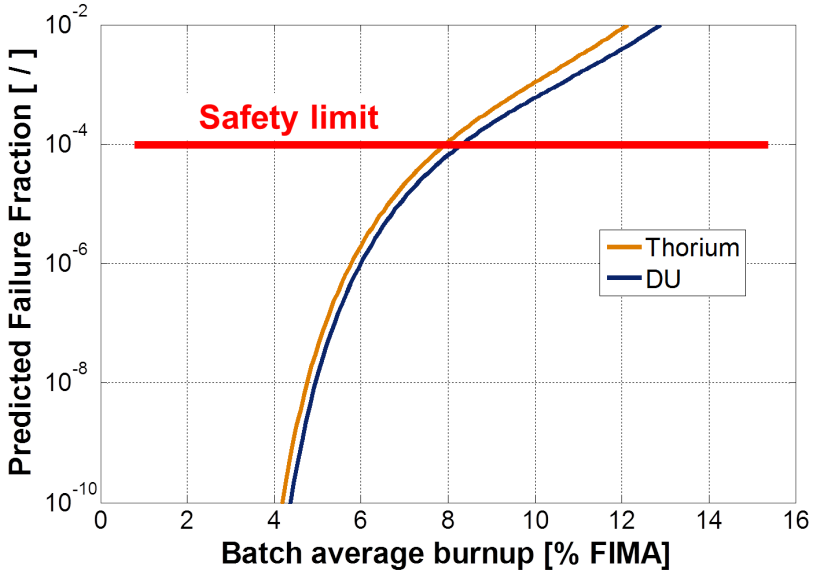

Figure 5.2: Predicted TRISO particle failure fractions as a function of batch average burnup for thorium and DU systems.

The neutronics analysis of the DU system looks substantially more promising than the thorium system: the DU system reaches plateau power in less than 30% of the time needed for the thorium system and achieves an end of plateau burnup that is nearly 75% greater on a relative basis. Multiple factors influence this outcome. As shown in Figure 5.1, ^{238}U has a higher resonance integral capture cross section than ^{232}Th does. In addition, as mentioned in Section 3.1.1, breeding fissile fuel from thorium involves significantly higher parasitic absorption rates in the intermediate nuclides. Both of these factors play into a key third item that largely determines the EOP burnup levels that the DU and thorium systems can achieve: the neutron flux spectrum spectrum for this study was a somewhat soft epithermal flux. The DU and thorium system would each exhibit better neutronic performance with a harder neutron energy spectrum, but DU optimizes to a significantly softer spectrum than thorium does. This is easily illustrated by the fact that past work showed that larger systems with harder neutron spectra showed fairly similar neutronic performance between thorium and DU; using a 40 MT initial fuel load with 30 % TRISO packing and a 16cm neutron multiplier thickness yielded EOP burnup levels of 78 %FIMA for DU and 76 %FIMA for thorium [54]. Similarly, Figure 4.6 shows that the EOP burnup predicted by neutronics codes for the 20MT thorium system more than doubles when hardening the spectrum by going to thinner neutron multiplier thicknesses and higher TRISO packing fractions.

From the perspective of neutronic performance, the DU system certainly appears better in this instance; however, fuel performance calculations indicate that the DU system achieves a maximum credible burnup that is a mere 0.1% higher on a relative basis and the discussion above explained some of why the neutronic performance looked better. Overall, the results

of this side study are largely inconclusive; the neutronic performance of the DU system fared much better than the thorium system for these epithermal neutron energy spectra but both fuels achieved roughly the same TRIUNE-calculated maximum credible burnup. While internal gas pressure due to fission product gases influences does have some influence, the maximum credible burnup predicted by TRIUNE appears to be largely driven by irradiation effect of fast neutron fluence accumulation in the PyC layers of the TRISO particles; the DU accumulates slightly less fast neutron fluence slightly slower and thorium systems The performance of both systems The DU system appears to be the better choice for neutronic performance in an epithermal neutron flux spectrum, and should perform better economically as well due to the short ramp-up time leading to better balance of plant utilization, but long-term waste repository impacts and other items could prove to be deciding factors. Nevertheless, if fuel performance limitations restrict LIFE hybrid blankets to softer neutron spectra for operation, then in that design space DU fuels offer better neutronic performance than thorium fuels though both at present achieve able the same maximum credible burnup as predicted by TRIUNE.

5.2 Uncertainty Quantification in Fuel Performance Modeling

TRISO fuel performance models are only as accurate as the material property values and correlations that they use. Given the uncertainties in measuring material properties, the inherent difficulty in ascertaining how some properties vary as a function of temperature and radiation damage, and the wide ranges of "acceptable" values and correlations for some parameters it stands to reason that there will be uncertainties in the properties employed by TRISO fuel performance models. This study seeks to quantify the effects of uncertainties in material properties used in TRIUNE by varying correlations and values one at a time over a range of values and adjustments determined by how much the data and recommendations in the literature appears to vary; for example, if multiple sources agree reasonably well on the value for a material property such as the Young's modulus for SiC then that property would not be varied much in this study but another property for which there are wide ranges of "recommended values" in the literature (e.g., SiC Weibull mean strength) would be varied considerably more. The goal of this study is to examine the impact of the uncertainty in each property by varying it over a reasonable range established by the uncertainty in that property and quantify the effect it has on the predicted maximum credible burnup; this process accounts for both the sensitivity of the system to a given parameter as well as the actual uncertainty in that parameter. The desired end result is to help guide future experimental work by identifying the material properties that are most important to refine for TRISO fuel performance modeling. This would ensure the effective use of research funding allocated to new experimental work while also hopefully improving the state of TRISO fuel performance models. Most of the variations performed during this study will be carried

out by applying multiplicative adjustment factors to existing values or correlations; where appropriate, actual new values or alternative correlations will be chosen and used for the property of interest. For all calculations, it should be kept in mind that stochastic noise in the calculation process is likely about 0.3% on a relative basis; thus, any relative percent differences smaller than this value or very close to it may not have any statistical significance. The first set of material properties varied during this study was thermal conductivities in the system. Thermal conductivities for PyC and SiC are fairly well known and thus were varied within a factor of 0.2 to 5.0 of their default value in TRIUNE. Uncertainties in the fuel thermal conductivity were found to be considerably higher, given the disagreement in the literature regarding correlations for use with UO_2 and a general lack of any correlations for other fuel species (e.g., thorium) or forms (e.g., oxycarbides), and thus the fuel thermal conductivity was varied within a factor of 0.1 to 10.0 of its default value in TRIUNE. The effective thermal conductivity of the gap that forms between the buffer and IPyC is likewise very uncertain [41] and thus was varied within a factor of 0.1 to 10.0 of its nominal assumed value of 0.1 W/m-K. Figure 5.3 shows the results of varying the thermal conductivities of the fuel ("kfuel"), buffer ("kbuff"), gap ("kgap"), PyC ("kpyc"), and SiC ("ksic").

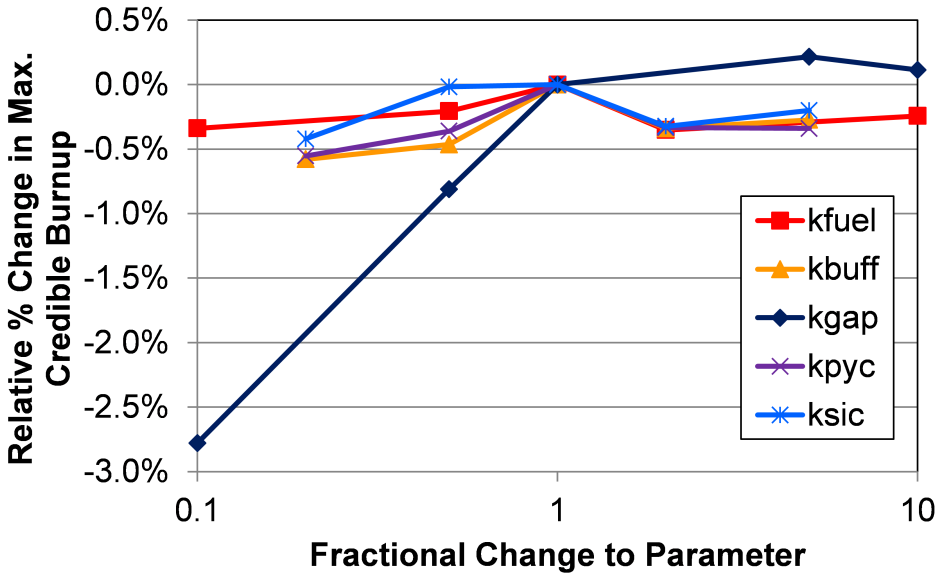

Figure 5.3: Relative percent change in the maximum credible burnup predicted by TRIUNE when varying thermal conductivities in the TRIUNE model.

These results indicate that a reasonable variation of the gap thermal conductivity within its uncertainties could impact overall fuel performance calculations by about 3% of the predicted value; all other thermal conductivities showed little effect.

Though the previous plot assessed the impact of uncertainties in the thermal conductivities for all materials simultaneously, the remainder of this study examined each material by itself. The key material properties and behaviors of each material were varied within

their uncertainties to see what impacts they had on overall fuel performance. The first material examined was PyC and it had its Young's modulus, coefficient of thermal expansion, irradiation creep, and irradiation-induced dimensional change correlations assessed. The elastic properties appear fairly well known and thus the Young's modulus was only varied over a factor of 0.5 to 2 of its nominal value in TRIUNE and the coefficient of thermal expansion was only varied over a factor of 0.66 to 1.5 of its nominal value. Uncertainties appear to be significantly greater in irradiation creep and IIDC correlations for PyC. The irradiation creep coefficient was varied over a factor of 0.2 to 3 times its nominal value with Poisson's ratio in creep also exercised to examine different values recommended for it by setting it at fixed values of 0.4 and 0.5 as well as the default behavior of letting it float from 0.5 down to 0.4 as a function of neutron fast fluence. PyC IIDC (shrinkage and swelling) correlations were exercised in two ways: the LLNL correlation [45] that TRIUNE uses by default was varied in magnitude over a factor of 0.1 to 10.0 and then a German correlation [19, 32] and a CEGA correlation (Correlation E) from the IAEA TRISO benchmark suite [68] were used in place of the LLNL correlation. It should be noted that neither of these correlations were originally intended for use at the neutron fast fluence values present in typical thorium LIFE calculations.

Figure 5.4 summarizes the effects of varying most of the PyC properties, Figure 5.5 focuses on the effect of varying Poisson's ratio in irradiation creep for PyC, and Figure 5.6 reports the effects of both varying the magnitude of the LLNL PyC IIDC correlation as well as employing the German and CEGA correlations.

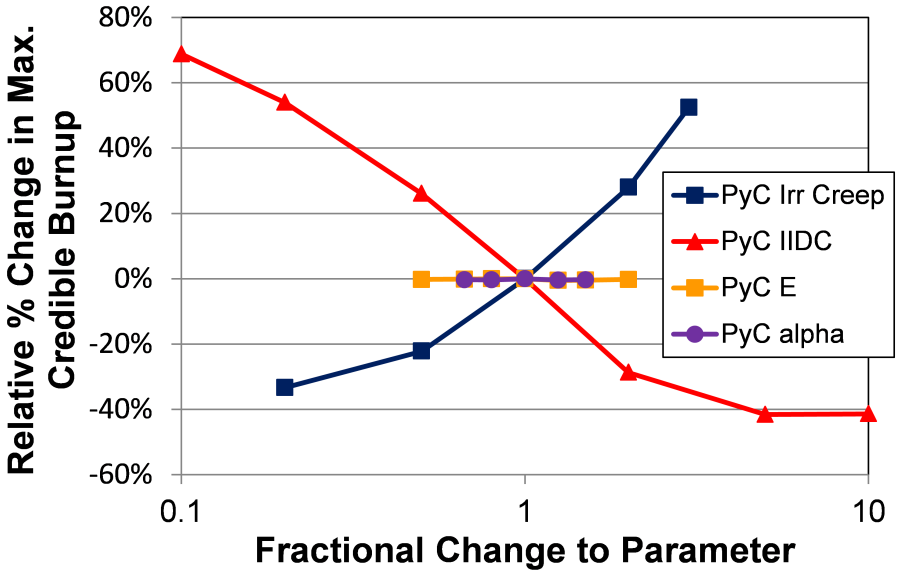

Figure 5.4: Relative percent change in the maximum credible burnup predicted by TRIUNE when varying PyC material property correlations in the TRIUNE model.

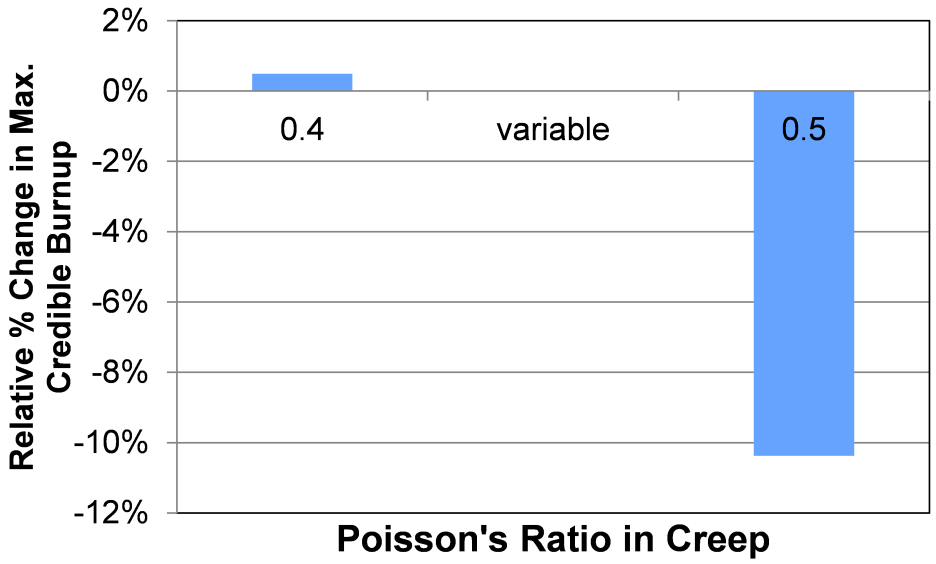

Figure 5.5: Relative percent change in the maximum credible burnup predicted by TRIUNE when varying Poisson's ratio in irradiation creep for PyC.

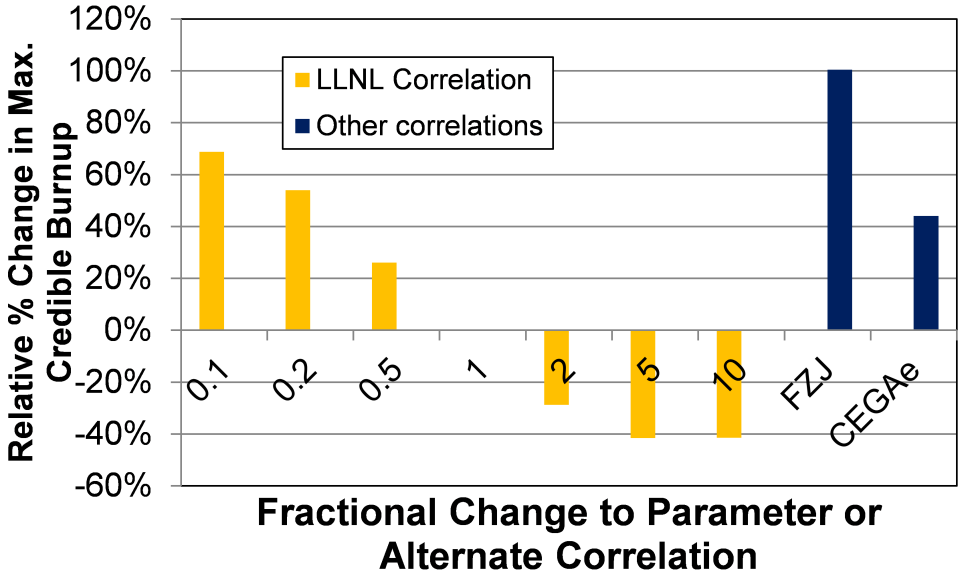

Figure 5.6: Relative percent change in the maximum credible burnup predicted by TRIUNE when varying the magnitude of the LLNL PyC IIDC correlation [45] or using other correlations [19, 25, 58, 68].

These results point to significant possible impacts on fuel performance calculations due to uncertainties and variations in correlations for PyC IIDC correlations as well as substantial effects due to uncertainties in the PyC irradiation creep constant. Despite some uncertainties in elastic properties for PyC, the overall fuel performance calculations do not seem likely to be impacted by them in any significant way.

Figure 5.7 summarizes the effects of varying material properties for SiC in the TRIUNE model. Similar to PyC, the Young's modulus and coefficient of thermal expansion are known fairly well for SiC and thus were only varied over factors of 0.5 to 2 and 0.66 to 1.5 respectively. The Weibull parameters for SiC, however, were found to have large uncertainties in the literature [26, 61]; recommended values for the Weibull mean strength of SiC ranged from 300 MPa to over 850 MPa and the recommended value for the SiC Weibull modulus ranged from 3.0 to 8.02. TRIUNE currently uses 600 MPa and 7.25, respectively, as the default values for these parameters.

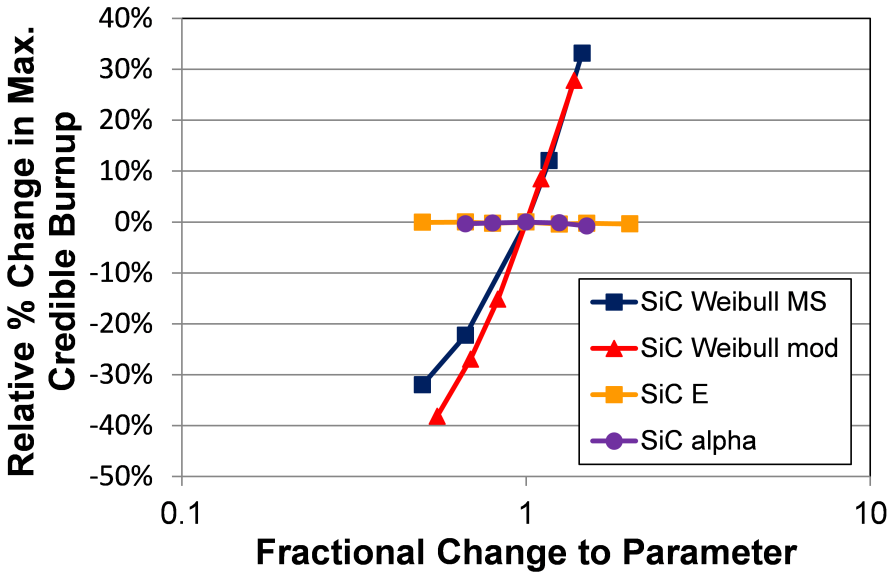

Figure 5.7: Relative percent change in the maximum credible burnup predicted by TRIUNE when varying SiC material property correlations in the TRIUNE model.

As one might expect, given that the Weibull parameters directly feed into calculating SiC pressure vessel failure probabilities, the sizable uncertainties in SiC Weibull parameters had noticeable effects on TRIUNE fuel performance calculations. The Young's modulus and coefficient of thermal expansion had very little effect on fuel performance calculations.

Lastly, Figure 5.8 shows the effect of varying the fuel kernel swelling rate used in TRIUNE, which had a default value of 0.6 % per %FIMA and was varied over the full range of recommended swelling rates from Olander's work [60]. Not considered in this study, but worth noting, is that the ATLAS code incorporates a fuel swelling model that switches behavior above 10 %FIMA to account for changes to the fuel kernel microstructure [19].

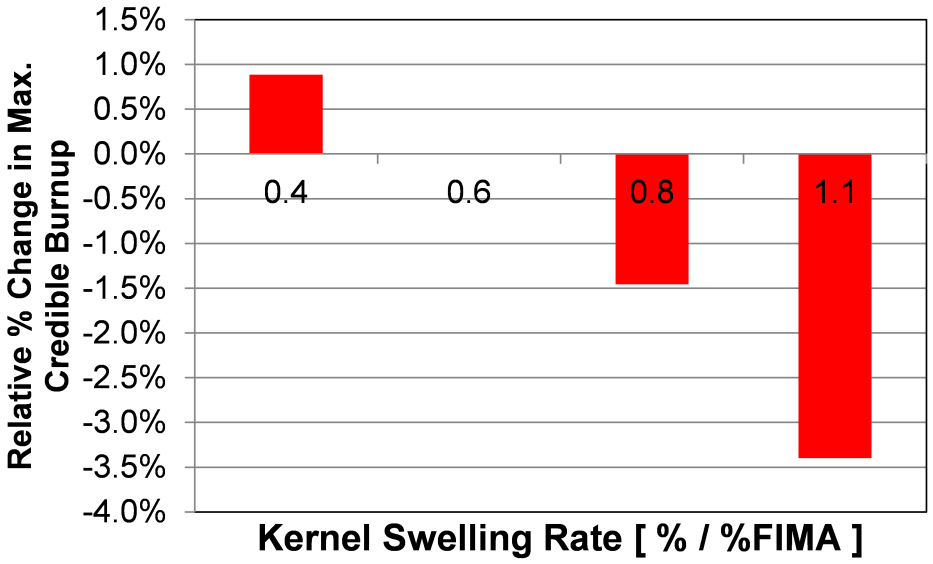

Figure 5.8: Relative percent change in the maximum credible burnup predicted by TRIUNE when varying the fuel kernel swelling rate in the TRIUNE model.

To summarize the overall results from this material property uncertainty quantification study, it appears fair to say that the biggest impacts on TRISO fuel performance calculations come from the significant uncertainties in and high sensitivity to irradiation creep and IIDC in PyC along with Weibull parameters in SiC. Uncertainties in elastic constants such as Young's modulus and coefficients of thermal expansion, along with most thermal conductivities, appear to have little effect if any on the fuel failure predictions in this study. Lastly, some work may be needed in refining the fuel kernel fission product swelling relationship as well as understanding and estimating the thermal conductivity of the gap that forms between the buffer and IPyC layers, but these effects appear relatively minor. In addition to reducing uncertainties in existing correlations and properties, substantial work is needed in extending the upper bound on neutron fast fluence to which several correlations are valid and temperature and porosity dependence should be added to several correlations to improve the accuracy of both the correlations and the fuel performance calculations they inform.

5.3 Pebble residence time

The TRISO particle lifetime history simulation process detailed in Appendix A has features that depend upon the pebble residence time, defined as the amount of time it takes a pebble to be discharged from the fuel blanket after being inserted, as well as features and methods that inherently rely upon the idea that a single fixed residence time exists. While some work might be done to characterize the expected pebble residence time with a fair bit of accuracy, ongoing work in pebble dynamics research indicates that a substantial

likelihood exists that there will be both a distribution of residence times centered around the expected residence time as well as some outlier points due to pebbles that got caught in a corner or other region with flow issues [87]. This side study varied the fixed value assumed for pebble residence time to try to assess how changes to the parameter might affect overall fuel performance.

The nominal pebble residence time assumed for design calculations in this work was 20 days. This study examines the impact on expected fuel performance when this default value was changes to residence time values of 10 days, 15 days, 30 days, and 40 days. The effect of changing the pebble residence time was measured by calculating the relative change in TRIUNE-calculated maximum credible burnup for each variant compared to the baseline assumption of a 20 day residence time. Figure 5.9 displays the results of these calculations.

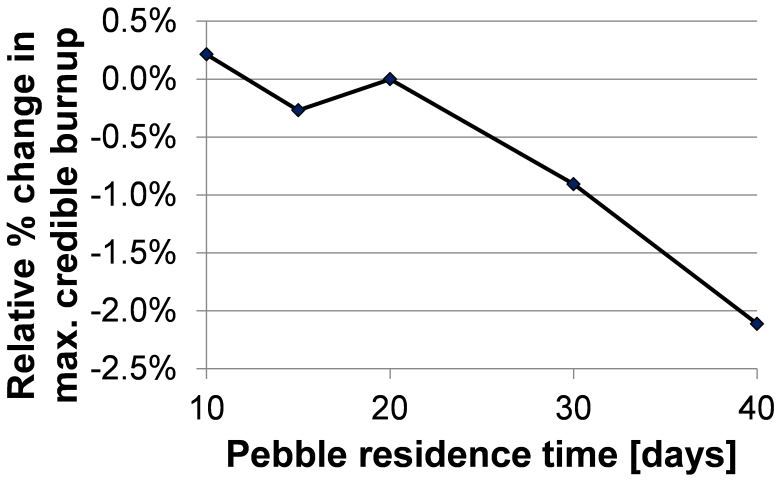

Figure 5.9: Relative percent change in the TRIUNE-calculated maximum credible burnup for several pebble residence times compared to the 20 day reference value.

Most of the relative changes were small enough to ignore because they are likely within the stochastic noise of the calculations. Even the impact of longer residence times (e.g., 40 days) appear small enough in magnitude to be neglected in these studies.

Chapter 6

Discussions and Conclusions

The results shown in Section 4.3 documenting the end of plateau burnup values predicted by neutronics analysis compared to the maximum credible burnup values predicted by TRIUNE accomplish one of the main goals of this work by demonstrating the importance of integrating fuel performance calculations into mainstream design studies and system-level trade-off studies.

Neutronic optimization of the 20MT thorium LIFE system appears to lend itself most easily to a fairly hard neutron energy spectrum; the neutron flux spectra in Figure 4.11 show that the design parameters that enable a higher EOP burnup value in neutronics analyses ("Case 1" with 40% TRISO packing with a 10cm neutron multiplier thickness) result in about three times more fast energy neutrons than in a softer spectrum system ("Case 2" with 15% TRISO packing and a 20cm neutron multiplier thickness). This makes sense given that neutron efficiency in a thorium system is actually better for faster neutron energies rather than thermal, as demonstrated in Figure 6.1 by the relative increase of the ^{232}Th capture cross section compared to the ^{233}Pa capture cross section from 0.1 to 1 MeV and the sharp lower energy resonance peaks in the ^{233}Pa capture cross section.

The neutronic optimization toward a fast neutron spectrum has adverse effects on TRISO fuel performance though, due to the sharp increases in the rate at which fast neutron fluence is accumulated compared to the relatively modest benefits to the neutron economy. While this relationship between the rate at which a TRISO particle accumulates fast neutron fluence compared to the rate at which it accumulates burnup cannot explain everything happening in the thorium LIFE system, it is certainly worth noting. Figure 6.2 plots the relationship between neutron fast fluence and batch average burnup level observed in multiple thorium LIFE design options alongside the fast fluence versus burnup relationship found in an irradiation experiment using LEU fuel kernels (HRB-22 [68, 69]) and one possible design for a Deep Burn critical fission reactor using TRU fuel kernels (DB-MHR [46, 70]). The curves for Cases 1 and 2, identified back in Section 4.3, are labeled in the figure for ease of reference.

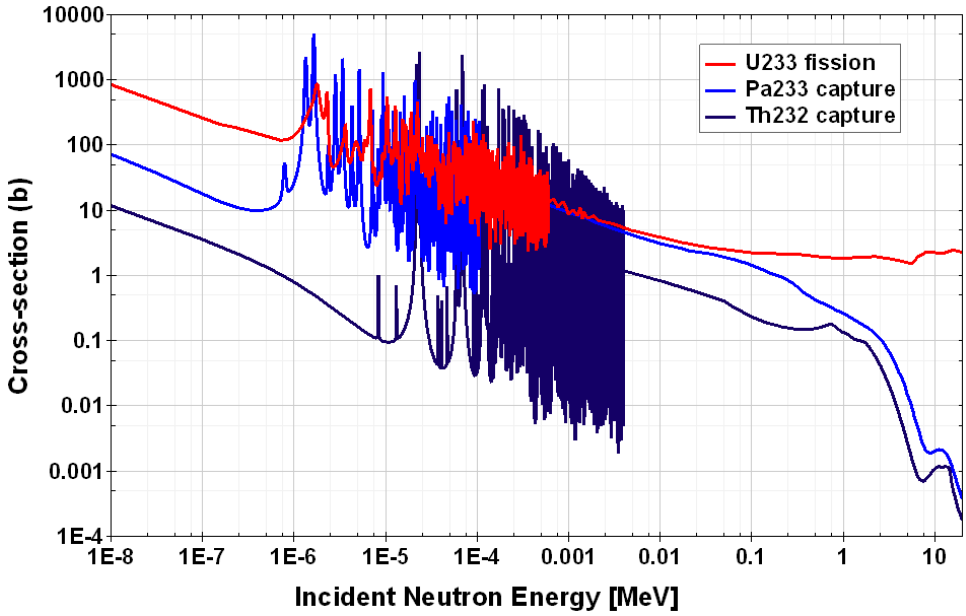

Figure 6.1: Important cross sections for thorium-fueled nuclear energy systems plotted using JANIS3.0 [86] with ENDF/B-VII.0 neutron cross section data [83].

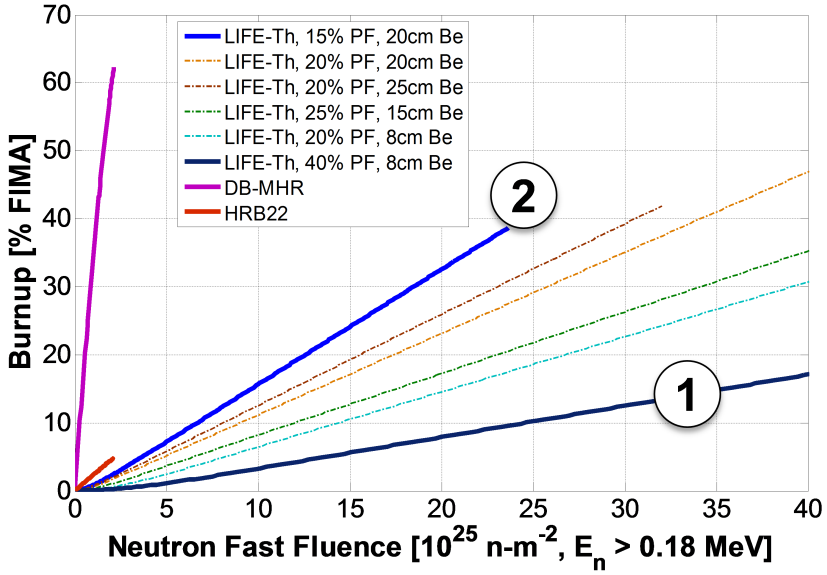

Figure 6.2: Plots of batch average fuel burnup level [% FIMA] as a function of accumulated neutron fast fluence for several different thorium LIFE design possibilities compared to representative data for the DB-MHR design [46, 70] and an actual irradiation experiment (HRB-22) [68, 69].

While no direct causal link can be shown that states that successful fuel designs must try to increase the rate at which they accumulate burnup relative to the rate at which they accumulate fast fluence, it is nevertheless a good rule of thumb; radiation damage effects on the TRISO particle will generally hurt it rather than help it, and many of the most severe behaviors known to occur in TRISO particles (e.g., irradiation-induced swelling) will appear and get worse as the accumulated fast fluence of a particle increases. It is important to note that during the course of this work no sound basis has been found for setting a concrete limit on the neutron fast fluence or radiation damage (in units of displacements per atom or dpa); logically the probability of fuel failures likely increases as these parameters increase, and there may be a good basis for a fast fluence or dpa limit at some point, but none has surfaced during the course of this work or literature surveys on the topic.

The maximum credible burnup values predicted by TRIUNE for the 20MT thorium system and shown in Figure 4.7 point quite clearly toward recommending a 20MT thorium LIFE system with a 20cm neutron multiplier thickness and a 15% TRISO packing fraction in the fuel pebbles. The system may use neutrons more efficiently at higher TRISO packing fractions and thinner neutron multiplier thicknesses but the end of plateau burnup levels predicted by neutronics analyses only provide an upper bound for how long the system can operate; in reality, the system can only reliably operate while it is both producing energy and doing so without exceeding safety limits such as fuel particle failure fraction limits. Pressure vessel failure of the SiC layer, which is the TRISO particle failure mechanism considered in this work, appears to be largely driven by a combination of both irradiation effects on PyC and internal gas pressure. The irradiation effects on PyC appear to be the dominant factor and depend mostly upon fast neutron fluence with minor contributions from other factors such as temperature. The internal gas pressure depends upon temperatures and burnup.

Given that the TRISO particle fuel performance in a thorium LIFE blanket has proven to be much more challenging and limiting than the neutronic performance of the blanket, system-level design optimization decisions should be made to benefit the fuel performance in any way possible.

6.1 Recommendations and Future Work

With specific regard to LIFE applications, this study provides a recommended thorium-fueled hybrid LIFE engine design using fairly "conventional" TRISO fuel particles that can reliably operate up to a burnup level of about 12–13 %FIMA and may be able to go higher with further optimization work and narrowing down uncertainties in material property correlations. Achieving a burnup level of 12–13 %FIMA using pure thorium without any enrichment or reprocessing facilities and also without any fissile material as a seed to start the conversion of the thorium to uranium could prove attractive given that it achieves a resource utilization about 25 times greater than the utilization of uranium in the existing light water reactor (LWR) fuel cycle. The thorium LIFE cycle also reduces proliferations risks by eliminating enrichment and reprocessing facilities from the fuel cycle.

This application of a TRISO fuel performance model to thorium LIFE operations is only intended to demonstrate the importance and use of such a code and evaluate how far a relatively standard existing technology such as TRISO fuel particles could be pushed in a LIFE system. Future LIFE design improvements, improvements to the TRISO design (e.g., thicker SiC coatings or optimizing PyC coating thicknesses to lower the effect of swelling), or possibly the development or use of new fuel technologies such as inert matrix fuels or other concepts could all offer significant improvements to the attainable burnup of a hybrid LIFE engine. Further design studies should look at optimizing the BOL lithium enrichments in the coolants, varying the fuel loading up to 30MT and 40MT levels to see if the predicted maximum credible burnup gets better, and using a different operational mode to eliminate the ramp-up phase of operation during which a disproportionate amount of fast neutron fluence is accumulated. In addition, this study was performed using 100% fertile material; if the decision were made to use fuels with a more substantial fissile content in a LIFE system, this should improve the maximum credible burnup predicted by TRIUNE or other fuel performance models.

As has been mentioned previously, a large amount of work is needed to improve material property correlations which are used for TRISO fuel performance modeling. There is a dearth of material properties for fuel materials other than UO_2, better oxygen release correlations are needed, correlations such as PyC irradiation-induced dimensional change need to be extended to higher fluence ranges, PyC irradiation creep correlations need to be more accurately determined, and SiC Weibull parameters need to be more accurate determined.

Researchers who many pick up future development of the TRIUNE model should consider adding a diffusion model that accounts for chemical (Fickian) and thermally-driven (Soret) diffusion of fission products away from the kernel and out through the coating layers. Failure models for TRIUNE could be expanded to account for 2-layer or 1-layer solutions for cases where the IPyC or OPyC layer might fail, multidimensional failure mechanisms could be accounted for through the use of an external finite element stress analysis tool (e.g., ABAQUS) or through other means, the Weibull mean strength for PyC and SiC should be adjusted to account for the volumes of the layers, and more realistic distribution functions could be investigated for sampling "as-manufactured" TRISO particle dimensions. As has been already previously mentioned, pebble residence times will have a distribution rather than being represented by a single fixed quantity [87]. Lastly, the model formulation in its current state encounters numerical instabilities for some situations involving very high neutron fast fluences combined with other factors; an exponential term in the solution explodes causing the solution to several parameters to assume values of either "Infinity" or "Not a Number". Future TRIUNE development efforts should look at reformulating this part of the model or adding an error check to handle it.

6.2 Conclusions

The goals of this study were to (1) create a new TRISO fuel performance model, (2) integrate this model into an existing system of neutronics and heat transfer codes to allow fuel performance calculations to inform design optimization and system-level trade-off studies, (3) demonstrate both the importance of incorporating fuel performance calculations into mainstream design studies and the impact that this new integrated analysis has on system-level design decisions by applying it to a thorium-fueled fusion-fission hybrid LIFE blanket design, and (4) establish a recommended design for a thorium LIFE engine. All of these goals have been met. The recommended thorium hybrid LIFE design has an initial fuel load of 20MT of pure thorium, 15% TRISO packing within fuel pebbles, and a neutron multiplier thickness of 20cm. It operated at a system power level of 2000 MW_{th}, took about 3.5 years to reach full plateau power, and was capable of an End of Plateau burnup of 38.7 %FIMA if considering just the neutronic constraints in the system design; however, its TRIUNE-predicted maximum credible burnup was 12.1 %FIMA due to a combination of internal gas pressure and irradiation effects on the TRISO materials (especially PyC) leading to SiC pressure vessel failures. The optimal neutron spectrum for the thorium-fueled blanket options evaluated seemed to favor a hard spectrum for optimizing neutronic performance but the fuel performance constraints demonstrated that a significantly softer spectrum would be needed to reduce radiation damage effects on the TRISO fuel particles and thereby enable higher burnup levels.

In addition to these goals, side studies were performed to compare thorium and DU versions of a 20MT LIFE system and some uncertainty quantification work was also conducted to assess the impact that existing uncertainties in material properties have on the fuel performance predicted for TRISO particles. The DU side study found that for the softer (epithermal) neutron flux chosen as part of the recommended thorium design, a DU system offered better neutronic performance (possible EOP burnup of 67.4 %FIMA for DU compared to 38.7 %FIMA for thorium) but both systems achieved about the same TRIUNE-predicted maximum credible burnup value (12.3 %FIMA for DU compared to 12.1 %FIMA for thorium). The material property sensitivity study illustrated that the maximum achievable burnup of the recommended thorium LIFE design was most heavily impacted by the uncertainties in PyC irradiation effects (irradiation creep and irradiation-induced shrinkage and swelling) as well as Weibull parameters for the SiC layer.

The results of this work are not specific to just LIFE systems; other nuclear energy design projects would benefit from integrating fuel performance calculations into their design optimization and trade-off studies as well. Furthermore, improvements in modeling material properties of TRISO fuel particles would benefit all systems that assume their use by increasing the accuracy and validity of the correlations used in TRISO fuel performance modeling; after all, the source data used for design work often has large impacts on how useful the design work ends up being. In addition, new experimental work could possibly extend the correlations to new valid ranges of fast fluence and burnup.

Bibliography

[1] "Energy Poverty: How to make modern energy access universal?" Special early excerpt of the World Energy Outlook 2010 for the UN General Assembly on the Millennium Development Goals, International Energy Agency, September 2010

[2] D. Kammen, "Lecture 4: Energy and Development", ER-280 course lecture presentation, version dated September 7, 2009.

[3] "Estimated U.S. Use in 2010," Lawrence Livermore National Laboratory, 2011. https://flowcharts.llnl.gov/index.html

[4] "World Energy Flow in 2007", Lawrence Livermore National Laboratory, 2011. https://flowcharts.llnl.gov/index.html

[5] IPCC, 2007: *Climate Change 2007: The Physical Science Basis. Contribution of Working Group I to the Fourth Assessment Report of the Intergovernmental Panel on Climate Change* [Solomon, S., D. Qin, M. Manning, Z. Chen, M. Marquis, K.B. Averyt, M. Tignor and H.L. Miller (eds.)]. Cambridge University Press, Cambridge, United Kingdom and New York, NY, USA, 996 pp.

[6] International Energy Agency. *Projected costs of generating electricity, 2010 update*. OECD publication, Paris, France, 2010.

[7] U.S. Energy Information Administration. Annual Energy Outlook 2011. DOE/EIA-0383(2011), April 2011.

[8] S. Pacala and R. Socolow, "Stabilization wedges: solving the climate problem for the next fifty years with current technologies," *Science*, **305** (2004): 968-971.

[9] W. C. Sailor, et al. "Nuclear Power: A Nuclear Solution to Climate Change?," *Science*, **288** (2000): 1177-1178. DOI: 10.1126/science.288.5469.1177

[10] J.J. Powers and B.D. Wirth,"A Review of TRISO Fuel Performance Models," *Journal of Nuclear Materials*, **405** (2010): 74-82.

[11] D.L. Hanson, "A Review of Radionuclide Release From HTGR Cores During Normal Operation." EPRI Report 1009382, Electric Power Research Institute, February 2004.

[12] K.J. Krueger and G.P. Ivens. "Safety-related experiences with the AVR reactor." Specialists' Meeting on Safety and Accident Analysis for Gas-cooled Reactors, Oak Ridge, TN, USA, 13–15 May, 1985, IAEA-TECDOC-358, pp:61–70.

[13] S. Brandes. "Core physics test of THTR pebble bed core at zero power." Specialists' Meeting on Safety and Accident Analysis for Gas-cooled Reactors, Oak Ridge, TN, USA, 13–15 May, 1985, IAEA-TECDOC-358, pp:285–298.

[14] R. Baumer, et al., "Construction and operating experience with the 300-MW THTR nuclear power plant," *Nuclear Engineering and Design*, **121** (1990): 155.

[15] Y. Xu and K. Zuo, "Overview of the 10 MW high temperature gas cooled reactortest module project," *Nuclear Engineering and Design*, **218** (2002): 13.

[16] F. Chen, et al., "Benchmark Calculation for the Steady-State Temperature Distribution of the HTR-10 under Full-Power Operation," *Journal of Nuclear Science and Technology*, **46** (2009): 572.

[17] S. Saito, et al. "Design of High Temperature Test Reactor (HTTR)." JAERI-1332, Japan Atomic Energy Research Institute, September (1994).

[18] P. Mills, R. Soto, G. Gibbs, et al. "Next Generation Nuclear Plant Pre-Conceptual Design Report." INL/EXT-07-12967, Idaho National Laboratory, November 2007.

[19] D. Petti, et al. "Development of Improved Models and Designs for Coated-Particle Gas Reactor Fuels." INEEL/EXT-05-02615, Idaho National Engineering and Environmental Laboratory, December 2004.

[20] K. Minato, et al., "Fission product release from ZrC-coated fuel particles during post-irradiation heating at 1800 and 2000C," *Journal of Nuclear Materials*, **249** (1997): 142.

[21] K. Minato,et al., "Deterioration of ZrC-coated fuel particle caused by failure of pyrolrytic carbon layer," *Journal of Nuclear Materials*, **252** (1998): 13.

[22] K. Minato,et al., "Retention of fission product caesium in ZrC-coated fuel particles for high-temperature gas-cooled reactors." *Journal of Nuclear Materials*, **279** (2000): 181.

[23] K. Minato,et al., "Irradiation experiment on ZrC-Coated fuel particles for high-temperature gas-cooled reactors," *Nuclear Technology*, **130** (2000): 272.

[24] D.A. Petti, et al., "Key differences in the fabrication, irradiation and high temperature accident testing of US and German TRISO-coated particle fuel, and their implications on fuel performance," *Nuclear Engineering and Design*, **222** (2003): 281.

[25] G.K. Miller, D.A. Petti, J.T. Maki, and D.L. Knudson. "PARFUME Theory and Model Basis Report." INL/EXT-08-14497, Idaho National Laboratory, September 2009.

[26] L.L. Snead, et al., "Handbook of SiC Properties for Fuel Performance Modeling," *Journal of Nuclear Materials*, **371** (2007): 329.

[27] D. Petti. "An Overview of the DOE Advanced Gas Reactor Fuel Development and Qualification Program." Presentation given at the Workshop on Advanced Reactors With Innovation Fuels (ARWIF), Oak Ridge, Tennessee, February 16, 2005.

[28] J. Wang, R.G. Ballinger, H.J. Maclean, and J.T. Decker. "TIMCOAT: An Integrated Fuel Performance Model for Coated Particle Fuel." Proc. of the 2nd International Topical Meeting on High Temp. Reactor Tech. (HTR2004), Beijing, China, September 22–24, 2004.

[29] J.T. Maki, D.A. Petti, D.L. Knudson, and G.K. Miller, "The Challenges Associated with High Burnup, High Temperature and Accelerated Irradiation for TRISO-coated Particle Fuel," *Journal of Nuclear Materials*, **371** (2007): 270.

[30] G.K. Miller, "Stresses in a Spherical Pressure Vessel Undergoing Creep and Dimensional Changes." *International Journal of Solids and Structures*, **32** (1995): 2077.

[31] G.K. Miller, D.A. Petti, J.T. Maki, and D.L. Knudson, "Updated Solution for Stresses and Displacements in TRISO-coated Fuel Particles," *Journal of Nuclear Materials*, **374** (2008): 129.

[32] B. Boer. "Optimized Core Design and Fuel Management of a Pebble-Bed Type Nuclear Reactor." Thesis. Delft University of Technology, 2009.

[33] D. Petti, et al. "Development of Improved Models and Design for Coated-Particle Gas Reactor Fuels." INEEL/EXT-02-01493, Idaho National Engineering and Environmental Laboratory, November 2002.

[34] D. Petti, et al. "Gas Reactor TRISO-coated Particle Fuel Modeling Activities at the Idaho National Engineering and Environmental Laboratory." Proc. of the 2nd Info. Exch. Meeting on Basic Studies in the Field of High-temp. Eng., Paris, France, October 10–12, 2001.

[35] G.K. Miller, D.A. Petti, and J.T. Maki. "Development of an Integrated Performance Model for TRISO-coated Gas Reactor Fuel." Proc. of the Conference on High Temp. Reactors (HTR2002), Petten, Netherlands, April 22–24, 2002.

[36] J. Wang. "An Integrated Performance Model for High Temperature Gas Cooled Reactor Coated Particle Fuel." Thesis. Massachusetts Institute of Technology, 2004.

[37] B. Boer, A.M. Ougouag, J.L. Kloosterman, and G.K. Miller, "Stress Analysis of Coated Particle fuel in Graphite of High-Temperature Reactors," *Nuclear Technology*, **162** (2008): 276.

[38] J. Jonnet, J.L. Kloosterman, and B. Boer. "Development of a Stress Analysis Code for TRISO Particles in HTRs." Proc. of International Conference on the Physics of Reactors (PHYSOR), Interlaken, Switzerland, September 14–19, 2008.

[39] B. Liu, T. Liang, and C. Tang, "A Review of TRISO-coated Particle Nuclear Fuel Performance Models," *Rare Metals*, **25** (2006): 337-342.

[40] M. Phélip, et al. "The ATLAS HTR Fuel Simulation Code Objectives, Description and First Results." Proc. of the 2nd International Topical Meeting on High Temp. Reactor Tech. (HTR2004), Beijing, China, September 22–24, 2004.

[41] D.G. Martin, "Considerations Pertaining to the Achievement of High Burn-ups in HTR Fuel," *Nuclear Engineering and Design*, **213** (2002): 241.

[42] K. Sawa, S. Shiozawa, K. Minato, and K. Fukuda, "Development of a Coated Fuel Particle Failure Model Under High Burnup Irradiation," *Journal of Nuclear Science and Technology*, **33** (1996): 712.

[43] W.J. Kovacs, K. Bongartz, D. Goodin. "TRISO-coated HTGR Fuel Pressure-Vessel Performance Models." GA-A16807, General Atomics, October 1983.

[44] M.F. Young. "HEISHI: A Fuel Performance Model for Space Nuclear Applications." SAND94-0169, Sandia National Laboratories, August 1994.

[45] P. DeMange, J. Marian, M. Caro, and A. Caro, " TRISO-fuel element thermo-mechanical performance modeling for the hybrid LIFE engine with Pu fuel blanket," *Journal of Nuclear Materials*, **405** (2010): 144-155. doi:10.1016/j.jnucmat.2010.08.004

[46] R. Versluis, et al. "Project Deep-Burn: Development of Transuranic Fuel for High-Temperature Helium-Cooled Reactors." Proc. of the 4th International Topical Meeting on High Temperature Reactor Technology (HTR2008), Washington, DC, USA, September 28 - October 1, 2008.

[47] G.K. Miller, D.A. Petti, and J.T. Maki, "Consideration of the Effects of Partial Debonding of the IPyC and Particle Asphericity on TRISO-coated Fuel Behavior," *Journal of Nuclear Materials*, **334** (2004): 79.

[48] E. Moses, et al., "A Sustainable Nuclear Fuel Cycle Based on Laser Inertial Fusion-fission Energy (LIFE)," *Fusion Science and Technology*, **56**, *2*, 547-565 (2009).

[49] K.J. Kramer, et al., "Neutron Transport and Nuclear Burnup Analysis for the Laser Inertial Confinement Fusion-Fission Energy (LIFE) Engine," *Fusion Science and Technology*, **56**, *2*, 625-631 (2009).

[50] R.P. Abbott, et al., "Thermal and Mechanical Design of the LIFE Engine," *Fusion Science and Technology*, **56**, *2*, 618-624 (2009).

[51] K.J. Kramer, et al., "Parameter study of the LIFE engine nuclear design," *Energy Conversion and Management*, **51** (2010): 1744-1750. doi:10.1016/j.enconman.2009.12.041

[52] K.J. Kramer, et al., "The Laser Inertial Fusion Engine as a Weapons Grade Plutonium Burner", *Transactions of the American Nuclear Society*, **102** (2010): 91.

[53] M. Fratoni, et al. "Attainable Burnup in a LIFE Engine Loaded With Depleted Uranium." *Proceedings of PHYSOR2010*, American Nuclear Society, Pittsburgh, PA, USA. May 9-14, 2010.

[54] J.J. Powers, et al. "Neutronics Design of a Thorium-Fueled Fission Blanket for LIFE (Laser Inertial Fusion-based Energy)," *Proceedings of the 2010 International Congress on Advances in Nuclear Power Plants (ICAPP '10)*, San Diego, CA, USA. June 13-17, 2010.

[55] J.J. Powers, et al. "Integrating TRISO Fuel Performance Modeling into Mainstream Design Analyses." Poster presented at the 2011 International Congress on Emerging Nuclear Energy Systems (ICENES 2011), San Francisco, CA, USA, 16 May 2011.

[56] J.T. Hunt, et al., "Laser design basis for the National Ignition Facility," *Fusion Technology*, **26**, 767-771 (1994).

[57] K.J. Kramer. "Laser Inertial Fusion-based Energy: Neutronic Design Aspects of a Hybrid Fusion-Fission Nuclear Energy System." Thesis. University of California, Berkeley, 2010.

[58] CEGA-002820, "NP-MHTGR Material Models of Pyrocarbon and Pyrolytic Silicon Carbide." CEGA Corporation, 1993.

[59] P.L. Walker, Jr., ed. Chemistry and Physics of Carbon. Vol. 5. Marcel Decker, Inc., 1969.

[60] D.R. Olander, Fundamental Aspects of Nuclear Reactor Fuel Elements. U.S. ERDA Report TID-26711-P1, 1976.

[61] T.S. Byun, et al. "Fracture Properties of SiC Layer in Triso-Coated Fuel Particles," in Ceramics in Nuclear Applications (eds Y. Katoh, A. Cozzi, D. Singh and J. Salem), John Wiley & Sons, Inc., Hoboken, NJ, USA, 2010. doi: 10.1002/9780470584002.ch12

[62] G.K. Miller, D.A. Petti, D.J. Varacalle, and J.T. Maki, "Consideration of the effects on fuel particle behavior from shrinkage cracks in the inner pyrocarbon layer," *Journal of Nuclear Materials*, **295** (2001): 205.

[63] G.K. Miller, J.T. Maki, D.L. Knudson, and D.A. Petti. "Current Capabilities of the Fuel Performance Modeling Code PARFUME." Proc. of the 2nd International Topical Meeting on High Temp. Reactor Tech. (HTR2004), Beijing, China, September 22–24, 2004.

[64] K. Morimoto, et al, "Thermal conductivities of hypostoichiometric (U,Pu,Am)O2-x oxide," *Journal of Nuclear Materials*, **374** (2008): 378.

[65] R.K. McCardell, et al. "NP-MHTGR Fuel Development Program Plan." EGG-NPR-8971 Revision C, September 1992.

[66] H.-J. Lee and B. Wirth. "TRISO Report: Assessment of Literature Data on Fuel Performance and Constitutive Properties of Component Layers." UCB-NE-5115, UC Berkeley Nuclear Engineering Department, July 2008.

[67] *Fuel performance and fission product behaviour in gas cooled reactors*, IAEA-TECDOC-978, International Atomic Energy Agency, Vienna, Austria, November 1997.

[68] J.T. Maki and G.K. Miller. "TRISO-Coated Particle Fuel Performance Benchmark Cases." INL-EDF-3981 Rev. 2, Idaho National Laboratory, March 2005.

[69] *Advances in HTGR Fuel Technology*, IAEA-TECDOC-????, International Atomic Energy Agency, Vienna, Austria, *in progress*.

[70] J.J. Powers. "Fuel Performance Modeling of High Burnup Transuranic TRISO Fuels." M.S. Thesis. University of California, Berkeley, 2009.

[71] D. L. Poston and H. R. Trellue, "User's Manual, Version 2.0 for MONTEBURNS Version 1.0," LA-UR-99-4999, Los Alamos National Laboratory (1999).

[72] X-5 MONTE CARLO TEAM, "MCNPA General Monte Carlo N-Particle Transport Code, Version 5," LA-CP-03-0245, Los Alamos National Laboratory (2003).

[73] A.G. Croff, "ORIGEN2: A Versatile Computer Code For Calculating the Nuclide Compositions and Characteristics of Nuclear Materials," *Nuclear Technology*, **62**, 335-352 (1983).

[74] *Thorium Based Fuel Options for the Generation of Electricity: Developments in the 1990s*, IAEA-TECDOC-1155, International Atomic Energy Agency, May 2000.

[75] *Thorium Fuel Utilization: Options and Trends*, IAEA-TECDOC-1319, International Atomic Energy Agency, November 2002.

[76] *Thorium Fuel CyclePotential Benefits and Challenges*, IAEA-TECDOC-1450, International Atomic Energy Agency, Vienna, Austria, May 2005.

[77] M. Lung and O. Gremm, "Perspectives of the Thorium Fuel Cycle," *Nuclear Engineering and Design*, **180** (1998): 133-146.

[78] "Use of Thorium as Nuclear Fuel," Position Statement 78, American Nuclear Society, La Grange Park, Illinois, United States (2006).

[79] J.B. Hendrick. "Thorium." Mineral Commodity Summaries, U.S. Geological Survey, January 2010.

[80] C.D. Heising, "Closing the Nuclear Fuel Cycle: Thorium and Advanced Alternatives," presentation given at University of California, Berkeley, CA. 6 APR 2009.

[81] J. Kang and F.N. von Hippel, "U-232 and the Proliferation Resistance of U-233 in Spent Fuel," *Science & Global Security*, **9** (2001): 1-32.

[82] B.W. Sleaford, et al. "Nuclear Material Attractiveness: An Assessment of Material from PHWR's in a Closed Thorium Fuel Cycle." Presented at the European Nuclear Conference, Barcelona, Spain, May 30 – June 2, 2010.

[83] M. B. Chadwick, et al., "ENDF/B-VII.0 Next Generation Evaluated Nuclear Data Library for Nuclear Science and Technology," *Nuclear Data Sheets*, **107**.12 (2006): 2931–3059.

[84] F. B. Brown, et al. "Stochastic Geometry and HTGR Modeling for MCNP5." ANS Monte Carlo 2005 Topical Meeting, Chattanooga, TN (2005).

[85] R. Plukiene and D. Ridikas, "Modelling of HTRs with Monte Carlo: from a homogenous to an exact heterogeneous core with microparticles," *Annals of Nuclear Energy*, **30** (2003): 1573-1585.

[86] N. Soppera, et al. "Recent Upgrades to the Nuclear Data Tool JANIS." Proceedings of the International Conference on Nuclear Data for Science and Technology 2010, Jeju Island, Korea, April 26-30, 2010.

[87] M. Laufer, Ph.D. thesis, University of California, Berkeley, *in preparation*.

[88] M.A. Stawicki. "Benchmarking of the MIT High Temperature Gas-Cooled Reactor TRISO-Coated Particle Fuel Performance Model." M.S. Thesis. Massachusetts Institute of Technology, 2006.

Appendix A

TRIUNE Particle Lifetime History Simulation Procedure

Setup calculations

$$\mathrm{P}^{i}_{insert} = \frac{\mathrm{N}^{i}_{pebbles}}{\sum_{i=1}^{\mathrm{N}_f}(\mathrm{N}^{i}_{pebbles})}$$

$$\mathrm{trackbreak}^{i} = \frac{\sum_{i=1}^{i}(\mathrm{P}^{i}_{insert})}{\sum_{i=1}^{\mathrm{N}_f}(\mathrm{P}^{i}_{insert})}$$

$$\Delta\mathrm{T}^{i}_{peb} = \mathrm{T}^{i}_{pc_{avg}} - \mathrm{T}^{i}_{ps_{avg}}$$

where:

$\mathbf{P}^{i}_{insert}$ is the probability of a pebble being inserted into track i

$\mathbf{N}^{i}_{pebbles}$ is the total number of fuel pebbles in track i .

$\mathbf{N}_f$ is the total number of pebble tracks or flux regions in the blanket

trackbreak^{i} establishes a breakpoint on a cumulative distribution function

$\Delta\mathbf{T}^{i}_{peb}$ is the temperature difference between the pebble surface and center in a pebble in track i

$\mathbf{T}_{pc_{avg}}$ is the average temperature at the center of a pebble in track i

$\mathbf{T}_{ps_{avg}}$ is the average temperature at the surface of a pebble in track i

and

$\mathbf{N}_f$ is read in from the parsed neutronics output data

$\mathbf{N}^{i}_{pebbles}$ is derived from N_f and other system design parameters

$\mathbf{T}_{pc_{avg}}$ **and** $\mathbf{T}_{ps_{avg}}$ are from the heat transfer calculations described in Section 4.1

for t=1 to ntottsteps:

$$\text{fracfiss}^{i,t} = \frac{\text{V}^{i}_{track} \times \dot{\text{f}}^{i,t}_{tot,nom}}{\sum_{i=1}^{\text{N}_f}(\text{V}^{i}_{track} \times \dot{\text{f}}^{i,t}_{tot,nom})}$$

$$\text{relfracfiss}^{i,t} = \frac{\text{fracfiss}_{i,t}}{\frac{\sum_{i=1}^{\text{N}_f}(\text{fracfiss}_{i,t})}{\text{N}_f}}$$

$$\left(\frac{d\tau}{d\text{days}}\right)^{i,t} = \frac{\tau^{t+1}_{nom} - \tau^{t}_{nom}}{\text{days}^{t+1}_{nom} - \text{days}^{t}_{nom}}$$

where:

ntottsteps is the total number of time steps in the neutronics results vectors

$\mathbf{V}^{i}_{track}$ is the total volume of track i [cm^3] .

$\dot{\mathbf{f}}^{i,t}_{tot,nom}$ is the total fission rate for a nominal particle in track i at time step t [fissions/s]

fracfiss^{i,t} is fraction of total fissions that are produced in track i at time step t

relfracfiss^{i,t} is the relative fission rate of track i at time step t scaled to the average fission rate per track in the full blanket

τ^{t}_{nom} **and** τ^{t+1}_{nom} are the batch average fuel burnup levels at the beginning of time step t and t+1 [% FIMA]

days$^{t}_{nom}$ **and days**$^{t+1}_{nom}$ represent the nominal cumulative irradiation duration that a nominal particle has experienced at the beginning of time step t or $t+1$ [days]

Main calculations

for n=1 to Ntotparticles:

$$\text{r}^{n}_{\text{TRISO}} = \left(\zeta \times (\text{r}_{\text{pebble}})^3\right)^{1/3}$$

for t=1

$$\text{track}^{n,t} = i \quad \text{such that} \quad \text{trackbreak}^{i-1} \leq \zeta < \text{trackbreak}^{i}$$

$$\tau^{n,t=1}_{\text{batch}} = \tau^{t=1}_{\text{nom}}$$

$$\text{days}^{n,t=1}_{\text{batch}} = \text{days}^{t=1}_{\text{nom}}$$

$$\text{qkern}^{n,t}_{\text{batch}} = \text{qkern}^{i=\text{track}^{n,t},t=1}_{\text{nom}} \times \left(\frac{\text{m}^{n,BOL}_{\text{kern}}}{\text{m}^{BOL}_{\text{kern,nom}}}\right)$$

$$\begin{aligned}
\text{qcoat}^{n,t}_{\text{batch}} &= \text{qcoat}^{i=\text{track}^{n,t},t=1}_{\text{nom}} \times \left(\frac{\text{m}^{n,BOL}_{\text{coat}}}{\text{m}^{BOL}_{\text{coat,nom}}}\right) \\
\text{dtimesecs}^{n,t} &= 0 \\
\text{nvt25}^{n,t}_{\text{batch}} &= \text{fastflux}^{i=\text{track}^{n,t},t=1}_{\text{nom}} \times (\text{dtimesecs}^{n,t}) \times \frac{10^4}{10^{25}} \\
\text{nXe_mol}^{n,t}_{\text{batch}} &= \text{nXe_mol}^{t=1}_{\text{nom}} \\
\text{nKr_mol}^{n,t}_{\text{batch}} &= \text{nKr_mol}^{t=1}_{\text{nom}} \\
\text{T}^{n,t}_{\text{bound}} &= \text{T}^{i=track^{n,t}}_{ps_avg} + \Delta\text{T}^{i=track^{n,t}}_{peb} \times interp(\text{PebTemp_rfrac,PebTemp_Tfrac,r}^{n}_{\text{TRISO}}))
\end{aligned}$$

for t=2 to ntotsteps

if $\tau^{\mathbf{n,t-1}}_{\mathbf{batch}} > max(\tau_{\text{nom}})$ **OR** $\mathbf{days}^{\mathbf{n,t-1}}_{\text{batch}} > max(\mathbf{days}_{\text{nom}})$ **OR** $\tau^{\mathbf{n,t-1}}_{\text{batch}} == \mathbf{NaN}$

$$\begin{aligned}
\tau^{n,t}_{\text{batch}} &= NaN \\
\text{days}^{n,t}_{\text{batch}} &= NaN \\
\text{dtimesecs}^{n,t}_{\text{batch}} &= NaN \\
\text{nvt25}^{n,t}_{\text{batch}} &= NaN \\
\text{track}^{n,t}_{\text{batch}} &= NaN
\end{aligned}$$

else

$$\begin{aligned}
\text{track}^{n,t} &= i \quad \text{such that} \quad \text{trackbreak}^{i-1} \leq \zeta < \text{trackbreak}^{i} \\
\tau^{n,t}_{\text{batch}} &= \tau^{n,t-1}_{\text{batch}} + interp(\tau_{\text{nom}}, \frac{d\tau}{\text{ddays}}, \tau^{n,t-1}_{\text{batch}}) \times (\text{t}_{\text{res}}) \\
&\quad \times interp(\tau_{\text{nom}}, \text{relfracfiss}^{i=\text{track}^{n,t-1}}, \tau^{n,t-1}_{\text{batch}}) \\
\text{days}^{n,t}_{\text{batch}} &= \text{days}^{n,t-1}_{\text{batch}} + \text{t}_{res} \\
\text{qkern}^{n,t}_{\text{batch}} &= interp(\tau_{\text{nom}}, \text{qkern}^{i=\text{track}^{n,t-1}}_{\text{nom}}, \tau^{n,t-1}_{\text{batch}}) \times \left(\frac{\text{m}^{n,BOL}_{\text{kern}}}{\text{m}^{BOL}_{\text{kern,nom}}}\right) \\
\text{qcoat}^{n,t}_{\text{batch}} &= interp(\tau_{\text{nom}}, \text{qcoat}^{i=\text{track}^{n,t-1}}_{\text{nom}}, \tau^{n,t-1}_{\text{batch}}) \times \left(\frac{\text{m}^{n,BOL}_{\text{coat}}}{\text{m}^{BOL}_{\text{coat,nom}}}\right) \\
\text{dtimesecs}^{n,t} &= (\text{days}^{n,t}_{\text{batch}} - \text{days}^{n,t-1}_{\text{batch}}) \times 24 \times 3600 \\
\text{nvt25}^{n,t}_{\text{batch}} &= \text{nvt25}^{n,t-1}_{\text{batch}} + interp(\text{days}_{\text{nom}}, \text{fastflux}^{i=\text{track}^{n,t-1}}_{\text{nom}}, \text{days}^{n,t-1}_{\text{batch}}) \\
&\quad \times (\text{dtimesecs}^{n,t}) \times \left(\frac{10^4}{10^{25}}\right)
\end{aligned}$$

$$\mathrm{nXe\_mol}^{n,t}_{\mathrm{batch}} = \mathit{interp}(\tau_{\mathrm{nom}}, \mathrm{nXe\_mol}_{\mathrm{nom}}, \tau^{n,t}_{\mathrm{batch}}) \times \left(\frac{\mathrm{m}^{n,BOL}_{\mathrm{kern}}}{\mathrm{m}^{BOL}_{\mathrm{kern,nom}}} \right)$$

$$\mathrm{nKr\_mol}^{n,t}_{\mathrm{batch}} = \mathit{interp}(\tau_{\mathrm{nom}}, \mathrm{nKr\_mol}_{\mathrm{nom}}, \tau^{n,t}_{\mathrm{batch}}) \times \left(\frac{\mathrm{m}^{n,BOL}_{\mathrm{kern}}}{\mathrm{m}^{BOL}_{\mathrm{kern,nom}}} \right)$$

$$\begin{aligned} \mathrm{T}^{n,t}_{\mathrm{bound}} &= \mathrm{T}^{i=\mathrm{track}^{n,t-1}}_{\mathrm{ps\_avg}} + \Delta\mathrm{T}^{i=\mathrm{track}^{n,t-1}}_{\mathrm{peb}} \\ &\quad \times \mathit{interp}(\mathrm{PebTemp\_rfrac,PebTemp\_Tfrac,r}^{n}_{\mathrm{TRISO}}) \end{aligned}$$

where:

Ntotparticles is the user-specified number of TRISO particles to be simulated

ζ is a pseudo-random number generated by MATLAB using a uniform distribution on the interval $0 < \zeta < 1$, with an independent generated every time it is called .

$\mathbf{r_{pebble}}$ is the radius of a fuel pebble in the system [cm]

$\mathbf{track}^{n,t}$ is the track into which the pebble containing particle n was inserted during timestep t

$\mathbf{m^{BOL}_{kern,nom}}$ **and** $\mathbf{m^{n,BOL}_{kern,nom}}$ are the BOL masses for the fuel kernel and combined coating layers for a nominal particle [g]

$\mathbf{m^{BOL}_{kern,nom}}$ **and** $\mathbf{m^{n,BOL}_{coat,nom}}$ are the BOL masses for the fuel kernel and combined coating layers for particle n [g]

$\mathbf{qkern}^{n,t}_{\mathbf{batch}}$ **and** $\mathbf{qcoat}^{n,t}_{\mathbf{batch}}$) are the power levels in the kernel and coating layers of particle n at time step t [W]

$\mathbf{dtimesecs}^{n,t}$ is the amount of time that particle n was irradiated between time steps $t-1$ and t [seconds]

$\mathbf{fastflux}^{i,t}_{\mathbf{nom}}$ is the fast flux ($\mathrm{E}_n > 0.18$ MeV) experienced by a nominal TRISO particle in track i at time step t $\left[\frac{n}{cm^2-s}\right]$

$\mathbf{nvt25}^{n,t}_{\mathbf{batch}}$ is the total fast neutron fluence ($\mathrm{E}_n > 0.18$ MeV) that particle n has accumulated at the beginning of time step t $\left[10^{25}\frac{n}{m^2}\right]$

$\mathbf{nXe\_mol}^{t}_{\mathbf{nom}}$ **and** $\mathbf{nKr\_mol}^{t}_{\mathbf{nom}}$ are the Xe and Kr fission product inventories of a nominal particle at the beginning of time step t

$\mathbf{nXe\_mol}^{n,t}_{\mathbf{batch}}$ **and** $\mathbf{nKr\_mol}^{n,t}_{\mathbf{batch}}$ are the Xe and Kr fission product inventories in particle n at the beginning of time step t

***interp*(x,y,x′)** is a built-in MATLAB command that interpolates on vectors x and y to find the value of y′ at a specified value x′

PebTemp_rfrac and PebTemp_Tfrac are arrays that contain normalized values for a temperature distribution within a representative fuel pebble in a LIFE blanket; these arrays provide a normalized temperature distribution within the fuel pebble and thus allow sampling actual temperatures as a function of pebble radius when given temperatures at the pebble surface and center. [/]

$\mathbf{T}_{\mathbf{bound}}^{n,t}$ is the boundary temperature found at the outer OPyC surface of particle n at time step t [K]

$\mathbf{t}_{\mathbf{res}}$ is the user-specified residence time between pebble insertion into the blanket and pebble extraction from the blanket [days]

Appendix B

Stress analysis in spherical pressure vessels

$$K_1 = -\frac{2r^3 r_a^3(1-2\mu) + r_a^3 r_b^3(1+\mu)}{2Er^2(r_b^3 - r_a^3)} \tag{B.1}$$

$$K_2 = \frac{2r^3 r_b^3(1-2\mu) + r_a^3 r_b^3(1+\mu)}{2Er^2(r_b^3 - r_a^3)} \tag{B.2}$$

$$K_3 = -\frac{2r^3 r_a^3(1-2\nu) + r_a^3 r_b^3(1+\nu)}{2r^2(r_b^3 - r_a^3)} \tag{B.3}$$

$$K_4 = \frac{2r^3 r_b^3(1-2\nu) + r_a^3 r_b^3(1+\nu)}{2r^2(r_b^3 - r_a^3)} \tag{B.4}$$

$$K_5 = \frac{r_a^3 r_b^3 \ln(\frac{r_a}{r_b})}{r^2(r_b^3 - r_a^3)} + \frac{r}{3} \tag{B.5}$$

$$K_6 = -\frac{r_a^3 r_b^3 \ln(\frac{r_a}{r_b})}{r^2(r_b^3 - r_a^3)} + \frac{2r}{3} \tag{B.6}$$

$$K_7 = \frac{r_a^3(\nu-\mu)}{3E(\nu-1)}\left[\frac{r_b^3(r^3 - r_a^3)\ln r_b - r_a^3(r^3 - r_b^3)\ln r_a}{r^2(r_b^3 - r_a^3)} - r\ln r\right] \tag{B.7}$$

$$Z = b_2 c_1 - (c_2 - d_1)(b_1 - a_2) \tag{B.8}$$

$$B_1 = \frac{a_4 c_I c_1}{Z} \tag{B.9}$$

$$B_2 = -\frac{d_3 c_O (b_1 - a_2)}{Z} \tag{B.10}$$

$$B_3 = -\frac{a_4 c_I (c_2 - d_1)}{Z} \tag{B.11}$$

$$B_4 = \frac{d_3 c_O b_2}{Z} \tag{B.12}$$

$$\begin{aligned} x_0 Z = {} & [-c_1 r_3 + (b_1 - a_2) r_4] \overline{\alpha}_s \frac{\Delta T_s}{\Delta t} + a_1 c_1 \frac{\Delta p}{\Delta t} - d_2 (b_1 - a_2) \frac{\Delta q}{\Delta t} \\ & + c_1 a_3 c_I \left(p_{n-1} - \frac{\Delta p}{\Delta t} t_{n-1} \right) - d_4 (b_1 - a_2) c_O \left(q_{n-1} - \frac{\Delta q}{\Delta t} t_{n-1} \right) \\ & + a_5 c_1 \left(\overline{S}_{rI} + \overline{\alpha}_{rI} \frac{\Delta T_I}{\Delta t} \right) + a_6 c_1 \left(\overline{S}_{tI} + \overline{\alpha}_{tI} \frac{\Delta T_I}{\Delta t} \right) \\ & - d_2 (b_1 - a_2) \left(\overline{S}_{rO} + \overline{\alpha}_{rO} \frac{\Delta T_O}{\Delta t} \right) - d_2 (b_1 - a_2) \left(\overline{S}_{tO} + \overline{\alpha}_{tO} \frac{\Delta T_O}{\Delta t} \right) \end{aligned} \tag{B.13}$$

$$x_1 = \frac{1}{Z} \left[c_2 a_3 c_I \frac{\Delta p}{\Delta t} - d_4 (b_1 - a_2) c_O \frac{\Delta q}{\Delta t} \right] \tag{B.14}$$

$$\begin{aligned} -y_0 Z = {} & [b_2 r_4 - (c_2 - d_1) r_3] \overline{\alpha}_s \frac{\Delta T_s}{\Delta t} + a_1 (c_2 - d_1) \frac{\Delta p}{\Delta t} - b_2 d_2 \frac{\Delta q}{\Delta t} \\ & + a_3 (c_2 - d_1) c_I \left(p_{n-1} - \frac{\Delta p}{\Delta t} t_{n-1} \right) - b_2 d_4 c_O \left(q_{n-1} - \frac{\Delta q}{\Delta t} t_{n-1} \right) \\ & + a_5 (c_2 - d_1) \left(\overline{S}_{rI} + \overline{\alpha}_{rI} \frac{\Delta T_I}{\Delta t} \right) + a_6 (c_2 - d_1) \left(\overline{S}_{tI} + \overline{\alpha}_{tI} \frac{\Delta T_I}{\Delta t} \right) \\ & - b_2 d_5 \left(\overline{S}_{rO} + \overline{\alpha}_{rO} \frac{\Delta T_O}{\Delta t} \right) - b_2 d_6 \left(\overline{S}_{tO} + \overline{\alpha}_{tO} \frac{\Delta T_O}{\Delta t} \right) \end{aligned} \tag{B.15}$$

$$y_1 = \frac{1}{Z}\left[a_3(c_2-d_1)c_I\frac{\Delta p}{\Delta t} - b_2 d_4 c_O \frac{\Delta q}{\Delta t}\right] \tag{B.16}$$

$$m_1, m_2 = \frac{1}{2}\left\{B_2 + B_3 \pm \sqrt{(B_2+B_3)^2 - 4(B_2B_3 - B_1B_4)}\right\} \tag{B.17}$$

$$\nu_1 = \frac{B_1 y_1 - B_3 x_1}{B_2 B_3 - B_1 B_4} \tag{B.18}$$

$$\nu_0 = \frac{(B_2+B_3)\nu_1 + x_1 - B_3 x_0 + B_1 y_0}{B_2 B_3 - B_1 B_4} \tag{B.19}$$

$$w_0 = \frac{\nu_1 - B_2\nu_0 - x_0}{B_1} \tag{B.20}$$

$$w_1 = \frac{B_2\nu_1 + x_1}{B_1} \tag{B.21}$$

Appendix C

Sample MCNP Input File

```
LIFE - TRISO fuel
c Thesis run for Jeff Powers.  Run tag: t13
c 20MT system mass, 15\% TRISO Packing Fraction, 20cm mult. thk.
c
1   1   -4.0E-006       -1
                        tmp=7.95478E-008  vol=6.54498E+007  imp:n,p 1
c
c  First wall armor: tungsten
3   3   -19.3          1 -2
                     21 22 23 24 25 26 27 28 29 30 31 32
                     33 34 35 36 37 38 39 40 41 42 43 44
                        tmp=7.95478E-008  vol=1.91439E+04  imp:n,p 1
c
c  First wall: ods
4   4   -8.0           2 -3
                     21 22 23 24 25 26 27 28 29 30 31 32
                     33 34 35 36 37 38 39 40 41 42 43 44
                        tmp=7.95478E-008  vol=2.10553E+05  imp:n,p 1
c
c  Dedicated first wall cooling: lipb
5   5   -9.40          3 -4
                     21 22 23 24 25 26 27 28 29 30 31 32
                     33 34 35 36 37 38 39 40 41 42 43 44
                        tmp=5.36968E-008  vol=2.33330E+06  imp:n,p 1
c
c  Second wall: ods
6   4   -8.0           4 -5
                     21 22 23 24 25 26 27 28 29 30 31 32
                     33 34 35 36 37 38 39 40 41 42 43 44
```

```
                        tmp=6.48989E-008  vol=2.37080E+05  imp:n,p 1
c
c  Main coolant injection plenum: flibe
7   7   -1.9820       5 -6
                     21 22 23 24 25 26 27 28 29 30 31 32
                     33 34 35 36 37 38 39 40 41 42 43 44
                        tmp=7.61010E-008  vol=2.38993E+06  imp:n,p 1
c
c  Third wall: ods
8   4   -6.0          6 -7
                     21 22 23 24 25 26 27 28 29 30 31 32
                     33 34 35 36 37 38 39 40 41 42 43 44
                        tmp=7.61829E-008  vol=2.42264E+05  imp:n,p 1
c
c  Beryllium/coolant mix (60/40 vol)
9   9   -1.9409       7 -8
                     21 22 23 24 25 26 27 28 29 30 31 32
                     33 34 35 36 37 38 39 40 41 42 43 44
                        tmp=7.62639E-008  vol=1.75428E+07  imp:n,p 1
c
c  Fourth wall: ods
10  4   -6.0          8 -9
                     21 22 23 24 25 26 27 28 29 30 31 32
                     33 34 35 36 37 38 39 40 41 42 43 44
                        tmp=7.72480E-008  vol=2.82946E+05  imp:n,p 1
c
c  Fuel zone -- mix of pebbles and flibe coolant (60/40 vol)
51  0                  9 -101
                     21 22 23 24 25 26 27 28 29 30 31 32
                     33 34 35 36 37 38 39 40 41 42 43 44  imp:n,p 1
          fill=101
c
52  0                101 -102
                     21 22 23 24 25 26 27 28 29 30 31 32
                     33 34 35 36 37 38 39 40 41 42 43 44  imp:n,p 1
          fill=102
c
53  0                102 -103
                     21 22 23 24 25 26 27 28 29 30 31 32
                     33 34 35 36 37 38 39 40 41 42 43 44  imp:n,p 1
          fill=103
c
```

```
54  0               103 -104
                    21 22 23 24 25 26 27 28 29 30 31 32
                    33 34 35 36 37 38 39 40 41 42 43 44  imp:n,p 1
          fill=104
c
55  0               104 -105
                    21 22 23 24 25 26 27 28 29 30 31 32
                    33 34 35 36 37 38 39 40 41 42 43 44  imp:n,p 1
          fill=105
c
56  0               105 -106
                    21 22 23 24 25 26 27 28 29 30 31 32
                    33 34 35 36 37 38 39 40 41 42 43 44  imp:n,p 1
          fill=106
c
57  0               106 -107
                    21 22 23 24 25 26 27 28 29 30 31 32
                    33 34 35 36 37 38 39 40 41 42 43 44  imp:n,p 1
          fill=107
c
58  0               107 -108
                    21 22 23 24 25 26 27 28 29 30 31 32
                    33 34 35 36 37 38 39 40 41 42 43 44  imp:n,p 1
          fill=108
c
59  0               108 -109
                    21 22 23 24 25 26 27 28 29 30 31 32
                    33 34 35 36 37 38 39 40 41 42 43 44  imp:n,p 1
          fill=109
c
60  0               109 -110
                    21 22 23 24 25 26 27 28 29 30 31 32
                    33 34 35 36 37 38 39 40 41 42 43 44  imp:n,p 1
          fill=110
c
61  0               110 -111
                    21 22 23 24 25 26 27 28 29 30 31 32
                    33 34 35 36 37 38 39 40 41 42 43 44  imp:n,p 1
          fill=111
c
62  0               111 -10
                    21 22 23 24 25 26 27 28 29 30 31 32
```

```
                    33 34 35 36 37 38 39 40 41 42 43 44  imp:n,p 1
         fill=112
c
c  Back wall to fuel region: ods
12  4   -6.0         10 -11
                    21 22 23 24 25 26 27 28 29 30 31 32
                    33 34 35 36 37 38 39 40 41 42 43 44
                       tmp=7.86861E-008  vol=8.97395E+05  imp:n,p 1
c
c  Graphite reflector
13  13  -1.8069      11 -12
                    21 22 23 24 25 26 27 28 29 30 31 32
                    33 34 35 36 37 38 39 40 41 42 43 44
                       tmp=7.87215E-008  vol=3.05769E+08  imp:n,p 1
c
c  Final wall: ods
14  4   -6.0         12 -13
                    21 22 23 24 25 26 27 28 29 30 31 32
                    33 34 35 36 37 38 39 40 41 42 43 44
                       tmp=7.86861E-008  vol=1.58277E+06  imp:n,p 1
c
c -------------------Pebble and TRISO lattice --------------------
c
101  51  -10.00000
                     -51
                       tmp=9.24733E-008  vol=1.87442E+05  imp:n,p 1 u=401
102  16  -1.7297       51
                       tmp=8.81648E-008  vol=6.66764E+06  imp:n,p 1 u=401
201  0               -53 54 -55 56 -57 58
          lat=1 fill=401                                  imp:n,p 1 u=301
c
c  Pebble unit cell--BCC
301  0                  -161
          fill=301                                        imp:n,p 1 u=201
302  17  -1.70         161 -162
                       tmp=7.95694E-008  vol=1.04893E+05  imp:n,p 1 u=201
303  0                  -163
          fill=301                                        imp:n,p 1 u=201
304  17  -1.70         163 -164
                       tmp=7.95694E-008  vol=1.31045E+04  imp:n,p 1 u=201
305  0                  -165
          fill=301                                        imp:n,p 1 u=201
```

```
306  17  -1.70         165 -166
                        tmp=7.95694E-008  vol=1.31396E+04  imp:n,p 1 u=201
307  0                   -167
          fill=301                                         imp:n,p 1 u=201
308  17  -1.70         167 -168
                        tmp=7.95694E-008  vol=1.30796E+04  imp:n,p 1 u=201
309  0                   -169
          fill=301                                         imp:n,p 1 u=201
310  17  -1.70         169 -170
                        tmp=7.95694E-008  vol=1.30687E+04  imp:n,p 1 u=201
311  0                   -171
          fill=301                                         imp:n,p 1 u=201
312  17  -1.70         171 -172
                        tmp=7.95694E-008  vol=1.30776E+04  imp:n,p 1 u=201
313  0                   -173
          fill=301                                         imp:n,p 1 u=201
314  17  -1.70         173 -174
                        tmp=7.95694E-008  vol=1.31322E+04  imp:n,p 1 u=201
315  0                   -175
          fill=301                                         imp:n,p 1 u=201
316  17  -1.70         175 -176
                        tmp=7.95694E-008  vol=1.31393E+04  imp:n,p 1 u=201
317  0                   -177
          fill=301                                         imp:n,p 1 u=201
318  17  -1.70         177 -178
                        tmp=7.95694E-008  vol=1.31011E+04  imp:n,p 1 u=201
c
319  18  -1.9700        162 164
                       166 168 170 172 174 176 178
                        tmp=7.82320E-008  vol=4.70550E+06  imp:n,p 1 u=201
901  0                 -181 182 -183 184 -185 186
          lat=1 fill=201                                   imp:n,p 1 u=101
c
c ------------------------------------------------------------
c
103  51  -10.00000
                       -51
                        tmp=9.24733E-008  vol=1.87379E+05  imp:n,p 1 u=402
104  16  -1.7297        51
                        tmp=8.81648E-008  vol=6.65999E+06  imp:n,p 1 u=402
202  0                 -53 54 -55 56 -57 58
          lat=1 fill=402                                   imp:n,p 1 u=302
```

```
c
c  Pebble unit cell--BCC
321  0                  -161
          fill=302                                          imp:n,p 1 u=202
322  17  -1.70         161 -162
                        tmp=7.95694E-008  vol=1.04717E+05  imp:n,p 1 u=202
323  0                  -163
          fill=302                                          imp:n,p 1 u=202
324  17  -1.70         163 -164
                        tmp=7.95694E-008  vol=1.30594E+04  imp:n,p 1 u=202
325  0                  -165
          fill=302                                          imp:n,p 1 u=202
326  17  -1.70         165 -166
                        tmp=7.95694E-008  vol=1.30861E+04  imp:n,p 1 u=202
327  0                  -167
          fill=302                                          imp:n,p 1 u=202
328  17  -1.70         167 -168
                        tmp=7.95694E-008  vol=1.30793E+04  imp:n,p 1 u=202
329  0                  -169
          fill=302                                          imp:n,p 1 u=202
330  17  -1.70         169 -170
                        tmp=7.95694E-008  vol=1.31028E+04  imp:n,p 1 u=202
331  0                  -171
          fill=302                                          imp:n,p 1 u=202
332  17  -1.70         171 -172
                        tmp=7.95694E-008  vol=1.30884E+04  imp:n,p 1 u=202
333  0                  -173
          fill=302                                          imp:n,p 1 u=202
334  17  -1.70         173 -174
                        tmp=7.95694E-008  vol=1.30714E+04  imp:n,p 1 u=202
335  0                  -175
          fill=302                                          imp:n,p 1 u=202
336  17  -1.70         175 -176
                        tmp=7.95694E-008  vol=1.31591E+04  imp:n,p 1 u=202
337  0                  -177
          fill=302                                          imp:n,p 1 u=202
338  17  -1.70         177 -178
                        tmp=7.95694E-008  vol=1.30911E+04  imp:n,p 1 u=202
c
339  18  -1.9700       162 164
                       166 168 170 172 174 176 178
                        tmp=7.82320E-008  vol=4.70303E+06  imp:n,p 1 u=202
```

```
902  0               -181 182 -183 184 -185 186
          lat=1 fill=202                                    imp:n,p 1 u=102
c
c ------------------------------------------------------------
c
105  51  -10.00000
                     -51
                       tmp=9.24733E-008  vol=1.87330E+05  imp:n,p 1 u=403
106  16  -1.7297       51
                       tmp=8.81648E-008  vol=6.65247E+06  imp:n,p 1 u=403
203  0               -53 54 -55 56 -57 58
          lat=1 fill=403                                    imp:n,p 1 u=303
c
c  Pebble unit cell--BCC
341  0                  -161
          fill=303                                          imp:n,p 1 u=203
342  17  -1.70         161 -162
                       tmp=7.95694E-008  vol=1.04653E+05  imp:n,p 1 u=203
343  0                  -163
          fill=303                                          imp:n,p 1 u=203
344  17  -1.70         163 -164
                       tmp=7.95694E-008  vol=1.31150E+04  imp:n,p 1 u=203
345  0                  -165
          fill=303                                          imp:n,p 1 u=203
346  17  -1.70         165 -166
                       tmp=7.95694E-008  vol=1.30954E+04  imp:n,p 1 u=203
347  0                  -167
          fill=303                                          imp:n,p 1 u=203
348  17  -1.70         167 -168
                       tmp=7.95694E-008  vol=1.30853E+04  imp:n,p 1 u=203
349  0                  -169
          fill=303                                          imp:n,p 1 u=203
350  17  -1.70         169 -170
                       tmp=7.95694E-008  vol=1.31104E+04  imp:n,p 1 u=203
351  0                  -171
          fill=303                                          imp:n,p 1 u=203
352  17  -1.70         171 -172
                       tmp=7.95694E-008  vol=1.30590E+04  imp:n,p 1 u=203
353  0                  -173
          fill=303                                          imp:n,p 1 u=203
354  17  -1.70         173 -174
                       tmp=7.95694E-008  vol=1.30553E+04  imp:n,p 1 u=203
```

```
355  0                    -175
          fill=303                                          imp:n,p 1 u=203
356  17  -1.70          175 -176
                         tmp=7.95694E-008  vol=1.30396E+04  imp:n,p 1 u=203
357  0                    -177
          fill=303                                          imp:n,p 1 u=203
358  17  -1.70          177 -178
                         tmp=7.95694E-008  vol=1.30610E+04  imp:n,p 1 u=203
c
359  18  -1.9700        162 164
                        166 168 170 172 174 176 178
                         tmp=7.82320E-008  vol=4.69977E+06  imp:n,p 1 u=203
903  0                 -181 182 -183 184 -185 186
          lat=1 fill=203                                    imp:n,p 1 u=103
c
c ------------------------------------------------------------
c
107  51  -10.00000
                       -51
                         tmp=9.24733E-008  vol=1.87040E+05  imp:n,p 1 u=404
108  16  -1.7297        51
                         tmp=8.81648E-008  vol=6.65031E+06  imp:n,p 1 u=404
204  0                 -53 54 -55 56 -57 58
          lat=1 fill=404                                    imp:n,p 1 u=304
c
c  Pebble unit cell--BCC
361  0                    -161
          fill=304                                          imp:n,p 1 u=204
362  17  -1.70          161 -162
                         tmp=7.95694E-008  vol=1.04679E+05  imp:n,p 1 u=204
363  0                    -163
          fill=304                                          imp:n,p 1 u=204
364  17  -1.70          163 -164
                         tmp=7.95694E-008  vol=1.30672E+04  imp:n,p 1 u=204
365  0                    -165
          fill=304                                          imp:n,p 1 u=204
366  17  -1.70          165 -166
                         tmp=7.95694E-008  vol=1.30503E+04  imp:n,p 1 u=204
367  0                    -167
          fill=304                                          imp:n,p 1 u=204
368  17  -1.70          167 -168
                         tmp=7.95694E-008  vol=1.30981E+04  imp:n,p 1 u=204
```

```
369  0                    -169
          fill=304                                          imp:n,p 1 u=204
370  17  -1.70          169 -170
                         tmp=7.95694E-008  vol=1.30765E+04  imp:n,p 1 u=204
371  0                    -171
          fill=304                                          imp:n,p 1 u=204
372  17  -1.70          171 -172
                         tmp=7.95694E-008  vol=1.30402E+04  imp:n,p 1 u=204
373  0                    -173
          fill=304                                          imp:n,p 1 u=204
374  17  -1.70          173 -174
                         tmp=7.95694E-008  vol=1.30828E+04  imp:n,p 1 u=204
375  0                    -175
          fill=304                                          imp:n,p 1 u=204
376  17  -1.70          175 -176
                         tmp=7.95694E-008  vol=1.30397E+04  imp:n,p 1 u=204
377  0                    -177
          fill=304                                          imp:n,p 1 u=204
378  17  -1.70          177 -178
                         tmp=7.95694E-008  vol=1.31047E+04  imp:n,p 1 u=204
c
379  18  -1.9700        162 164
                        166 168 170 172 174 176 178
                         tmp=7.82320E-008  vol=4.70058E+06  imp:n,p 1 u=204
904  0                 -181 182 -183 184 -185 186
          lat=1 fill=204                                    imp:n,p 1 u=104
c
c ------------------------------------------------------------
c
109  51  -10.00000
                        -51
                         tmp=9.24733E-008  vol=1.87406E+05  imp:n,p 1 u=405
110  16  -1.7297        51
                         tmp=8.81648E-008  vol=6.65988E+06  imp:n,p 1 u=405
205  0                 -53 54 -55 56 -57 58
          lat=1 fill=405                                    imp:n,p 1 u=305
c
c  Pebble unit cell--BCC
381  0                    -161
          fill=305                                          imp:n,p 1 u=205
382  17  -1.70          161 -162
                         tmp=7.95694E-008  vol=1.04840E+05  imp:n,p 1 u=205
```

```
383  0                    -163
          fill=305                                          imp:n,p 1 u=205
384  17  -1.70          163 -164
                          tmp=7.95694E-008  vol=1.30495E+04  imp:n,p 1 u=205
385  0                    -165
          fill=305                                          imp:n,p 1 u=205
386  17  -1.70          165 -166
                          tmp=7.95694E-008  vol=1.30848E+04  imp:n,p 1 u=205
387  0                    -167
          fill=305                                          imp:n,p 1 u=205
388  17  -1.70          167 -168
                          tmp=7.95694E-008  vol=1.31125E+04  imp:n,p 1 u=205
389  0                    -169
          fill=305                                          imp:n,p 1 u=205
390  17  -1.70          169 -170
                          tmp=7.95694E-008  vol=1.30976E+04  imp:n,p 1 u=205
391  0                    -171
          fill=305                                          imp:n,p 1 u=205
392  17  -1.70          171 -172
                          tmp=7.95694E-008  vol=1.30869E+04  imp:n,p 1 u=205
393  0                    -173
          fill=305                                          imp:n,p 1 u=205
394  17  -1.70          173 -174
                          tmp=7.95694E-008  vol=1.31403E+04  imp:n,p 1 u=205
395  0                    -175
          fill=305                                          imp:n,p 1 u=205
396  17  -1.70          175 -176
                          tmp=7.95694E-008  vol=1.31361E+04  imp:n,p 1 u=205
397  0                    -177
          fill=305                                          imp:n,p 1 u=205
398  17  -1.70          177 -178
                          tmp=7.95694E-008  vol=1.31024E+04  imp:n,p 1 u=205
c
399  18  -1.9700         162 164
                        166 168 170 172 174 176 178
                          tmp=7.82320E-008  vol=4.70011E+06  imp:n,p 1 u=205
905  0                 -181 182 -183 184 -185 186
          lat=1 fill=205                                    imp:n,p 1 u=105
c
c ------------------------------------------------------------
c
111  51  -10.00000
```

```
                     -51
                       tmp=9.24733E-008  vol=1.86988E+05  imp:n,p 1 u=406
112  16  -1.7297       51
                       tmp=8.81648E-008  vol=6.64722E+06  imp:n,p 1 u=406
206  0               -53 54 -55 56 -57 58
          lat=1 fill=406                                  imp:n,p 1 u=306
c
c  Pebble unit cell--BCC
401  0                  -161
          fill=306                                        imp:n,p 1 u=206
402  17  -1.70         161 -162
                       tmp=7.95694E-008  vol=1.04518E+05  imp:n,p 1 u=206
403  0                  -163
          fill=306                                        imp:n,p 1 u=206
404  17  -1.70         163 -164
                       tmp=7.95694E-008  vol=1.30458E+04  imp:n,p 1 u=206
405  0                  -165
          fill=306                                        imp:n,p 1 u=206
406  17  -1.70         165 -166
                       tmp=7.95694E-008  vol=1.30834E+04  imp:n,p 1 u=206
407  0                  -167
          fill=306                                        imp:n,p 1 u=206
408  17  -1.70         167 -168
                       tmp=7.95694E-008  vol=1.30618E+04  imp:n,p 1 u=206
409  0                  -169
          fill=306                                        imp:n,p 1 u=206
410  17  -1.70         169 -170
                       tmp=7.95694E-008  vol=1.30502E+04  imp:n,p 1 u=206
411  0                  -171
          fill=306                                        imp:n,p 1 u=206
412  17  -1.70         171 -172
                       tmp=7.95694E-008  vol=1.30510E+04  imp:n,p 1 u=206
413  0                  -173
          fill=306                                        imp:n,p 1 u=206
414  17  -1.70         173 -174
                       tmp=7.95694E-008  vol=1.30630E+04  imp:n,p 1 u=206
415  0                  -175
          fill=306                                        imp:n,p 1 u=206
416  17  -1.70         175 -176
                       tmp=7.95694E-008  vol=1.30441E+04  imp:n,p 1 u=206
417  0                  -177
          fill=306                                        imp:n,p 1 u=206
```

```
418  17  -1.70         177 -178
                         tmp=7.95694E-008  vol=1.30548E+04  imp:n,p 1 u=206
c
419  18  -1.9700       162 164
                       166 168 170 172 174 176 178
                         tmp=7.82320E-008  vol=4.69363E+06  imp:n,p 1 u=206
906  0                -181 182 -183 184 -185 186
          lat=1 fill=206                                    imp:n,p 1 u=106
c
c ------------------------------------------------------------
c
113  51  -10.00000
                       -51
                         tmp=9.24733E-008  vol=1.87260E+05  imp:n,p 1 u=407
114  16  -1.7297       51
                         tmp=8.81648E-008  vol=6.65780E+06  imp:n,p 1 u=407
207  0                -53 54 -55 56 -57 58
          lat=1 fill=407                                    imp:n,p 1 u=307
c
c  Pebble unit cell--BCC
421  0                  -161
          fill=307                                          imp:n,p 1 u=207
422  17  -1.70         161 -162
                         tmp=7.95694E-008  vol=1.04848E+05  imp:n,p 1 u=207
423  0                  -163
          fill=307                                          imp:n,p 1 u=207
424  17  -1.70         163 -164
                         tmp=7.95694E-008  vol=1.31106E+04  imp:n,p 1 u=207
425  0                  -165
          fill=307                                          imp:n,p 1 u=207
426  17  -1.70         165 -166
                         tmp=7.95694E-008  vol=1.30975E+04  imp:n,p 1 u=207
427  0                  -167
          fill=307                                          imp:n,p 1 u=207
428  17  -1.70         167 -168
                         tmp=7.95694E-008  vol=1.30724E+04  imp:n,p 1 u=207
429  0                  -169
          fill=307                                          imp:n,p 1 u=207
430  17  -1.70         169 -170
                         tmp=7.95694E-008  vol=1.30760E+04  imp:n,p 1 u=207
431  0                  -171
          fill=307                                          imp:n,p 1 u=207
```

```
432  17  -1.70         171 -172
                         tmp=7.95694E-008  vol=1.30887E+04  imp:n,p 1 u=207
433  0                    -173
          fill=307                                          imp:n,p 1 u=207
434  17  -1.70         173 -174
                         tmp=7.95694E-008  vol=1.30857E+04  imp:n,p 1 u=207
435  0                    -175
          fill=307                                          imp:n,p 1 u=207
436  17  -1.70         175 -176
                         tmp=7.95694E-008  vol=1.31486E+04  imp:n,p 1 u=207
437  0                    -177
          fill=307                                          imp:n,p 1 u=207
438  17  -1.70         177 -178
                         tmp=7.95694E-008  vol=1.30948E+04  imp:n,p 1 u=207
c
439  18  -1.9700       162 164
                       166 168 170 172 174 176 178
                         tmp=7.82320E-008  vol=4.70208E+06  imp:n,p 1 u=207
907  0                -181 182 -183 184 -185 186
          lat=1 fill=207                                    imp:n,p 1 u=107
c
c ------------------------------------------------------------------
c
115  51  -10.00000
                       -51
                         tmp=9.24733E-008  vol=1.87355E+05  imp:n,p 1 u=408
116  16  -1.7297        51
                         tmp=8.81648E-008  vol=6.66341E+06  imp:n,p 1 u=408
208  0                -53 54 -55 56 -57 58
          lat=1 fill=408                                    imp:n,p 1 u=308
c
c  Pebble unit cell--BCC
441  0                    -161
          fill=308                                          imp:n,p 1 u=208
442  17  -1.70         161 -162
                         tmp=7.95694E-008  vol=1.04802E+05  imp:n,p 1 u=208
443  0                    -163
          fill=308                                          imp:n,p 1 u=208
444  17  -1.70         163 -164
                         tmp=7.95694E-008  vol=1.30865E+04  imp:n,p 1 u=208
445  0                    -165
          fill=308                                          imp:n,p 1 u=208
```

```
446  17  -1.70         165 -166
                        tmp=7.95694E-008  vol=1.30913E+04  imp:n,p 1 u=208
447  0                   -167
         fill=308                                          imp:n,p 1 u=208
448  17  -1.70         167 -168
                        tmp=7.95694E-008  vol=1.30984E+04  imp:n,p 1 u=208
449  0                   -169
         fill=308                                          imp:n,p 1 u=208
450  17  -1.70         169 -170
                        tmp=7.95694E-008  vol=1.30748E+04  imp:n,p 1 u=208
451  0                   -171
         fill=308                                          imp:n,p 1 u=208
452  17  -1.70         171 -172
                        tmp=7.95694E-008  vol=1.31004E+04  imp:n,p 1 u=208
453  0                   -173
         fill=308                                          imp:n,p 1 u=208
454  17  -1.70         173 -174
                        tmp=7.95694E-008  vol=1.30977E+04  imp:n,p 1 u=208
455  0                   -175
         fill=308                                          imp:n,p 1 u=208
456  17  -1.70         175 -176
                        tmp=7.95694E-008  vol=1.31599E+04  imp:n,p 1 u=208
457  0                   -177
         fill=308                                          imp:n,p 1 u=208
458  17  -1.70         177 -178
                        tmp=7.95694E-008  vol=1.30725E+04  imp:n,p 1 u=208
c
459  18  -1.9700       162 164
                       166 168 170 172 174 176 178
                        tmp=7.82320E-008  vol=4.70646E+06  imp:n,p 1 u=208
908  0                 -181 182 -183 184 -185 186
         lat=1 fill=208                                    imp:n,p 1 u=108
c
c ------------------------------------------------------------
c
117  51  -10.00000
                       -51
                        tmp=9.24733E-008  vol=1.87421E+05  imp:n,p 1 u=409
118  16  -1.7297        51
                        tmp=8.81648E-008  vol=6.66209E+06  imp:n,p 1 u=409
209  0                 -53 54 -55 56 -57 58
         lat=1 fill=409                                    imp:n,p 1 u=309
```

```
c
c  Pebble unit cell--BCC
461  0                   -161
          fill=309                                          imp:n,p 1 u=209
462  17  -1.70          161 -162
                         tmp=7.95694E-008  vol=1.04896E+05  imp:n,p 1 u=209
463  0                   -163
          fill=309                                          imp:n,p 1 u=209
464  17  -1.70          163 -164
                         tmp=7.95694E-008  vol=1.31425E+04  imp:n,p 1 u=209
465  0                   -165
          fill=309                                          imp:n,p 1 u=209
466  17  -1.70          165 -166
                         tmp=7.95694E-008  vol=1.30987E+04  imp:n,p 1 u=209
467  0                   -167
          fill=309                                          imp:n,p 1 u=209
468  17  -1.70          167 -168
                         tmp=7.95694E-008  vol=1.31089E+04  imp:n,p 1 u=209
469  0                   -169
          fill=309                                          imp:n,p 1 u=209
470  17  -1.70          169 -170
                         tmp=7.95694E-008  vol=1.31353E+04  imp:n,p 1 u=209
471  0                   -171
          fill=309                                          imp:n,p 1 u=209
472  17  -1.70          171 -172
                         tmp=7.95694E-008  vol=1.30819E+04  imp:n,p 1 u=209
473  0                   -173
          fill=309                                          imp:n,p 1 u=209
474  17  -1.70          173 -174
                         tmp=7.95694E-008  vol=1.30923E+04  imp:n,p 1 u=209
475  0                   -175
          fill=309                                          imp:n,p 1 u=209
476  17  -1.70          175 -176
                         tmp=7.95694E-008  vol=1.31075E+04  imp:n,p 1 u=209
477  0                   -177
          fill=309                                          imp:n,p 1 u=209
478  17  -1.70          177 -178
                         tmp=7.95694E-008  vol=1.31351E+04  imp:n,p 1 u=209
c
479  18  -1.9700        162 164
                        166 168 170 172 174 176 178
                         tmp=7.82320E-008  vol=4.70632E+06  imp:n,p 1 u=209
```

```
909  0               -181 182 -183 184 -185 186
          lat=1 fill=209                                    imp:n,p 1 u=109
c
c ------------------------------------------------------------
c
119  51  -10.00000
                     -51
                       tmp=9.24733E-008  vol=1.87342E+05  imp:n,p 1 u=410
120  16  -1.7297       51
                       tmp=8.81648E-008  vol=6.66233E+06  imp:n,p 1 u=410
210  0               -53 54 -55 56 -57 58
          lat=1 fill=410                                    imp:n,p 1 u=310
c
c  Pebble unit cell--BCC
481  0                  -161
          fill=310                                          imp:n,p 1 u=210
482  17  -1.70         161 -162
                       tmp=7.95694E-008  vol=1.04746E+05  imp:n,p 1 u=210
483  0                  -163
          fill=310                                          imp:n,p 1 u=210
484  17  -1.70         163 -164
                       tmp=7.95694E-008  vol=1.31023E+04  imp:n,p 1 u=210
485  0                  -165
          fill=310                                          imp:n,p 1 u=210
486  17  -1.70         165 -166
                       tmp=7.95694E-008  vol=1.30835E+04  imp:n,p 1 u=210
487  0                  -167
          fill=310                                          imp:n,p 1 u=210
488  17  -1.70         167 -168
                       tmp=7.95694E-008  vol=1.30700E+04  imp:n,p 1 u=210
489  0                  -169
          fill=310                                          imp:n,p 1 u=210
490  17  -1.70         169 -170
                       tmp=7.95694E-008  vol=1.30980E+04  imp:n,p 1 u=210
491  0                  -171
          fill=310                                          imp:n,p 1 u=210
492  17  -1.70         171 -172
                       tmp=7.95694E-008  vol=1.30706E+04  imp:n,p 1 u=210
493  0                  -173
          fill=310                                          imp:n,p 1 u=210
494  17  -1.70         173 -174
                       tmp=7.95694E-008  vol=1.30432E+04  imp:n,p 1 u=210
```

```
495  0                    -175
          fill=310                                          imp:n,p 1 u=210
496  17  -1.70          175 -176
                          tmp=7.95694E-008  vol=1.31581E+04  imp:n,p 1 u=210
497  0                    -177
          fill=310                                          imp:n,p 1 u=210
498  17  -1.70          177 -178
                          tmp=7.95694E-008  vol=1.30474E+04  imp:n,p 1 u=210
c
499  18  -1.9700        162 164
                        166 168 170 172 174 176 178
                          tmp=7.82320E-008  vol=4.70451E+06  imp:n,p 1 u=210
910  0                 -181 182 -183 184 -185 186
          lat=1 fill=210                                    imp:n,p 1 u=110
c
c ------------------------------------------------------------
c
121  51  -10.00000
                        -51
                          tmp=9.24733E-008  vol=1.87607E+05  imp:n,p 1 u=411
122  16  -1.7297         51
                          tmp=8.81648E-008  vol=6.66714E+06  imp:n,p 1 u=411
211  0                 -53 54 -55 56 -57 58
          lat=1 fill=411                                    imp:n,p 1 u=311
c
c  Pebble unit cell--BCC
501  0                    -161
          fill=311                                          imp:n,p 1 u=211
502  17  -1.70          161 -162
                          tmp=7.95694E-008  vol=1.04943E+05  imp:n,p 1 u=211
503  0                    -163
          fill=311                                          imp:n,p 1 u=211
504  17  -1.70          163 -164
                          tmp=7.95694E-008  vol=1.31111E+04  imp:n,p 1 u=211
505  0                    -165
          fill=311                                          imp:n,p 1 u=211
506  17  -1.70          165 -166
                          tmp=7.95694E-008  vol=1.30761E+04  imp:n,p 1 u=211
507  0                    -167
          fill=311                                          imp:n,p 1 u=211
508  17  -1.70          167 -168
                          tmp=7.95694E-008  vol=1.30865E+04  imp:n,p 1 u=211
```

```
509  0                    -169
          fill=311                                          imp:n,p 1 u=211
510  17  -1.70          169 -170
                         tmp=7.95694E-008  vol=1.30860E+04  imp:n,p 1 u=211
511  0                    -171
          fill=311                                          imp:n,p 1 u=211
512  17  -1.70          171 -172
                         tmp=7.95694E-008  vol=1.31548E+04  imp:n,p 1 u=211
513  0                    -173
          fill=311                                          imp:n,p 1 u=211
514  17  -1.70          173 -174
                         tmp=7.95694E-008  vol=1.31546E+04  imp:n,p 1 u=211
515  0                    -175
          fill=311                                          imp:n,p 1 u=211
516  17  -1.70          175 -176
                         tmp=7.95694E-008  vol=1.31254E+04  imp:n,p 1 u=211
517  0                    -177
          fill=311                                          imp:n,p 1 u=211
518  17  -1.70          177 -178
                         tmp=7.95694E-008  vol=1.31134E+04  imp:n,p 1 u=211
c
519  18  -1.9700        162 164
                        166 168 170 172 174 176 178
                         tmp=7.82320E-008  vol=4.71151E+06  imp:n,p 1 u=211
911  0                 -181 182 -183 184 -185 186
          lat=1 fill=211                                    imp:n,p 1 u=111
c
c ------------------------------------------------------------
c
123  51  -10.00000
                       -51
                         tmp=9.24733E-008  vol=1.87714E+05  imp:n,p 1 u=412
124  16  -1.7297        51
                         tmp=8.81648E-008  vol=6.67355E+06  imp:n,p 1 u=412
212  0                 -53 54 -55 56 -57 58
          lat=1 fill=412                                    imp:n,p 1 u=312
c
c  Pebble unit cell--BCC
521  0                    -161
          fill=312                                          imp:n,p 1 u=212
522  17  -1.70          161 -162
                         tmp=7.95694E-008  vol=1.05063E+05  imp:n,p 1 u=212
```

```
523  0                   -163
          fill=312                                          imp:n,p 1 u=212
524  17  -1.70          163 -164
                          tmp=7.95694E-008  vol=1.31179E+04  imp:n,p 1 u=212
525  0                   -165
          fill=312                                          imp:n,p 1 u=212
526  17  -1.70          165 -166
                          tmp=7.95694E-008  vol=1.31164E+04  imp:n,p 1 u=212
527  0                   -167
          fill=312                                          imp:n,p 1 u=212
528  17  -1.70          167 -168
                          tmp=7.95694E-008  vol=1.30881E+04  imp:n,p 1 u=212
529  0                   -169
          fill=312                                          imp:n,p 1 u=212
530  17  -1.70          169 -170
                          tmp=7.95694E-008  vol=1.31563E+04  imp:n,p 1 u=212
531  0                   -171
          fill=312                                          imp:n,p 1 u=212
532  17  -1.70          171 -172
                          tmp=7.95694E-008  vol=1.31522E+04  imp:n,p 1 u=212
533  0                   -173
          fill=312                                          imp:n,p 1 u=212
534  17  -1.70          173 -174
                          tmp=7.95694E-008  vol=1.31903E+04  imp:n,p 1 u=212
535  0                   -175
          fill=312                                          imp:n,p 1 u=212
536  17  -1.70          175 -176
                          tmp=7.95694E-008  vol=1.31087E+04  imp:n,p 1 u=212
537  0                   -177
          fill=312                                          imp:n,p 1 u=212
538  17  -1.70          177 -178
                          tmp=7.95694E-008  vol=1.30792E+04  imp:n,p 1 u=212
c
539  18  -1.9700         162 164
                        166 168 170 172 174 176 178
                          tmp=7.82320E-008  vol=4.71823E+06  imp:n,p 1 u=212
912  0                 -181 182 -183 184 -185 186
          lat=1 fill=212                                    imp:n,p 1 u=112
c
c ------------------------------------------------------------------
c ------------------------------------------------------------------
c  Leakage zone
```

```
15  0                13                                    imp:n,p 0
c
c  Beamports
21  1   -4.0E-006      1 -13 -21          tmp=7.95478E-008 imp:n,p 1
22  1   -4.0E-006      1 -13 -22          tmp=7.95478E-008 imp:n,p 1
23  1   -4.0E-006      1 -13 -23          tmp=7.95478E-008 imp:n,p 1
24  1   -4.0E-006      1 -13 -24          tmp=7.95478E-008 imp:n,p 1
25  1   -4.0E-006      1 -13 -25          tmp=7.95478E-008 imp:n,p 1
26  1   -4.0E-006      1 -13 -26          tmp=7.95478E-008 imp:n,p 1
27  1   -4.0E-006      1 -13 -27          tmp=7.95478E-008 imp:n,p 1
28  1   -4.0E-006      1 -13 -28          tmp=7.95478E-008 imp:n,p 1
29  1   -4.0E-006      1 -13 -29          tmp=7.95478E-008 imp:n,p 1
30  1   -4.0E-006      1 -13 -30          tmp=7.95478E-008 imp:n,p 1
31  1   -4.0E-006      1 -13 -31          tmp=7.95478E-008 imp:n,p 1
32  1   -4.0E-006      1 -13 -32          tmp=7.95478E-008 imp:n,p 1
33  1   -4.0E-006      1 -13 -33          tmp=7.95478E-008 imp:n,p 1
34  1   -4.0E-006      1 -13 -34          tmp=7.95478E-008 imp:n,p 1
35  1   -4.0E-006      1 -13 -35          tmp=7.95478E-008 imp:n,p 1
36  1   -4.0E-006      1 -13 -36          tmp=7.95478E-008 imp:n,p 1
37  1   -4.0E-006      1 -13 -37          tmp=7.95478E-008 imp:n,p 1
38  1   -4.0E-006      1 -13 -38          tmp=7.95478E-008 imp:n,p 1
39  1   -4.0E-006      1 -13 -39          tmp=7.95478E-008 imp:n,p 1
40  1   -4.0E-006      1 -13 -40          tmp=7.95478E-008 imp:n,p 1
41  1   -4.0E-006      1 -13 -41          tmp=7.95478E-008 imp:n,p 1
42  1   -4.0E-006      1 -13 -42          tmp=7.95478E-008 imp:n,p 1
43  1   -4.0E-006      1 -13 -43          tmp=7.95478E-008 imp:n,p 1
44  1   -4.0E-006      1 -13 -44          tmp=7.95478E-008 imp:n,p 1

c Surface cards
1 so 250.00000000
2 so 250.02500000
3 so 250.30000000
4 so 253.30000000
5 so 253.60000000
6 so 256.60000000
7 so 256.90000000
8 so 276.90000000
9 so 277.20000000
101 so 289.15012792
102 so 300.18657448
103 so 310.46620053
104 so 320.10676529
```

```
105 so 329.19919275
106 so 337.81532352
107 so 346.01302320
108 so 353.83966808
109 so 361.33459419
110 so 368.53086197
111 so 375.45655569
10 so 382.13575857
11 so 382.63575857
12 so 507.63575857
13 so 508.13575857
c
21 1 kz 0 0.00183397
22 2 kz 0 0.00183397
23 3 kz 0 0.00183397
24 4 kz 0 0.00183397
25 5 kz 0 0.00183397
26 6 kz 0 0.00183397
27 7 kz 0 0.00183397
28 8 kz 0 0.00183397
29 9 kz 0 0.00183397
30 10 kz 0 0.00183397
31 11 kz 0 0.00183397
32 12 kz 0 0.00183397
33 13 kz 0 0.00183397
34 14 kz 0 0.00183397
35 15 kz 0 0.00183397
36 16 kz 0 0.00183397
37 17 kz 0 0.00183397
38 18 kz 0 0.00183397
39 19 kz 0 0.00183397
40 20 kz 0 0.00183397
41 21 kz 0 0.00183397
42 22 kz 0 0.00183397
43 23 kz 0 0.00183397
44 24 kz 0 0.00183397
c
51 so  0.03000000
53 px  0.07963948
54 px -0.07963948
55 py  0.07963948
56 py -0.07963948
```

```
57 pz  0.07963948
58 pz -0.07963948
c
c BCC unit cell segment  1
161 so  0.99000000
163 s   1.20399807  1.20399807  1.20399807  0.99000000
165 s   1.20399807  1.20399807 -1.20399807  0.99000000
167 s   1.20399807 -1.20399807 -1.20399807  0.99000000
169 s   1.20399807 -1.20399807  1.20399807  0.99000000
171 s  -1.20399807  1.20399807  1.20399807  0.99000000
173 s  -1.20399807  1.20399807 -1.20399807  0.99000000
175 s  -1.20399807 -1.20399807 -1.20399807  0.99000000
177 s  -1.20399807 -1.20399807  1.20399807  0.99000000
162 so  1.00000000
164 s   1.20399807  1.20399807  1.20399807  1.00000000
166 s   1.20399807  1.20399807 -1.20399807  1.00000000
168 s   1.20399807 -1.20399807 -1.20399807  1.00000000
170 s   1.20399807 -1.20399807  1.20399807  1.00000000
172 s  -1.20399807  1.20399807  1.20399807  1.00000000
174 s  -1.20399807  1.20399807 -1.20399807  1.00000000
176 s  -1.20399807 -1.20399807 -1.20399807  1.00000000
178 s  -1.20399807 -1.20399807  1.20399807  1.00000000
181 px  1.20399807
182 px -1.20399807
183 py  1.20399807
184 py -1.20399807
185 pz  1.20399807
186 pz -1.20399807
c

c ******************** RUN DATA ********************
c
c  Source definition
sdef par=1 erg=14.1 x=0 y=0 z=0
nps 1
c kcode 1e4 1 50 100
c ksrc  300.964  0. 0. -300.964 0. 0.
c      0. 300.964 0. 0. -300.964 0. 0.
c      0. 0. 300.964 0 0 -300.964
prdmp 10000 10000 0 1 10000
mode n p
totnu
```

```
print  40 130 140
c
c ******************* TALLIES ********************
c
F6:n    3 4 5 6 7 8 9 10 12 13 14
        101 102 319
        302 304 306 308 310 312 314 316 318
        103 104 339
        322 324 326 328 330 332 334 336 338
        105 106 359
        342 344 346 348 350 352 354 356 358
        107 108 379
        362 364 366 368 370 372 374 376 378
        109 110 399
        382 384 386 388 390 392 394 396 398
        111 112 419
        402 404 406 408 410 412 414 416 418
        113 114 439
        422 424 426 428 430 432 434 436 438
        115 116 459
        442 444 446 448 450 452 454 456 458
        117 118 479
        462 464 466 468 470 472 474 476 478
        119 120 499
        482 484 486 488 490 492 494 496 498
        121 122 519
        502 504 506 508 510 512 514 516 518
        123 124 539
        522 524 526 528 530 532 534 536 538
F16:p   3 4 5 6 7 8 9 10 12 13 14
        101 102 319
        302 304 306 308 310 312 314 316 318
        103 104 339
        322 324 326 328 330 332 334 336 338
        105 106 359
        342 344 346 348 350 352 354 356 358
        107 108 379
        362 364 366 368 370 372 374 376 378
        109 110 399
        382 384 386 388 390 392 394 396 398
        111 112 419
        402 404 406 408 410 412 414 416 418
```

```
        113 114 439
        422 424 426 428 430 432 434 436 438
        115 116 459
        442 444 446 448 450 452 454 456 458
        117 118 479
        462 464 466 468 470 472 474 476 478
        119 120 499
        482 484 486 488 490 492 494 496 498
        121 122 519
        502 504 506 508 510 512 514 516 518
        123 124 539
        522 524 526 528 530 532 534 536 538
f204:n  3 4 5 6 7 8 9 10 12 13 14
        101 102 319
        302 304 306 308 310 312 314 316 318
        103 104 339
        322 324 326 328 330 332 334 336 338
        105 106 359
        342 344 346 348 350 352 354 356 358
        107 108 379
        362 364 366 368 370 372 374 376 378
        109 110 399
        382 384 386 388 390 392 394 396 398
        111 112 419
        402 404 406 408 410 412 414 416 418
        113 114 439
        422 424 426 428 430 432 434 436 438
        115 116 459
        442 444 446 448 450 452 454 456 458
        117 118 479
        462 464 466 468 470 472 474 476 478
        119 120 499
        482 484 486 488 490 492 494 496 498
        121 122 519
        502 504 506 508 510 512 514 516 518
        123 124 539
        522 524 526 528 530 532 534 536 538
e204 1.00E-11 1.05E-11 1.10E-11 1.15E-11 1.20E-11 1.26E-11
     1.32E-11 1.38E-11 1.45E-11 1.51E-11 1.58E-11 1.66E-11
     1.74E-11 1.82E-11 1.91E-11 2.00E-11 2.09E-11 2.19E-11
     2.29E-11 2.40E-11 2.51E-11 2.63E-11 2.75E-11 2.88E-11
     3.02E-11 3.16E-11 3.31E-11 3.47E-11 3.63E-11 3.80E-11
```

```
3.98E-11 4.17E-11 4.37E-11 4.57E-11 4.79E-11 5.01E-11
5.25E-11 5.50E-11 5.75E-11 6.03E-11 6.31E-11 6.61E-11
6.92E-11 7.24E-11 7.59E-11 7.94E-11 8.32E-11 8.71E-11
9.12E-11 9.55E-11 1.00E-10 1.05E-10 1.10E-10 1.15E-10
1.20E-10 1.26E-10 1.32E-10 1.38E-10 1.45E-10 1.51E-10
1.58E-10 1.66E-10 1.74E-10 1.82E-10 1.91E-10 2.00E-10
2.09E-10 2.19E-10 2.29E-10 2.40E-10 2.51E-10 2.63E-10
2.75E-10 2.88E-10 3.02E-10 3.16E-10 3.31E-10 3.47E-10
3.63E-10 3.80E-10 3.98E-10 4.17E-10 4.37E-10 4.57E-10
4.79E-10 5.01E-10 5.25E-10 5.50E-10 5.75E-10 6.03E-10
6.31E-10 6.61E-10 6.92E-10 7.24E-10 7.59E-10 7.94E-10
8.32E-10 8.71E-10 9.12E-10 9.55E-10 1.00E-09 1.05E-09
1.10E-09 1.15E-09 1.20E-09 1.26E-09 1.32E-09 1.38E-09
1.45E-09 1.51E-09 1.58E-09 1.66E-09 1.74E-09 1.82E-09
1.91E-09 2.00E-09 2.09E-09 2.19E-09 2.29E-09 2.40E-09
2.51E-09 2.63E-09 2.75E-09 2.88E-09 3.02E-09 3.16E-09
3.31E-09 3.47E-09 3.63E-09 3.80E-09 3.98E-09 4.17E-09
4.37E-09 4.57E-09 4.79E-09 5.01E-09 5.25E-09 5.50E-09
5.75E-09 6.03E-09 6.31E-09 6.61E-09 6.92E-09 7.24E-09
7.59E-09 7.94E-09 8.32E-09 8.71E-09 9.12E-09 9.55E-09
1.00E-08 1.05E-08 1.10E-08 1.15E-08 1.20E-08 1.26E-08
1.32E-08 1.38E-08 1.45E-08 1.51E-08 1.58E-08 1.66E-08
1.74E-08 1.82E-08 1.91E-08 2.00E-08 2.09E-08 2.19E-08
2.29E-08 2.40E-08 2.51E-08 2.63E-08 2.75E-08 2.88E-08
3.02E-08 3.16E-08 3.31E-08 3.47E-08 3.63E-08 3.80E-08
3.98E-08 4.17E-08 4.37E-08 4.57E-08 4.79E-08 5.01E-08
5.25E-08 5.50E-08 5.75E-08 6.03E-08 6.31E-08 6.61E-08
6.92E-08 7.24E-08 7.59E-08 7.94E-08 8.32E-08 8.71E-08
9.12E-08 9.55E-08 1.00E-07 1.05E-07 1.10E-07 1.15E-07
1.20E-07 1.26E-07 1.32E-07 1.38E-07 1.45E-07 1.51E-07
1.58E-07 1.66E-07 1.74E-07 1.82E-07 1.91E-07 2.00E-07
2.09E-07 2.19E-07 2.29E-07 2.40E-07 2.51E-07 2.63E-07
2.75E-07 2.88E-07 3.02E-07 3.16E-07 3.31E-07 3.47E-07
3.63E-07 3.80E-07 3.98E-07 4.17E-07 4.37E-07 4.57E-07
4.79E-07 5.01E-07 5.25E-07 5.50E-07 5.75E-07 6.03E-07
6.31E-07 6.61E-07 6.92E-07 7.24E-07 7.59E-07 7.94E-07
8.32E-07 8.71E-07 9.12E-07 9.55E-07 1.00E-06 1.05E-06
1.10E-06 1.15E-06 1.20E-06 1.26E-06 1.32E-06 1.38E-06
1.45E-06 1.51E-06 1.58E-06 1.66E-06 1.74E-06 1.82E-06
1.91E-06 2.00E-06 2.09E-06 2.19E-06 2.29E-06 2.40E-06
2.51E-06 2.63E-06 2.75E-06 2.88E-06 3.02E-06 3.16E-06
3.31E-06 3.47E-06 3.63E-06 3.80E-06 3.98E-06 4.17E-06
```

```
4.37E-06 4.57E-06 4.79E-06 5.01E-06 5.25E-06 5.50E-06
5.75E-06 6.03E-06 6.31E-06 6.61E-06 6.92E-06 7.24E-06
7.59E-06 7.94E-06 8.32E-06 8.71E-06 9.12E-06 9.55E-06
1.00E-05 1.05E-05 1.10E-05 1.15E-05 1.20E-05 1.26E-05
1.32E-05 1.38E-05 1.45E-05 1.51E-05 1.58E-05 1.66E-05
1.74E-05 1.82E-05 1.91E-05 2.00E-05 2.09E-05 2.19E-05
2.29E-05 2.40E-05 2.51E-05 2.63E-05 2.75E-05 2.88E-05
3.02E-05 3.16E-05 3.31E-05 3.47E-05 3.63E-05 3.80E-05
3.98E-05 4.17E-05 4.37E-05 4.57E-05 4.79E-05 5.01E-05
5.25E-05 5.50E-05 5.75E-05 6.03E-05 6.31E-05 6.61E-05
6.92E-05 7.24E-05 7.59E-05 7.94E-05 8.32E-05 8.71E-05
9.12E-05 9.55E-05 1.00E-04 1.05E-04 1.10E-04 1.15E-04
1.20E-04 1.26E-04 1.32E-04 1.38E-04 1.45E-04 1.51E-04
1.58E-04 1.66E-04 1.74E-04 1.82E-04 1.91E-04 2.00E-04
2.09E-04 2.19E-04 2.29E-04 2.40E-04 2.51E-04 2.63E-04
2.75E-04 2.88E-04 3.02E-04 3.16E-04 3.31E-04 3.47E-04
3.63E-04 3.80E-04 3.98E-04 4.17E-04 4.37E-04 4.57E-04
4.79E-04 5.01E-04 5.25E-04 5.50E-04 5.75E-04 6.03E-04
6.31E-04 6.61E-04 6.92E-04 7.24E-04 7.59E-04 7.94E-04
8.32E-04 8.71E-04 9.12E-04 9.55E-04 1.00E-03 1.05E-03
1.10E-03 1.15E-03 1.20E-03 1.26E-03 1.32E-03 1.38E-03
1.45E-03 1.51E-03 1.58E-03 1.66E-03 1.74E-03 1.82E-03
1.91E-03 2.00E-03 2.09E-03 2.19E-03 2.29E-03 2.40E-03
2.51E-03 2.63E-03 2.75E-03 2.88E-03 3.02E-03 3.16E-03
3.31E-03 3.47E-03 3.63E-03 3.80E-03 3.98E-03 4.17E-03
4.37E-03 4.57E-03 4.79E-03 5.01E-03 5.25E-03 5.50E-03
5.75E-03 6.03E-03 6.31E-03 6.61E-03 6.92E-03 7.24E-03
7.59E-03 7.94E-03 8.32E-03 8.71E-03 9.12E-03 9.55E-03
1.00E-02 1.05E-02 1.10E-02 1.15E-02 1.20E-02 1.26E-02
1.32E-02 1.38E-02 1.45E-02 1.51E-02 1.58E-02 1.66E-02
1.74E-02 1.82E-02 1.91E-02 2.00E-02 2.09E-02 2.19E-02
2.29E-02 2.40E-02 2.51E-02 2.63E-02 2.75E-02 2.88E-02
3.02E-02 3.16E-02 3.31E-02 3.47E-02 3.63E-02 3.80E-02
3.98E-02 4.17E-02 4.37E-02 4.57E-02 4.79E-02 5.01E-02
5.25E-02 5.50E-02 5.75E-02 6.03E-02 6.31E-02 6.61E-02
6.92E-02 7.24E-02 7.59E-02 7.94E-02 8.32E-02 8.71E-02
9.12E-02 9.55E-02 1.00E-01 1.05E-01 1.10E-01 1.15E-01
1.20E-01 1.26E-01 1.32E-01 1.38E-01 1.45E-01 1.51E-01
1.58E-01 1.66E-01 1.74E-01 1.82E-01 1.91E-01 2.00E-01
2.09E-01 2.19E-01 2.29E-01 2.40E-01 2.51E-01 2.63E-01
2.75E-01 2.88E-01 3.02E-01 3.16E-01 3.31E-01 3.47E-01
3.63E-01 3.80E-01 3.98E-01 4.17E-01 4.37E-01 4.57E-01
```

```
     4.79E-01 5.01E-01 5.25E-01 5.50E-01 5.75E-01 6.03E-01
     6.31E-01 6.61E-01 6.92E-01 7.24E-01 7.59E-01 7.94E-01
     8.32E-01 8.71E-01 9.12E-01 9.55E-01 1.00E+00 1.05E+00
     1.10E+00 1.15E+00 1.20E+00 1.26E+00 1.32E+00 1.38E+00
     1.45E+00 1.51E+00 1.58E+00 1.66E+00 1.74E+00 1.82E+00
     1.91E+00 2.00E+00 2.09E+00 2.19E+00 2.29E+00 2.40E+00
     2.51E+00 2.63E+00 2.75E+00 2.88E+00 3.02E+00 3.16E+00
     3.31E+00 3.47E+00 3.63E+00 3.80E+00 3.98E+00 4.17E+00
     4.37E+00 4.57E+00 4.79E+00 5.01E+00 5.25E+00 5.50E+00
     5.75E+00 6.03E+00 6.31E+00 6.61E+00 6.92E+00 7.24E+00
     7.59E+00 7.94E+00 8.32E+00 8.71E+00 9.12E+00 9.55E+00
     1.00E+01 1.05E+01 1.10E+01 1.15E+01 1.20E+01 1.26E+01
     1.32E+01 1.38E+01 1.45E+01 1.51E+01 1.58E+01 1.66E+01
     1.74E+01 1.82E+01 1.91E+01 2.00E+01
c
fc207  Fission energy deposition tally
f207:n    101 103 105 107 109 111 113 115 117 119 121 123
c
c ***********************************************************
c *******   ADD DPA AND REACTION RATE CALCULATIONS   *******
c ***********************************************************
c
c  ODS steel dpa w/ Ed=40eV to 1stwall
f244:n 4
fm244 (1 4 444) (1 44 444)
c   beryllium dpa w/ Ed=31eV (dpa.v2.pdf) to Be/flibe region
f344:n 9
fm344 (1 40 444)
c  carbon dpa w/ Ed=20eV (dpa.v2.pdf) in pyc/sic/matrix zone
f444:n  101 103 105 107 109 111 113 115 117 119 121 123
fm444 (1 42 444)
c materials needed for dpa calculations
M40 4009.72c 1.0
M42 6000.72c 1.0
M44 26054 0.05845 26056.72c 0.91754 26057.72c 0.02119
c
c
c FISSION REACTION RATE TALLY FOR FPM CALC INPUT
f504:n  101 103 105 107 109 111 113 115 117 119 121 123
fm504 (-1 51 -6)
c
c
```

```
c ***********************************************************
c  Rotation matrixes for the 48 beamports
*tr1   0 0 0   79.7  25.9 66.5 168.8  78.8 90  94.5 113.  23.5
*tr2   0 0 0  154.1  79.7 66.5 101.3 168.8 90  67.   94.5 23.5
*tr3   0 0 0  100.3 154.1 66.5  11.3 101.3 90  85.5  67.  23.5
*tr4   0 0 0   25.9 100.3 66.5  78.8  11.3 90 113.   85.5 23.5
*tr5   0 0 0   44.7  61.  59.4 124.3  34.3 90 114.8 106.7 30.6
*tr6   0 0 0  118.8  43.9 60.  146.3 123.8 90  73.9 114.6 30.
*tr7   0 0 0  135.3 119.  59.4  55.7 145.7 90  65.2  73.3 30.6
*tr8   0 0 0   61.2 136.1 60.   33.8  56.3 90 106.1  65.4 30.
*tr9   0 0 0   46.8  78.5 45.5 106.3  16.3 90 132.3 101.3 44.5
*tr10  0 0 0   70.7  50.8 45.5 152.5  62.5 90 108.9 128.4 44.5
*tr11  0 0 0  101.5  46.8 45.5 163.7 106.3 90  78.7 132.3 44.5
*tr12  0 0 0  129.2  70.7 45.5 117.5 152.5 90  51.6 108.9 44.5
*tr13  0 0 0  133.2 101.5 45.5  73.7 163.7 90  47.7  78.7 44.5
*tr14  0 0 0  109.3 129.2 45.5  27.5 117.5 90  71.1  51.6 44.5
*tr15  0 0 0   78.5 133.2 45.5  16.3  73.7 90 101.3  47.7 44.5
*tr16  0 0 0   50.8 109.3 45.5  62.5  27.5 90 128.4  71.1 44.5
*tr17  0 0 0   60.3  65.8 40.  129.7  39.7 90 126.1 119.3 50.
*tr18  0 0 0   86.4  50.2 40.  174.4  84.4 90  94.3 139.7 50.
*tr19  0 0 0  114.1  60.2 40.  140.6 129.4 90  60.9 126.3 50.
*tr20  0 0 0  129.8  86.4 40.   95.6 174.4 90  40.3  94.3 50.
*tr21  0 0 0  119.7 114.2 40.   50.3 140.3 90  53.9  60.7 50.
*tr22  0 0 0   93.6 129.8 40.    5.6  95.6 90  85.7  40.3 50.
*tr23  0 0 0   65.9 119.8 40.   39.4  50.6 90 119.1  53.7 50.
*tr24  0 0 0   50.2  93.6 40.   84.4   5.6 90 139.7  85.7 50.
c
c ******************** MATERIALS ********************
c
c Scattering kernels
mt4   fe56.15t
mt9   fe56.15t be.15t
mt16  grph.15t
mt17  grph.15t
mt13  grph.15t
c
m1   54131.72c  1.
m3   74182.72c  2.66200E-001
     74183.72c  1.43100E-001
     74184.72c  3.06400E-001
     74186.72c  2.84300E-001
m4   26054.72c  4.96578E-002
```

```
      26056.72c  7.79522E-001
      26057.72c  1.80026E-002
      26058.72c  2.39581E-003
      24050.72c  5.80127E-003
      24052.72c  1.11872E-001
      24053.72c  1.26854E-002
      24054.72c  3.15765E-003
      74182.72c  2.45170E-003
      74183.72c  1.31795E-003
      74184.72c  2.82194E-003
      74186.72c  2.61840E-003
      22046.72c  3.79418E-004
      22047.72c  3.42166E-004
      22048.72c  3.39038E-003
      22049.72c  2.48806E-004
      22050.72c  2.38228E-004
      39089.72c  1.23900E-003
       8016.72c  1.85349E-003
       8017.72c  4.51494E-006
m5     3006.71c  1.19000E-002
       3007.71c  1.58100E-001
      82204.71c  1.16200E-002
      82206.71c  2.00030E-001
      82207.71c  1.83430E-001
      82208.71c  4.34920E-001
m7     3006.72c  2.85714E-004
       3007.72c  2.85429E-001
       4009.72c  1.42857E-001
       9019.72c  5.71429E-001
m9     4009.72c  7.26502E-001
      26054.72c  2.46297E-004
      26056.72c  3.86633E-003
      26057.72c  8.92905E-005
      26058.72c  1.18829E-005
      24050.72c  2.87736E-005
      24052.72c  5.54870E-004
      24053.72c  6.29178E-005
      24054.72c  1.56616E-005
      74182.72c  1.21601E-005
      74183.72c  6.53688E-006
      74184.72c  1.39965E-005
      74186.72c  1.29870E-005
```

```
     22046.72c  1.88186E-006
     22047.72c  1.69710E-006
     22048.72c  1.68159E-005
     22049.72c  1.23405E-006
     22050.72c  1.18158E-006
     39089.72c  6.14529E-006
      8016.72c  9.19306E-006
      8017.72c  2.23936E-008
      3006.72c  8.95127E-005
      3007.72c  8.94232E-002
      9019.72c  1.79025E-001
m13   6000.72c  6.04259E-001
      3006.72c  1.13069E-004
      3007.72c  1.12956E-001
      4009.72c  5.65344E-002
      9019.72c  2.26138E-001
m16   6000.72c  9.82520E-001
     14028.72c  1.61217E-002
     14029.72c  8.18622E-004
     14030.72c  5.39641E-004
m17   6000.72c  1.00000E+000
m18   3006.72c  2.85714E-004
      3007.72c  2.85429E-001
      4009.72c  1.42857E-001
      9019.72c  5.71429E-001
m51   6000.72c  1.37931E-001
      8016.72c  5.15984E-001
      8017.72c  1.25690E-003
     90232.72c  3.44828E-001
```

Appendix D

Verification and Validation of TRIUNE

As discussed in Section 2.4, an extensive verification and validation (V&V) effort was conducted for the TRIUNE model using the IAEA Normal Operation Steady-State TRISO-Coated Particle Fuel Performance Benchmark Cases [68, 69]. Detailed results from this verification and validation effort, including relevant tables and/or figures for each benchmark case with TRIUNE results compared to PARFUME results, are provided in this Appendix. The specifications for the benchmark cases, which were developed with international cooperation as part of the IAEA's Coordinated Research Program 6 (CRP6), are documented in [68]. There are fourteen (14) total benchmark cases specified with three distinct types of benchmarks constructed. Cases 1–8 are computational benchmarks where single nominal particles are analyzed using simplified irradiation histories to test specific aspects of TRISO fuel performance models such as the thermomechanical stress calculations or how they handle irradiation-induced shrinkage and swelling in PyC. Cases 9–12 cover actual TRISO irradiation experiments that have been performed. They involve calculations for both a nominal TRISO particle and a simulated batch of particles using more detailed irradiation histories and provide some of the only true opportunities for validating TRISO FPM failure fraction predictions. Cases 13 and 14 were based upon future planned irradiation experiments. Almost all of the input data needed for fuel performance calculations is provided in the benchmark specification and the comparison metrics vary by case but generally include the maximum tangential stress calculated for SiC during the case and/or internal gas pressure as a function of fast neutron fluence. An upcoming IAEA CRP6 report will review these benchmark specifications and provide the results of a large code comparison effort where the results from a number of international TRISO fuel performance codes are compared for each benchmark case [69].

Overall, TRIUNE benchmark results agree well with PARFUME benchmark results. TRIUNE nominal particle calculations for Cases 1 through 8 agree exactly or very closely with PARFUME results. Cases 9 through 14 exhibit some gas pressure differences that, after a major debugging and analysis effort as well as consultation with Dave Petti and

John Maki of the PARFUME development team at INL, have been determined to likely be due to differences in CO production rate correlations (Proksch or Homan correlation in TRIUNE compared to HSCcalculated reaction rates and inventories used in PARFUME) as well as different fission product diffusion coefficients (TRIUNE benchmark calculations were performed using fixed diffusion coefficients for Xe and Kr that did not vary with temperature and were different in magnitude than the PARFUME temperature-dependent diffusion coefficients). When PARFUME gas pressures were provided as input to TRIUNE, the resultant nominal particle stress calculations and batch failure fraction calculations from TRIUNE both agreed very well with PARFUME, which means that the thermomechanical stress calculations and irradiation-effect modules in TRIUNE performed as desired. The differences between TRIUNE and PARFUME failure fraction curves likely stem from the small differences in stress calculations as well as undocumented items such as as-manufactured failure fractions in the PARFUME results. It is worth noting that the PARFUME gas pressures generally vastly exceed not just TRIUNE results but gas pressures calculated by almost all other TRISO fuel performance models [69]; the PARFUME results could easily be correct and this may simply be highlighting a deficiency in existing oxygen release correlations. It must also be noted that TRIUNE does not currently support IPyC cracking or IPyC/SiC debonding as failure modes; therefore, no such curves are come from TRIUNE for benchmark cases where such curves do exist from PARFUME.

Case 1: Elastic SiC

Table D.1: Maximum tangential stress predicted for Benchmark Case 1 by TRIUNE, PARFUME, and an ABAQUS model used by INL.

Maximum Tangential Stress [MPa]		
TRIUNE	**PARFUME**	**ABAQUS (INL)**
125.19	125.2	125.0

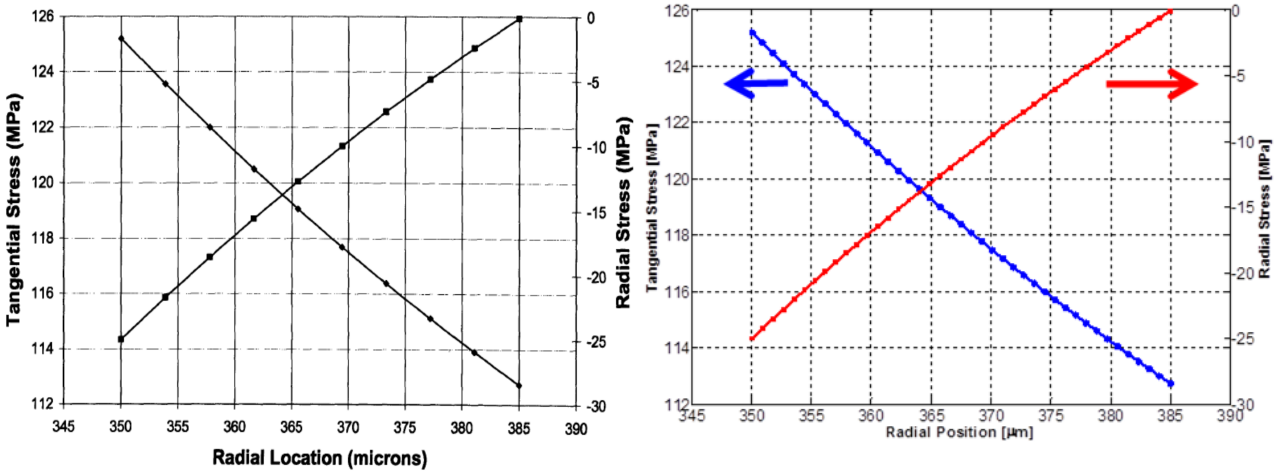

(a) (b)

Figure D.1: Radial and tangential stresses for Benchmark Case 1 as a function of radial position within the TRISO particle as calculated by (a) TIMCOAT [88] and (b) TRIUNE.

Case 2: Simple BISO

Table D.2: Maximum tangential stress predicted for Benchmark Case 2 by TRIUNE, PARFUME, and an ABAQUS model used by INL.

Maximum Tangential Stress [MPa]		
TRIUNE	**PARFUME**	**ABAQUS (INL)**
50.2	50.14	50.33

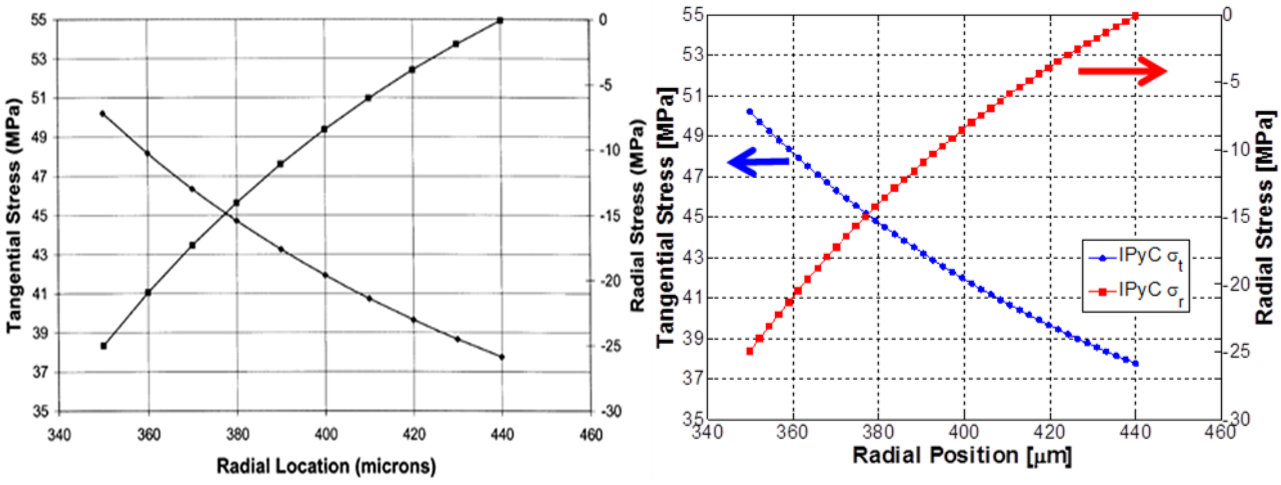

(a) (b)

Figure D.2: Radial and tangential stresses for Benchmark Case 2 as a function of radial position within the TRISO particle as calculated by (a) TIMCOAT [88] and (b) TRIUNE.

Case 3: IPyC/SiC Composite without fluence

Table D.3: Maximum tangential stress predicted for Benchmark Case 3 by TRIUNE, PARFUME, and an ABAQUS model used by INL.

Maximum Tangential Stress [MPa] (IPyC/SiC)		
TRIUNE	**PARFUME**	**ABAQUS (INL)**
8.778 / 104.38	8.770 / 104.3	8.802 / 104.2

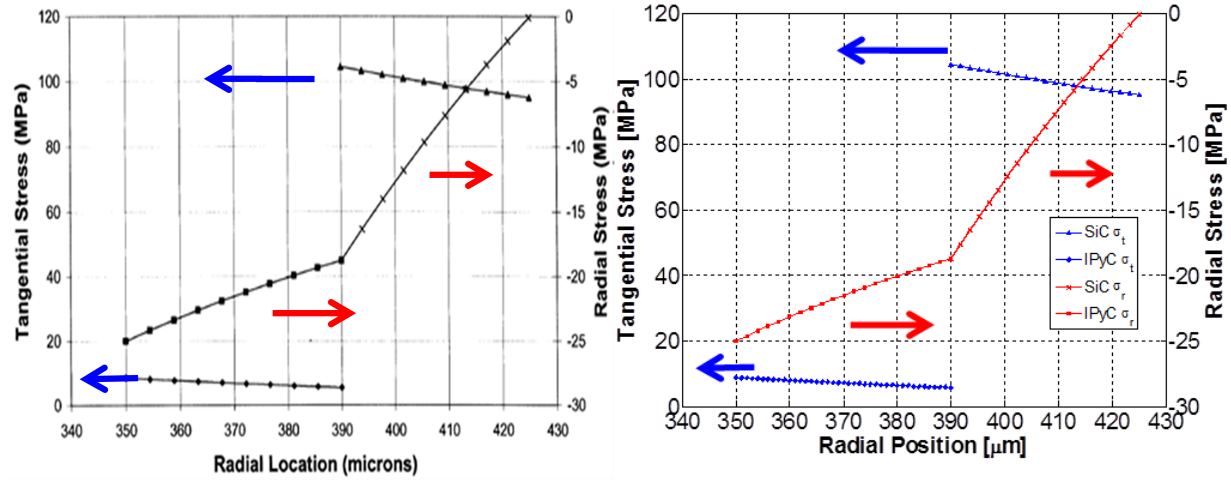

(a) (b)

Figure D.3: Radial and tangential stresses for Benchmark Case 3 as a function of radial position within the TRISO particle as calculated by (a) TIMCOAT [88] and (b) TRIUNE.

Case 4a: IPyC/SiC Composite with no creep and constant swelling

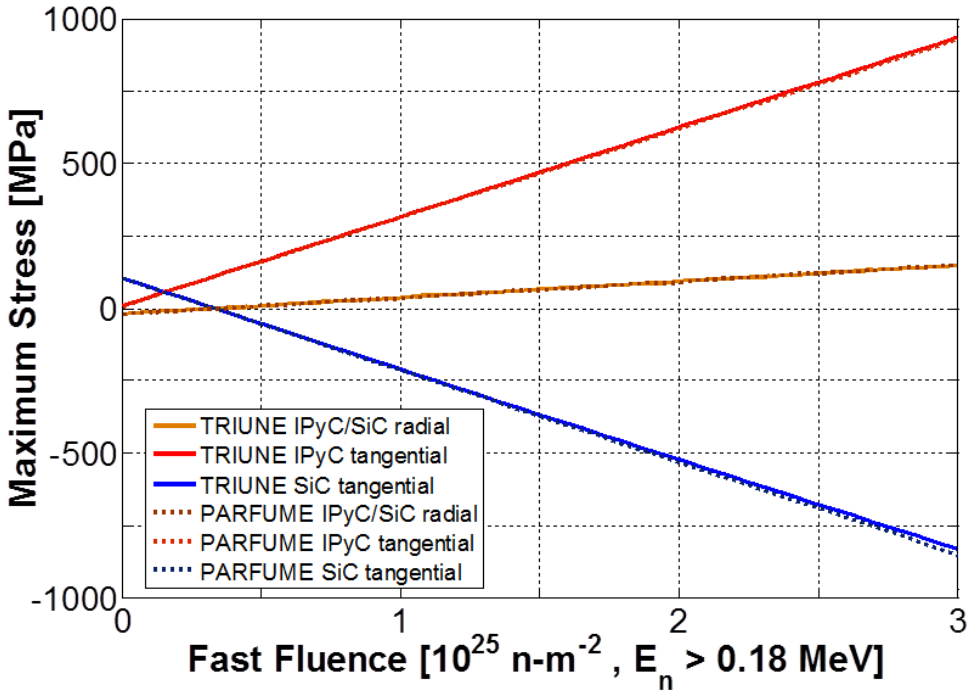

Figure D.4: Maximum stresses predicted for Benchmark Case 4a by TRIUNE and PARFUME as a function of neutron fast fluence.

Case 4b: IPyC/SiC Composite with constant creep and no swelling

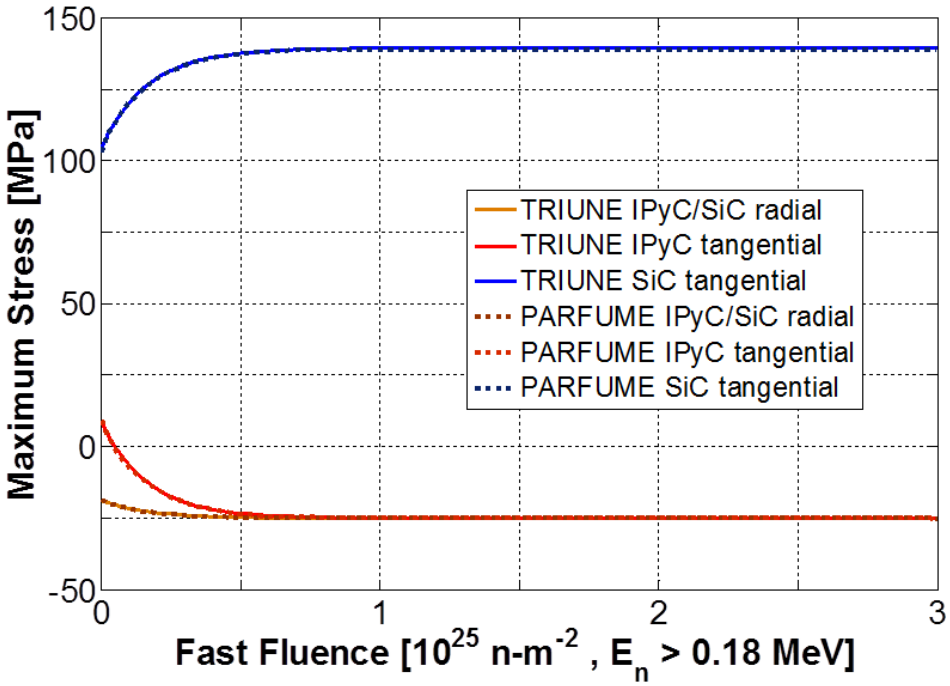

Figure D.5: Maximum stresses predicted for Benchmark Case 4b by TRIUNE and PARFUME as a function of neutron fast fluence.

Case 4c: IPyC/SiC Composite with constant creep and constant swelling

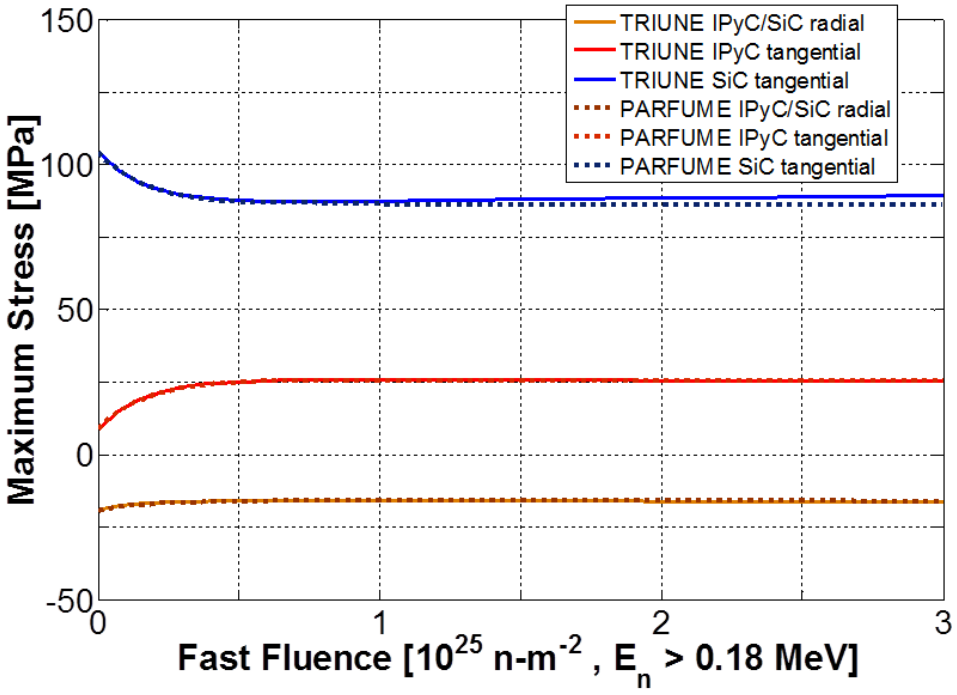

Figure D.6: Maximum stresses predicted for Benchmark Case 4c by TRIUNE and PARFUME as a function of neutron fast fluence.

Case 4d: IPyC/SiC Composite with constant creep and fluence dependent swelling

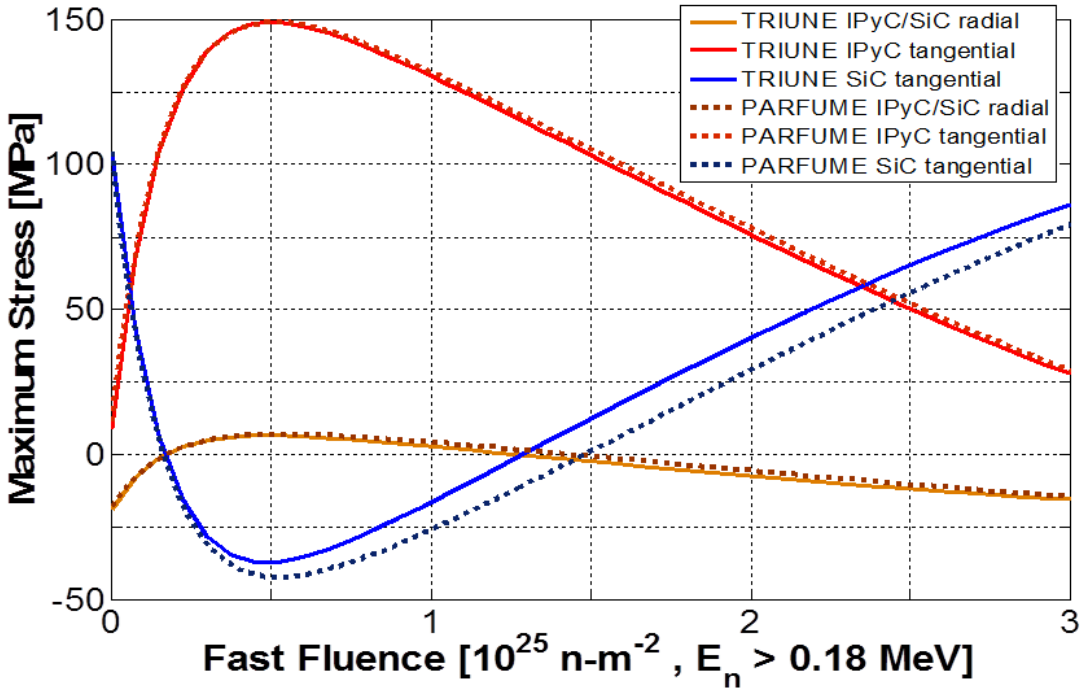

Figure D.7: Maximum stresses predicted for Benchmark Case 4d by TRIUNE and PARFUME as a function of neutron fast fluence.

Case 5: TRISO, 350 m kernel

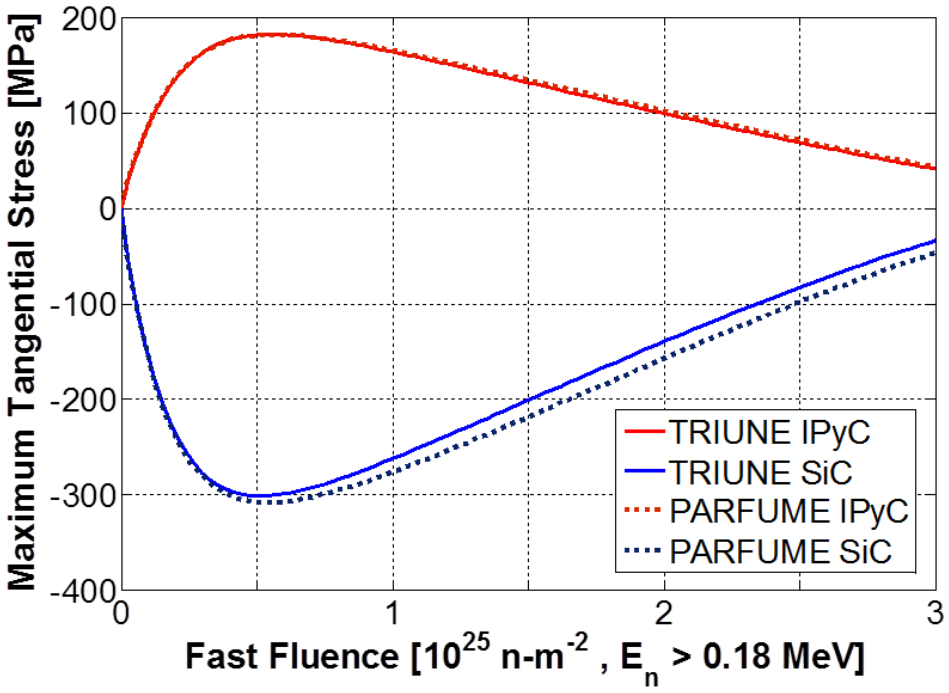

Figure D.8: Maximum stresses predicted for Benchmark Case 5 by TRIUNE and PARFUME as a function of neutron fast fluence.

Case 6: TRISO, 500 m kernel

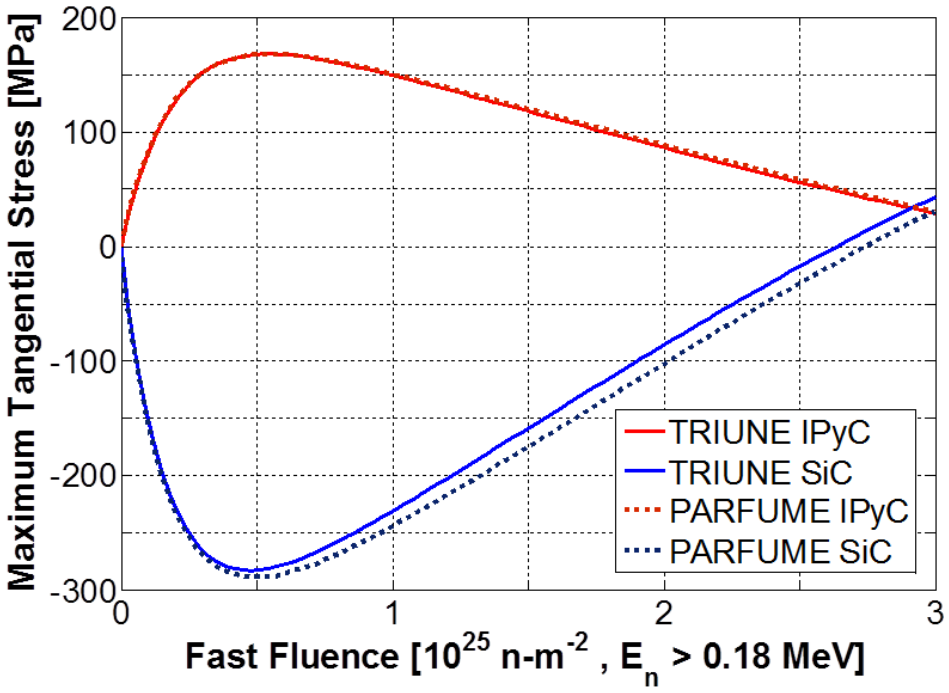

Figure D.9: Maximum stresses predicted for Benchmark Case 6 by TRIUNE and PARFUME as a function of neutron fast fluence.

Case 7: TRISO, high BAF

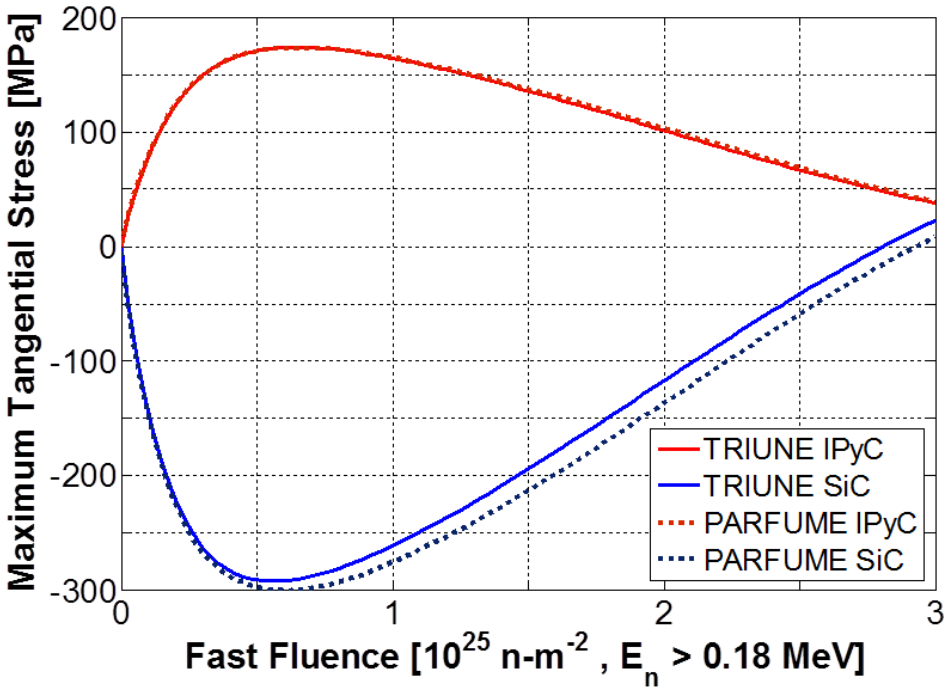

Figure D.10: Maximum stresses predicted for Benchmark Case 7 by TRIUNE and PARFUME as a function of neutron fast fluence.

Case 8: TRISO, cyclic temperature history

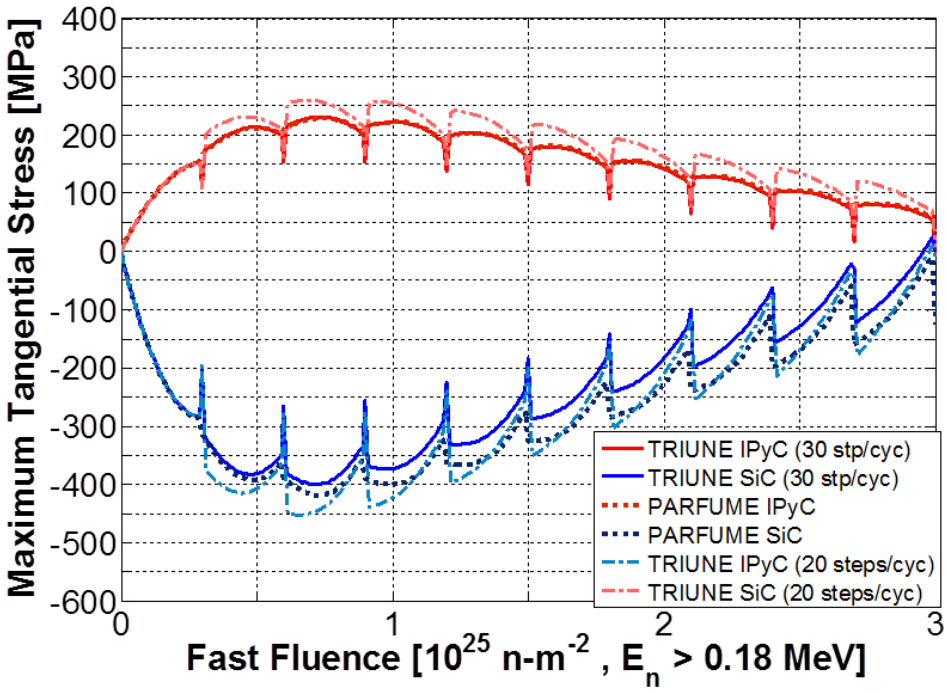

Figure D.11: Maximum stresses predicted for Benchmark Case 8 by TRIUNE and PARFUME as a function of neutron fast fluence.

Case 9: HRB-22

Starting with Benchmark Case 9, predicted internal gas pressures and particle failure fractions are reported and compared in addition to stress levels. TRIUNE was exercised using the Homan and Proksch correlations described in Section 2.3.4 to predict CO gas generation. Curves labeled "Homan" or "Proksch" in figures presented for Cases 9 through 14 display data from TRIUNE calculations using those correlations for oxygen release from the fuel kernel. All stress curves come from TRIUNE unless specifically labeled "PARFUME".

Due to differences in internal gas pressures predicted by TRIUNE and PARFUME, various attempts were made to account for differences between the two codes by applying various adjustment factors to the results calculated by TRIUNE; some of these attempts are shown in the figures for Benchmark Cases 9 through 14. For example, Figure D.12(b) contains legend entries labeled "(Proksch, 365*EFPD)"; this indicates that the Proksch oxygen release correlation was used to produce that curve and the pressures/inventories in the calculation were multiplied by a factor of 365 to see how the adjusted pressure compared to PARFUME results. Curves labeled "TRIUNE w/ INL pressures", such as in Figure D.13, indicate that the pressures calculated by PARFUME for that benchmark case were used as inputs for the TRIUNE calculations associated with that label to try to eliminate possible differences between TRIUNE and PARFUME calculations. All of these efforts resulted in identifying two key factors: PARFUME uses the HSC code to calculation CO gas production instead of either of the correlations incorporated into TRIUNE and other fuel performance models, and the fission product diffusion coefficients used by TRIUNE needed to be updated. For V&V purposes, these efforts showed an acceptable thermomechanical model and associated functional modules with a possible gas production issue. In design calculations in the bulk of this document, these issues have been eliminated by using an oxycarbide fuel form that avoids CO gas production entirely and dynamically calculating fission product diffusion coefficients in the fuel kernel by interpolating on temperature-dependent data [67].

No failure probabilities from TRIUNE calculations are shown for Case 9 because TRIUNE focuses on pressure vessel failure of the SiC as the failure mode while IPyC cracking is the failure mode present for this benchmark case.

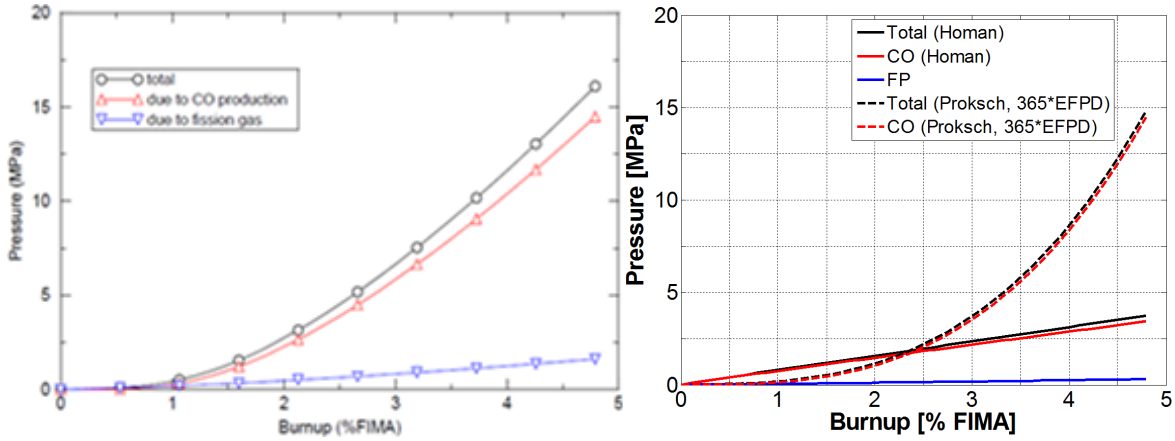

(a) (b)

Figure D.12: Total and partial internal gas pressures within a nominal TRISO particle predicted for Benchmark Case 9 as calculated by (a) PARFUME and (b) TRIUNE.

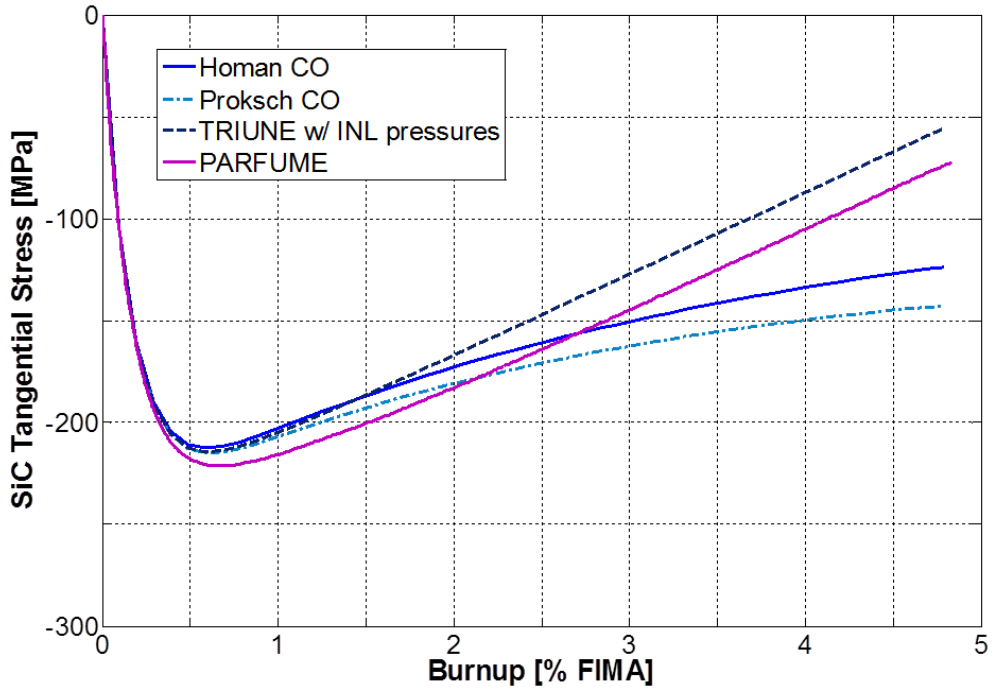

Figure D.13: SiC tangential stress calculated by TRIUNE and PARFUME as a function of neutron fast fluence for Benchmark Case 9 using a Poisson's ratio in creep of 0.4.

Case 10: HFR-K3 B/2

No failure probabilities from TRIUNE calculations are shown for Case 10 because TRIUNE focuses on pressure vessel failure of the SiC as the failure mode while IPyC cracking is the failure mode present for this benchmark case.

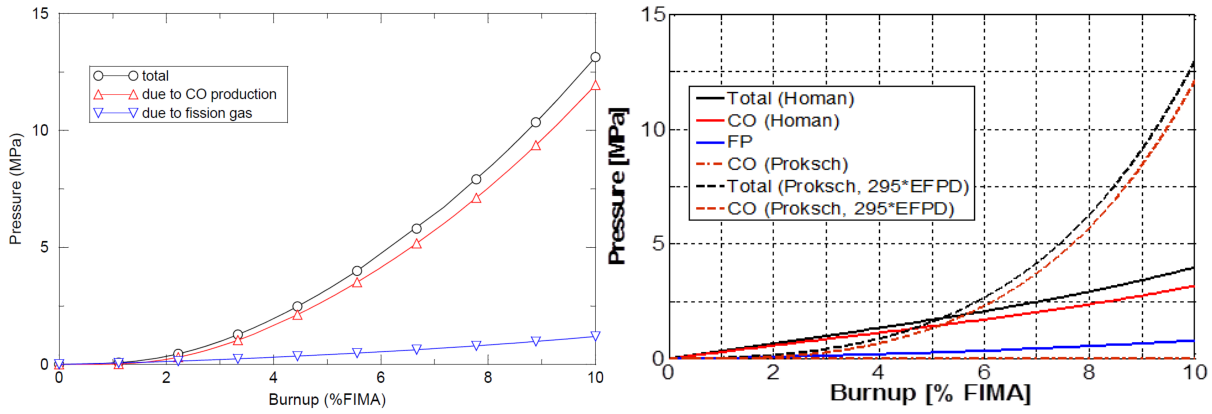

(a) (b)

Figure D.14: Total and partial internal gas pressures within a nominal TRISO particle predicted for Benchmark Case 10 as calculated by (a) PARFUME and (b) TRIUNE.

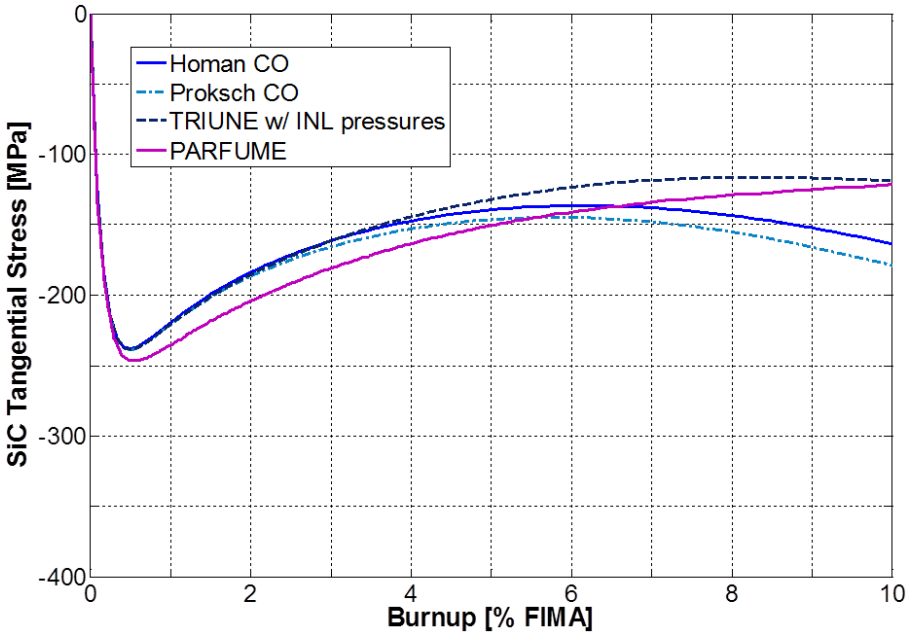

Figure D.15: SiC tangential stress calculated by TRIUNE and PARFUME as a function of neutron fast fluence for Benchmark Case 10 using a Poisson's ratio in creep of 0.4.

Case 11: HFR-P4 3

Gas pressures, SiC tangential stresses, and failure probabilities due to SiC pressure vessel failure are shown for Case 11. The failure probability curve in Figure D.18 labeled "TRIUNE w/ adj" displays TRIUNE fuel performance results using PARFUME gas pressures instead of TRIUNE's gas generation modules.

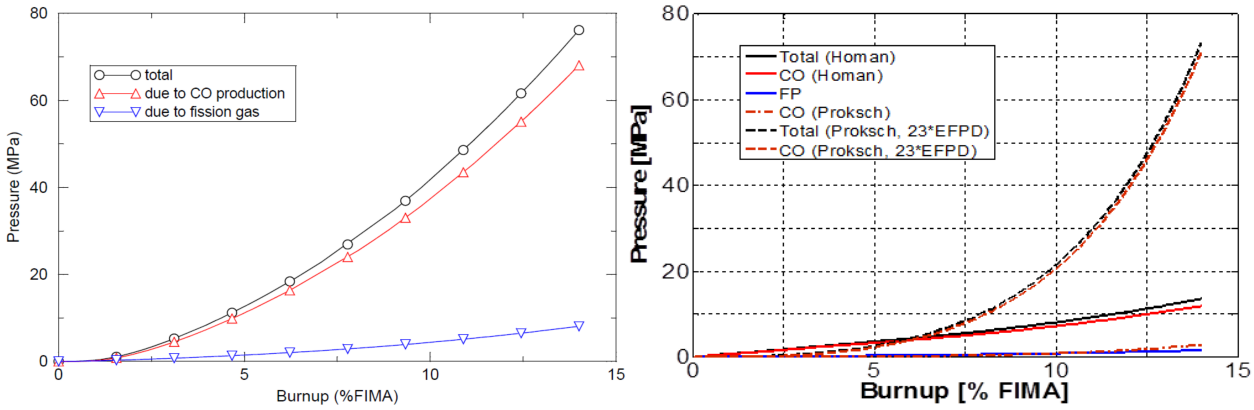

(a) (b)

Figure D.16: Total and partial internal gas pressures within a nominal TRISO particle predicted for Benchmark Case 11 as calculated by (a) PARFUME and (b) TRIUNE.

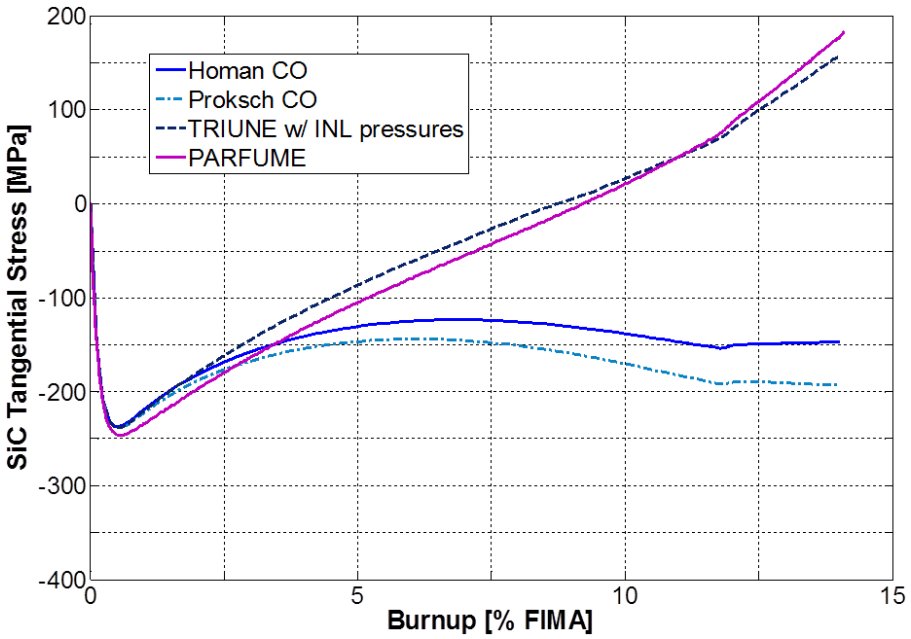

Figure D.17: SiC tangential stress calculated by TRIUNE and PARFUME as a function of neutron fast fluence for Benchmark Case 11 using a Poisson's ratio in creep of 0.4.

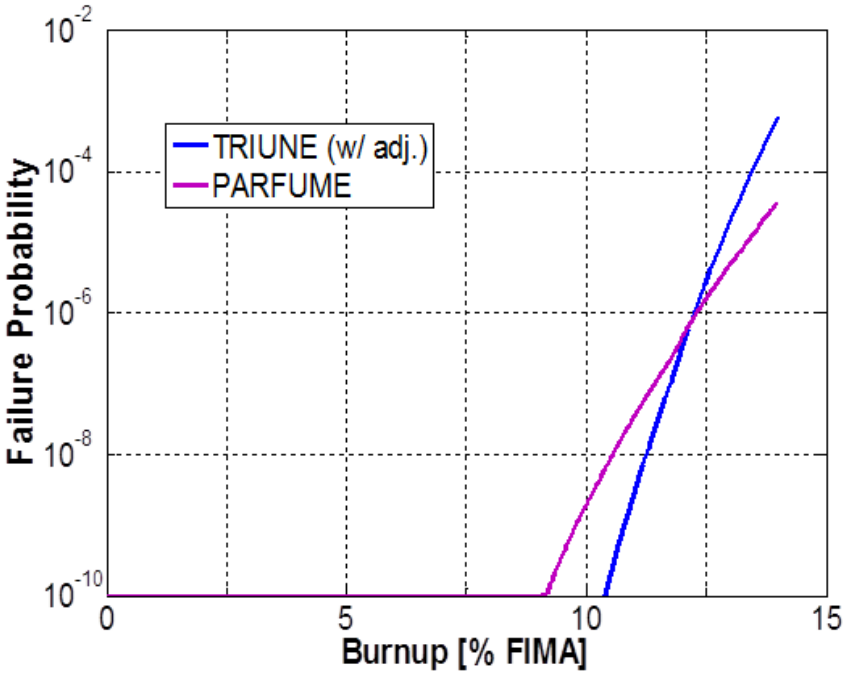

Figure D.18: TRISO particle failure probabilities due to SiC pressure vessel failure as a function of fuel burnup level for Benchmark Case 11, as calculated by TRIUNE and PARFUME.

Case 12: NPR-1 A5

No failure probabilities from TRIUNE calculations are shown for Case 12 because TRIUNE focuses on pressure vessel failure of the SiC as the failure mode while IPyC cracking and IPyC/SiC debonding are the failure modes present for this benchmark case.

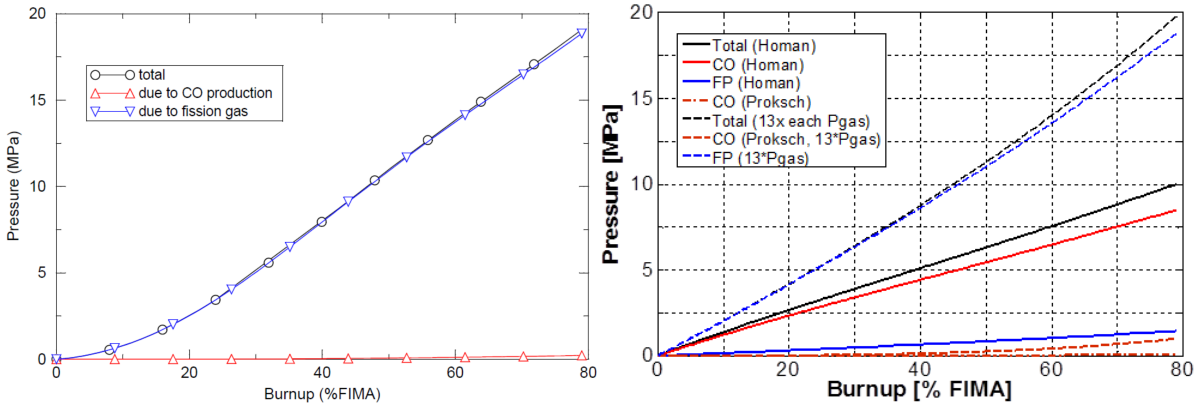

(a) (b)

Figure D.19: Total and partial internal gas pressures within a nominal TRISO particle predicted for Benchmark Case 12 as calculated by (a) PARFUME and (b) TRIUNE.

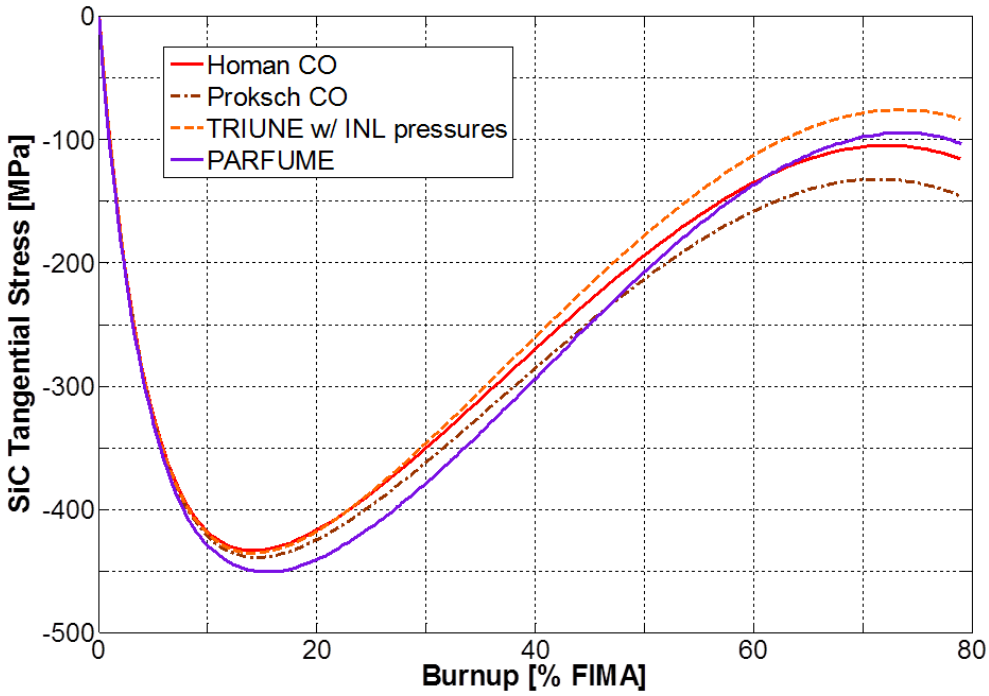

Figure D.20: SiC tangential stress calculated by TRIUNE and PARFUME as a function of neutron fast fluence for Benchmark Case 12 using a Poisson's ratio in creep of 0.4.

Case 13: HFR EU-1

Gas pressures, calculated SiC tangential stresses, and failure probabilities due to SiC pressure vessel failure are shown for Case 13. The failure probability curve in Figure D.23 labeled "TRIUNE w/ adj" displays fuel performance results calculated using TRIUNE with PARFUME gas pressure as input data for stress calculations instead of using TRIUNE's gas generation modules.

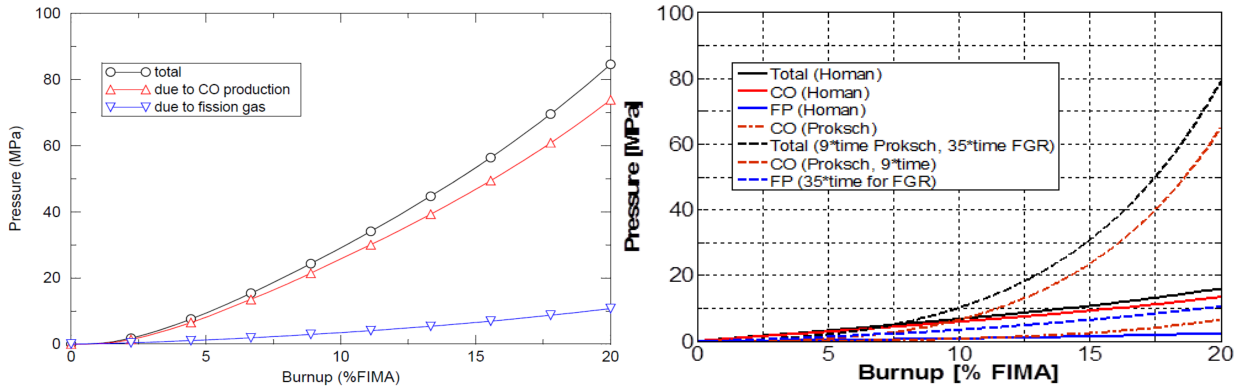

(a) (b)

Figure D.21: Total and partial internal gas pressures within a nominal TRISO particle predicted for Benchmark Case 13 as calculated by (a) PARFUME and (b) TRIUNE.

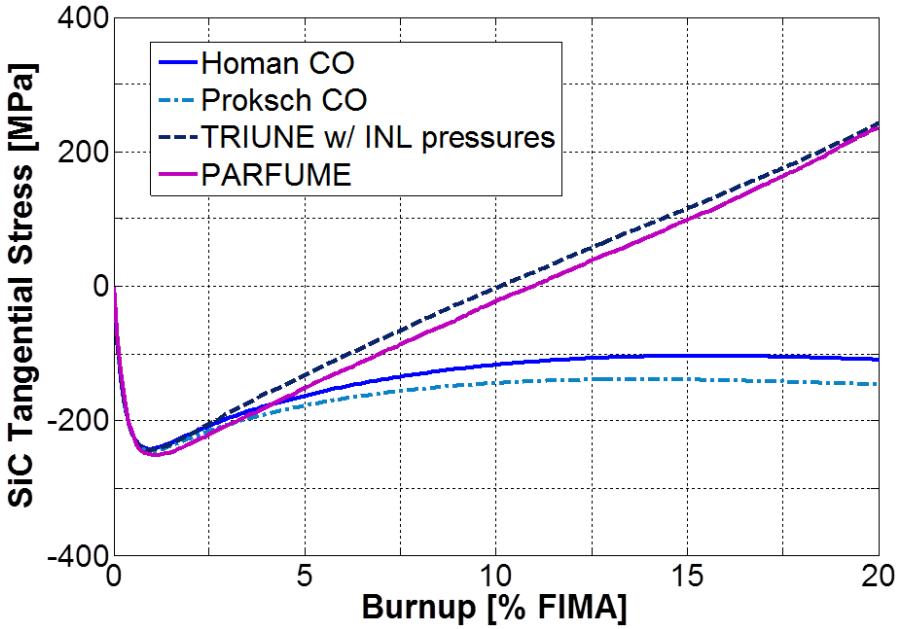

Figure D.22: SiC tangential stress calculated by TRIUNE and PARFUME as a function of neutron fast fluence for Benchmark Case 13 using a Poisson's ratio in creep of 0.4.

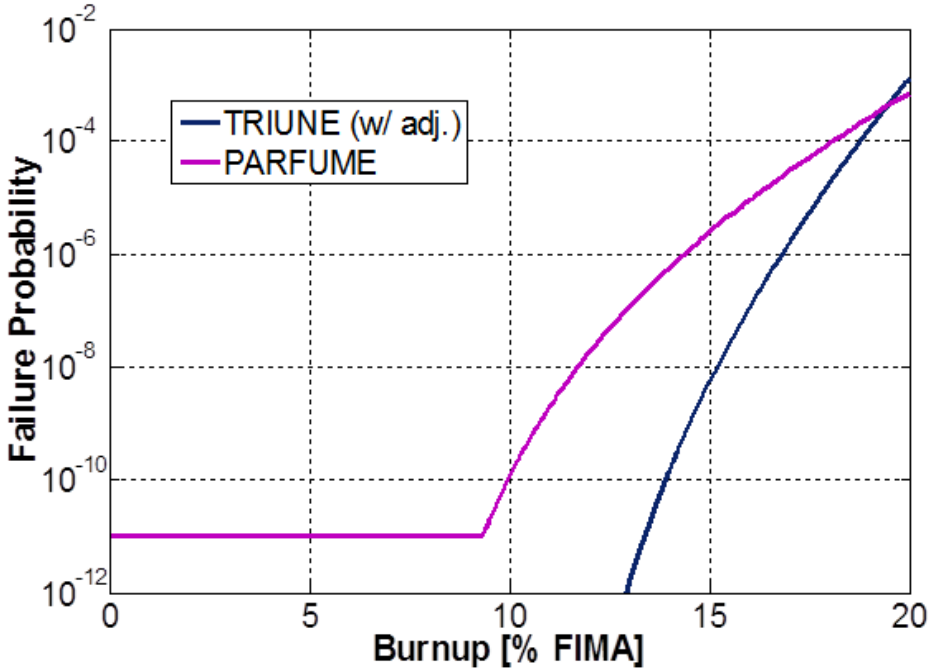

Figure D.23: TRISO particle failure probabilities due to SiC pressure vessel failure as a function of fuel burnup level for Benchmark Case 13, as calculated by TRIUNE and PARFUME.

Case 14: HFR EU-2

Gas pressures, calculated SiC tangential stresses, and failure probabilities due to SiC pressure vessel failure are shown for Case 14. The failure probability curve in Figure D.26 labeled "TRIUNE w/ adj" displays fuel performance results calculated using TRIUNE with PARFUME gas pressure as input data for stress calculations instead of using TRIUNE's gas generation modules.

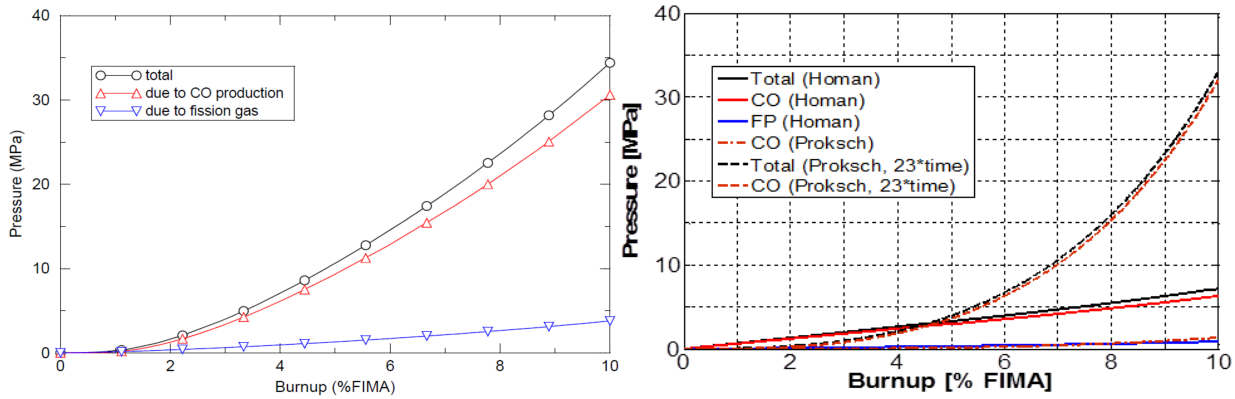

(a) (b)

Figure D.24: Total and partial internal gas pressures within a nominal TRISO particle predicted for Benchmark Case 14 as calculated by (a) PARFUME and (b) TRIUNE.

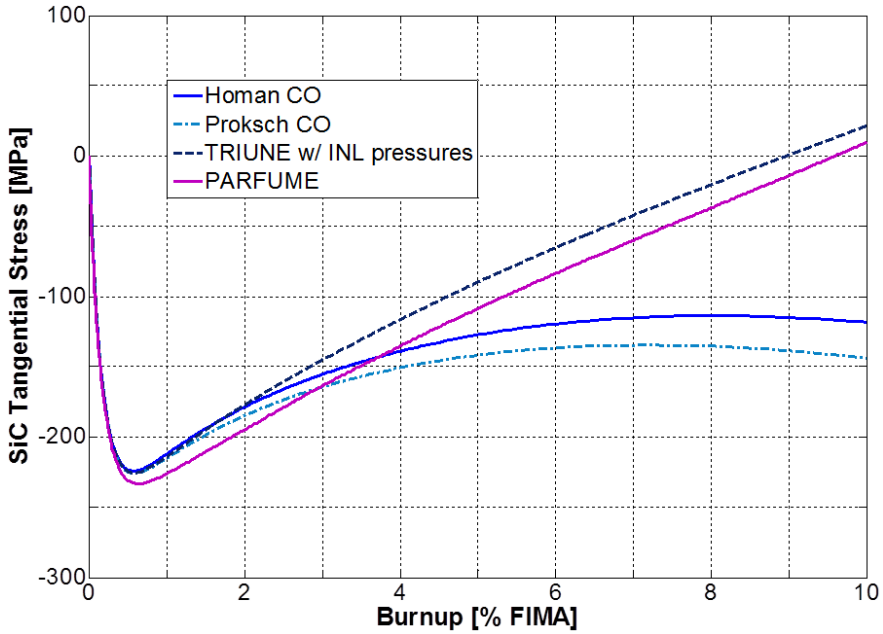

Figure D.25: SiC tangential stress calculated by TRIUNE and PARFUME as a function of neutron fast fluence for Benchmark Case 14 using a Poisson's ratio in creep of 0.4.

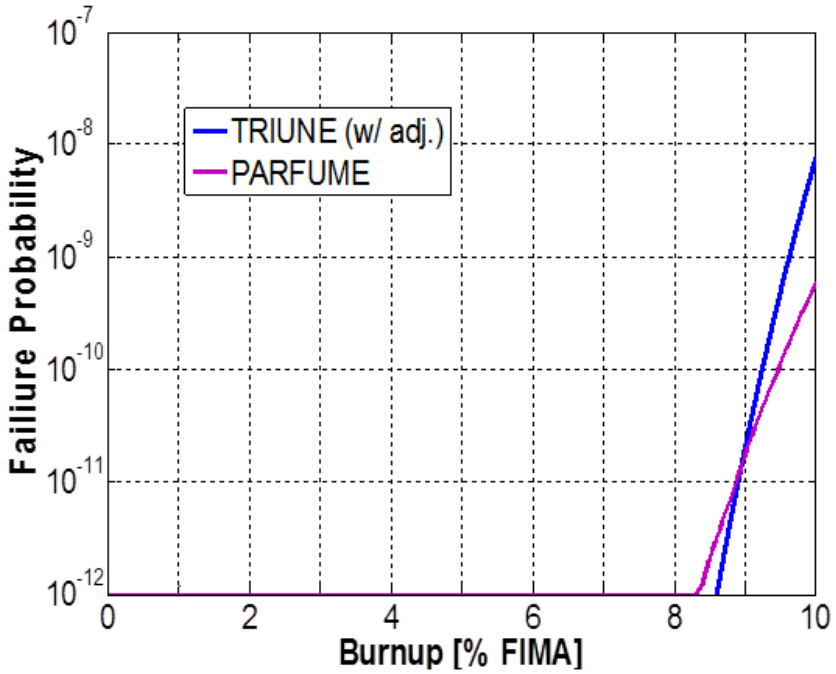

Figure D.26: TRISO particle failure probabilities due to SiC pressure vessel failure as a function of fuel burnup level for Benchmark Case 14, as calculated by TRIUNE and PARFUME.